Formation and surface exchange of nitrous acid

Dissertation zur Erlangung des Grades

„Doktor der Naturwissenschaften“

im Promotionsfach Chemie

am Fachbereich Chemie, Pharmazie und Geowissenschaften

der Johannes Gutenberg-Universität in Mainz

Robert Oswald

geb. in Lahnstein

Mainz, den 12.02.2014

“Wirkliches Neuland in einer Wissenschaft kann wohl nur gewonnen werden, wenn man an einer entscheidenden Stelle bereit ist, den Grund zu verlassen, auf dem die bisherige Wissenschaft ruht, und gewissermaßen ins Leere zu springen.“

Werner Heisenberg (1901-1976)

Zusammenfassung

Der globale Stickstoffkreislauf umfasst die Prozesse der Stickstoffumsetzung und den gegenseitigen Austausch der einzelnen Komponenten zwischen der Atmosphäre, den Gewässern und dem Boden. Hierbei ist die Stickstofffixierung aus der Atmosphäre durch Mikroben im Boden und in Gewässern von großer Bedeutung für das Leben auf der Erde. Der vermehrte Einsatz von Düngemitteln in Folge der Entwicklung des Haber-Bosch Verfahrens führte zu einem enormen Anstieg des Stickstoffeintrags in die Böden. Dieser anthropogene Eintrag verdoppelte den bisherigen natürlichen Eintrag an reaktiven Stickstoffs. Das Gleichgewicht zwischen den einzelnen Systemen stellt sich neu ein und führt zu erhöhten Werten an reaktivem Stickstoff in der Atmosphäre und den Gewässern. Zum reaktiven Stickstoff gehören unter anderem Stickoxide (NO_x), die salpetrige Säure (HONO), sowie die Salpetersäure (HNO_3). Reaktiver Stickstoff ist eine treibende Kraft bei der Bildung von Ozon (O_3) und dem Hydroxylradikal (OH) und beeinflusst dadurch maßgeblich die Reaktivität der Atmosphäre.

Bislang sind die genauen Bildungswege von HONO in der Atmosphäre und im Boden, sowie der gegenseitige Austausch von HONO zwischen Atmosphäre und Boden noch nicht vollständig aufgedeckt. HONO besitzt tagsüber aufgrund der Photolyse im UV-Bereich in der Atmosphäre eine durchschnittliche Lebensdauer von etwa 15 bis 30 min. Bei der HONO-Photolyse entstehen OH und Stickstoffmonooxid (NO), was die Bedeutsamkeit von HONO für die atmosphärische Photochemie widerspiegelt.

Um die genannte Bildung von HONO im Boden und dessen anschließenden Austausch mit der Atmosphäre zu untersuchen, wurden Messungen mit dynamischen Kammern durchgeführt. Es wurden Bodenproben aus verschiedenen Regionen der Erde genommen, vorbereitet und in der dynamischen Kammer unter geregelten Laborbedingungen gemessen. Die Emissionsflüsse von Wasser, NO und HONO wurden während dem Spülen der Kammer mit sauberer Luft (frei von reaktivem Stickstoff, Wasser und O_3) aufgezeichnet. Die Ergebnisse zeigen, dass die Emission von HONO im gleichen Bodenfeuchtebereich stattfindet wie die für NO (von 6.5 bis 56.0 % WHC), dessen Prozesse weitestgehend bekannt sind. HONO wurde in vergleichbarem Umfang

wie NO emittiert und bei drei von 17 Bodenproben überstiegen die Werte sogar jene von NO. Der maximale Emissionsfluss von HONO betrug (257.5 ± 0.1) N-ng m^{-2} s^{-1}. Des Weiteren waren die beobachteten Flüsse von HONO für Böden mit neutralen bis basischen pH-Werten unerwartet hoch. Dies und die ermittelten Aktivierungsenergie für den HONO-Emissionsfluss von 80 kJ mol^{-1} einer ausgewählten Bodenprobe im Vergleich mit Literaturwerten der mikrobiellen Nitrifikation führten zu der Annahme, dass die mikrobielle Nitrifikation die Hauptquelle für die HONO-Emission ist. Inhibierungsexperimente mit einer Bodenprobe und die Messung einer Reinkultur von *Nitrosomonas europaea* (eine Bakterienart, die Nitrifikation durchführt und in Böden sehr verbreitet ist) bestärkten diese Theorie. Als Schlussfolgerung wurde das konzeptionelle Model der Bodenemission verschiedener Stickstoffkomponenten in Abhängigkeit von dem Wasserhaushalt des Bodens für HONO erweitert.

In einem weiteren Versuch mit einer hervorragend charakterisierten Bodenprobe von einem Maisfeld aus der Region Grignon in Frankreich, wurde zum Spülen der dynamischen Kammer Luft mit erhöhtem Mischungsverhältnis von HONO verwendet. Es konnten für diese Bodenprobe bidirektionale Flüsse von HONO von minimal -25 N-ng m^{-2} s^{-1} bei 10 ppb bis maximal von 20 N-ng m^{-2} s^{-1} bei 0 ppb beobachtet werden. Das zeigt, dass Böden nicht nur als HONO-Quelle, sondern auch je nach Bedingungen als effektive Senke dienen können. Der sogenannte Kompensationspunkt für HONO wurde speziell für diese Bodenprobe über die gesamte Bodenfeuchte bestimmt. Der maximale Kompensationspunkt liegt mit ca. 12 ppb weit über den Werten, die in der Regel am Tag in der Atmosphäre für HONO beobachtet werden.

Ein erniedrigter pH-Wert im Boden führt zu einem deutlich verringerten Verhältnis von HONO- zu NO-Emissionen. Dies ließe sich damit erklären, dass die Reaktivität von HONO mit sinkendem pH-Wert zunimmt. Niedrige pH-Werte finden sich vornehmlich in Böden mit einem hohen Anteil an organischem Material, das zusätzlich mit HONO reagieren kann. Außerdem finden die Emissionsflüsse von HONO und NO dieser Böden bevorzugt bei erhöhtem Wassergehalt statt, was dazu führt, dass die Gasdiffusion zum Zeitpunkt der Emission im Boden relativ gering ist und somit die Aufenthaltsdauer von HONO und NO im Vergleich zu anderen Böden erhöht ist. Die längere Aufenthaltszeit bedeutet, dass HONO mehr Zeit hat im Boden zu reagieren und sich das Gleichgewicht zwischen Bodenlösung und der Atmosphäre länger einstellen kann. So

konnte gezeigt werden, dass die effektive Diffusion von Gasen im Bodenporenraum und die effektive Diffusion von Ionen in der Bodenlösung die HONO-Produktion und den Austausch von HONO mit der Atmosphäre begrenzen. Zum Beispiel setzt die vermehrte Freisetzung von HONO und NO erst bei Bodenfeuchten unterhalb von (61 ± 10) % ein, wenn die relativen Diffusionskoeffizienten für Gase im Bodenporenraum ($D_{eff,gas}/D_{0,gas}$) und Ionen in der Bodenlösung ($D_{eff,ion}/D_{0,ion}$) sich entsprechen. Im Durchschnitt liegt dieser Wert bei $10^{-(1.37 \pm 0.7)}$.

Ergänzend zu den Messungen im Labor wurde HONO während der Messkampagne HUMPPA-COPEC 2010 im borealen Nadelwald simultan in der Höhe von 1 m über dem Boden und 2 - 3 m über dem Blätterdach gemessen. Um den Einfluss bekannter Quellen und Senken abzuschätzen, wurde eine Budgetberechnung für HONO durchgeführt. Es stellte sich heraus, dass für HONO sämtliche bekannte Quellen und Senken in Bezug auf die übermächtige HONO-Photolyserate vernachlässigbar sind (< 20%). Wie erwartet haben die Bodenemissionen von HONO nur einen geringen Einfluss auf das Budget, da der Boden einen niedrigen pH-Wert und einen hohen Organikanteil aufweist. Eine weitere postulierte Quelle ist die verstärkte Photolyse von an Oberflächen adsorbierter HNO_3. Diese müsste mindestens zehnmal so hoch sein wie veranschlagt um der fehlenden Quelle von HONO zu entsprechen. Die lichtinduzierte Reduktion von Stickstoffdioxid (NO_2) am Boden oder an anderen Oberflächen konnte nicht ausgeschlossen werden und in Kombination mit der Photolyse von adsorbierter HNO_3 könnte es sich zumindest teilweise um die fehlende Quelle handeln. Es zeigte sich jedoch, dass eine stärkere Korrelation zwischen der fehlenden Quelle und der HONO-Photolyserate besteht, als zwischen der fehlenden Quelle und der entsprechenden Photolysefrequenz. Diese ist proportional zur Photolysefrequenz von NO_2. Das wiederum deutet daraufhin, dass der in Erwägung gezogene Ansatz nicht zutreffend ist. Somit lässt sich schlussfolgern, dass entweder die Photolyserate von HONO überschätzt wird oder dass immer noch eine unbekannte HONO-Quelle existiert.

Summary

The global nitrogen cycle encompasses the processes of nitrogen transformation and exchange between the terrestrial, marine, and atmospheric system. As an essential nutrient for plants and animals, nitrogen fixation from the atmosphere to marine and terrestrial system is of major importance for life on earth. The enhanced use of fertilizer following the invention of the Haber-Bosch process led to an increased nitrogen input to the terrestrial system by a factor of about two. Reaching for an equilibrium state, the enhancement of reactive nitrogen in the terrestrial system also leads to an increase of reactive nitrogen in the atmosphere and the oceans. In the atmosphere reactive nitrogen comprises, among others, nitrogen oxides (NO_x) as well as nitrous acid (HONO) and nitric acid (HNO_3), which are driving forces in the formation of ozone (O_3) and hydroxyl radical (OH) and hence, strongly influence the reactivity of the atmosphere.

By now, the exact formation pathways of HONO in the atmosphere and pedosphere and the exchange between these is not well understood. Due to its photolysis in the UV, forming NO and OH, HONO is a very short lived molecule with an average atmospheric lifetime of about 15 to 30 min during daytime and of special interest for atmospheric photo-chemistry, hence, the exchange processes of HONO between soil and atmosphere are of major importance.

In order to investigate the formation of HONO in soil and its subsequent emission to the atmosphere, in this thesis measurements using a dynamic chamber system were performed. A survey of soils from different ecosystems were sampled, prepared and measured in the dynamic chamber under controlled laboratory conditions. The emission fluxes of water vapor, NO and HONO were observed by flushing the chamber with clean air (free of reactive nitrogen, water and O_3). The results showed that both HONO and NO, for which the processes are well known, are emitted at the same soil water content (SWC) range of 6.5 to 56.0 % WHC. The emission fluxes of HONO were comparable to that of NO, and even higher for three of 17 different soil samples with a maximum value of (257.5 ± 0.1) N-ng m^{-2} s^{-1}. The emission fluxes of HONO were unexpectedly high for soils with neutral to basic pH. This novel finding together with

typical activation energies of microbial nitrification rates found for the emission fluxes of HONO (80 kJ mol^{-1}), led to the assumption of direct release of HONO by nitrifying microbes. Inhibition experiments with a soil sample and measurement of a pure culture suspension of *Nitrosomonas europaea* (a nitrifying bacterium that occurs in nearly every soil) strengthened this theory. As a result the conceptual model of the SWC dependency of soil nitrogen emissions could be extended for HONO.

In a subsequent dynamic chamber experiment, utilizing a well characterized soil sample from a maize field in France, elevated mixing ratios of HONO were added to the purging air flow through the chamber. Bidirectional exchange fluxes of HONO were found for this soil sample ranging between minimal -25 N-ng m^{-2} s^{-1} at 10 ppb inlet mixing ratio to maximal 20 N-ng m^{-2} s^{-1} at 0 ppb inlet mixing ratio, indicating that soil not only acts as a source, but also as a strong sink for HONO under certain conditions. A compensation point mixing ratio for the analyzed soil sample was calculated dependent on the SWC. At optimum SWC (SWC_{opt}) the compensation point mixing ratio of HONO reached about 12 ppb, which exceeds the mixing ratios typically found for HONO during daytime in the atmosphere by more than ten to a hundred times and, hence, impressively shows the possible strength of this source. However, soil acidity leads to a decrease in the ratio of HONO to NO, which is due to several processes. First the reactivity of HONO is increased with lower soil pH, which generally occurs together with an increasing organic matter content being also reactive to HONO. Furthermore, the maximal emission fluxes of HONO and NO occur at higher soil water contents where pH is decreased, leading to a longer residence time due to slower diffusion in soil and, consequently, to increased time for reactions and partitioning with the soil solution. The effective diffusion of gases in soil pores and the effective diffusion of ions in soil solution have been found to set the boundaries for HONO production and exchange with the atmosphere. For example, HONO and NO emission start to increase when SWC decreases below (61 ± 10) % WHC when relative diffusion coefficients of gases in soil ($D_{eff,gas}/D_{0,gas}$) and ions in soil solution ($D_{eff,ion}/D_{0,ion}$) are equal, with a mean value of $10^{-(1.37 \pm 0.7)}$.

In addition to the laboratory experiments, the sinks and sources of HONO in boreal forest ecosystem were investigated during a field campaign (HUMPPA-COPEC 2010). HONO was measured simultaneously at a height of about 1 m above ground and at

about 2 to 3 m above the canopy. To estimate the influence of known sources and sinks budgets of HONO from measurements of all relevant species were calculated. The budgets derived at both measurement heights clearly demonstrate that all known production and loss terms for HONO during daytime are of minor importance (< 20%) and even negligible compared to the strong photolytic loss of HONO. As indicated by the laboratory measurements direct emission of HONO by the acidic soil with high organic content is of minor importance. Another postulated source is the enhanced photolysis of surface adsorbed HNO_3 producing HONO and NO_x. However, the enhancement of photolysis needs to be 10 times stronger than assumed in order to compete with the missing source. Light-induced conversion of nitrogen dioxide (NO_2) on the ground and other surfaces cannot be ruled out as a formation process of HONO and together with the photolysis of adsorbed HNO_3 may at least partly explain the missing source. However, since the missing source term correlates stronger with the photolytic loss of HONO than with its photolysis frequency, which is linearly correlated to the photolysis frequency of NO_2, a large contribution of this pathway is very unlikely. This leads to the assumption that either the photolysis rate of HONO is generally overestimated or a yet unknown production term is still missing.

Contents

1. Introduction

Nitrogen in its elemental form (N_2) is the most abundant gas in the atmosphere accounting for about 78 % (Seinfeld et al., 2006). Due to its triple bond, one of the most stable molecular bonds, it is used in chemistry and industry as an inert gas. However, once the triple bond is "broken" and oxygen (O_2) is allowed to react with nitrogen, the highly reactive nitrogen oxides are formed. These may react further with water vapor (H_2O) to form acids, like nitrous acid (HNO_2) or nitric acid (HNO_3). While the mentioned compounds are primary important for the reactivity of the atmosphere by formation of ozone (O_3) (Crutzen, 1979) and partly responsible for the acidity of rain causing plant diseases (van Breemen et al., 1982), the corresponding bases of HNO_2 (i.e., nitrite, NO_2^-) and HNO_3 (i.e. nitrate, NO_3^-) are together with ammonia (NH_3) and its corresponding acid ammonium (NH_4^+) essential for plant growth and life in general. Therefore, N_2 from the atmosphere needs to be fixed to the soil in order to be available for plants and animals. Beside natural fixation of N_2 by microbes (biological nitrogen fixation), the invention of the Haber-Bosch process in 1913 led to anthropogenic nitrogen fixation and doubling of the amount of nitrogen available for plant growth (Fowler et al., 2013; Galloway et al., 2013). Fig. 1 gives an overview of the exchange processes of nitrogen between the atmosphere, land and ocean.

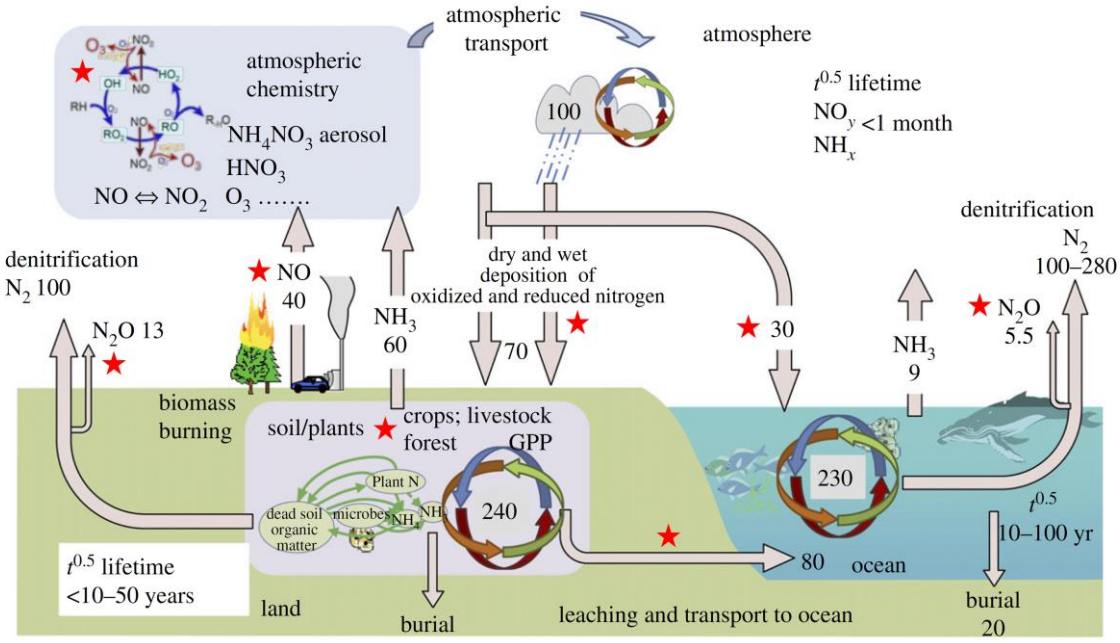

Figure 1. Overview of the processes and their related exchange fluxes of nitrogen and reactive nitrogen (Tg N yr^{-1}) is presented for the terrestrial and marine systems and the atmosphere. The approximated lifetimes of reactive nitrogen integrated over global scales is shown. Additionally, the occurrence of HNO_2 in the nitrogen cycle is marked by the red stars. (adapted from Fowler et al., 2013)

Since HNO_2 is a highly reactive compound with a lifetime during day in the troposphere of about 15 to 30 min and its transformation rates by soil microbes might be even faster, it is often not considered in the global nitrogen cycle although it can be more abundant than other long-living nitrogen species. In Fig.1 its occurrence is indicated by the red stars. The exact mechanisms of formation and exchange of HNO_2 in these processes is not well understood and hence, needs to be further investigated.

1.1 The chemistry of nitrous acid

The sum formula HNO_2 comprises five important structural isomers, three of them having two stereo isomers (Fig. 2); nitrous acid (trans-HONO and cis-HONO), isonitrous acid or hydrogen nitryl (HNO_2), imine peroxide (trans-HNOO and cis-HNOO), hydroperoxynitrene (trans-HOON and cis-HOON), and cyclic dioxaciridine (HcyNOO).

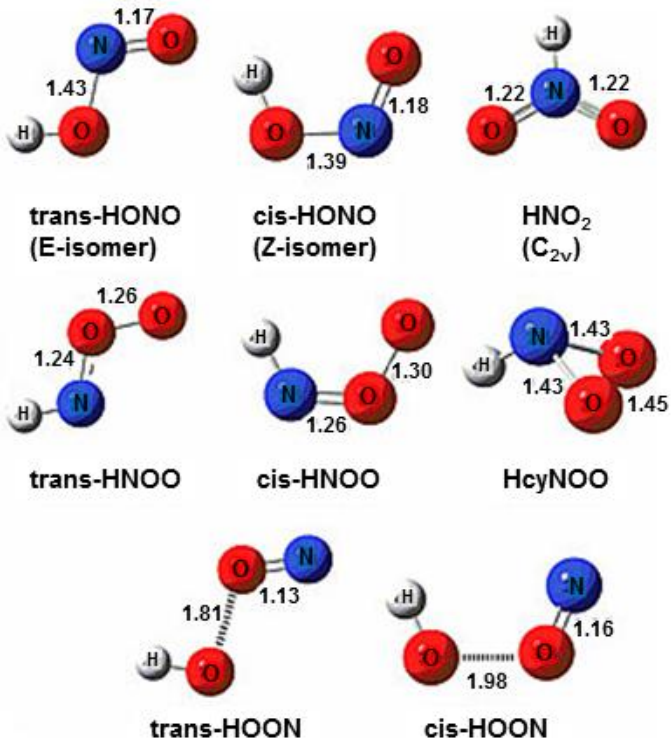

Figure 2. Structures and bond lengths (Å) for the eight main isomers of HNO_2 are shown. (adapted from Asatryan et al., 2007)

The first three isomers provide negative heat of formation ($\Delta H_f < 0$), while the others have positive ΔH_f, being less important for most applications. The energetic difference between trans- and cis-HONO is about + 1.69 kJ mol^{-1} (± 0.42 kJ mol^{-1}) (De Mare and Moussaoui, 1999), possibly resulting from the stronger steric hindrance at cis-conformation than at trans-conformation and being larger than the formed intramolecular hydrogen bonding at cis-conformation. Steric hindrance is positively correlated with the bond angles, weakening the overlap of the high energetic π-orbitals

between nitrogen and oxygen, expressed as difference in bond length for trans- and cis-conformation, $\Delta_{\text{bond length}}(N=O) \approx 0.01$ Å (Asatryan et al., 2007) (Fig. 2). The isomerization energy for the torsion of cis- to trans-HONO constitutes about 40.6 kJ mol^{-1} (De Mare and Moussaoui, 1999), while the one for HNO_2 to trans-HONO is about 198.7 kJ mol^{-1} (Asatryan et al., 2007).

In the following the chemistry of nitrous acid and its isomers for the four classical elements water, fire, air and earth is outlined.

1.1.1 WATER: Aqueous chemistry of nitrous acid

Pure HONO is not stable due to its disproportion reaction (R1) and, hence, only stable in diluted solution or in the form of its corresponding salt NO_2^-.

$$3\,\mathrm{HO}\overset{+3}{\mathrm{N}}\mathrm{O} \Leftrightarrow \overset{+5}{\mathrm{N}}\mathrm{O}_3^- + 2\overset{+2}{\mathrm{N}}\mathrm{O} + \mathrm{H_3O^+} \qquad \text{(R1)}$$

This reaction is part of the commercial Ostwald process (Ostwald, 1902), gaining NO_3^- by oxidation of NH_3, which is produced by the Haber-Bosch process (Schlögl, 2003). The disproportion reaction can be separated into a reduction reaction, where HONO gets reduced to nitric oxide (NO), and into an oxidation reaction, where HONO acts as reducing agent, forming NO_3^-.

$$\overset{+5}{\mathrm{N}}\mathrm{O}_3^- + 3\mathrm{H_3O^+} + 2\mathrm{e^-} \Leftrightarrow \mathrm{HO}\overset{+3}{\mathrm{N}}\mathrm{O} + 4\mathrm{H_2O} \qquad \text{(R2)}$$

$$\mathrm{HO}\overset{+3}{\mathrm{N}}\mathrm{O} + \mathrm{H_3O^+} + \mathrm{e^-} \Leftrightarrow \overset{+2}{\mathrm{N}}\mathrm{O} + 2\mathrm{H_2O} \qquad \text{(R3)}$$

The standard reduction potentials for the two reactions are $E^{\theta}_{red}\left(NO_3^-/HONO\right) = 0.934\,V$ and $E^{\theta}_{red}\left(HONO/NO\right) = 0.983\,V$ (Haynes and Lide, 2011). The resulting difference of standard potentials yields in E^{θ}_{red} of 0.049 V, which is about 1.7 times the pre-logarithm factor of the Nernst equation at standard conditions:

$$\Delta E = \Delta E_{red}^{\theta} + \frac{R \times T}{z \times F} \ln\left(\frac{[HONO]^3}{[NO_3^-] \times [NO]^2 \times [H_3O^+]}\right) \quad (1)$$

where R is the ideal gas constant (8.314 J mol^{-1} K^{-1}), *T* is the absolute temperature (K), *z* is the number of electrons being transferred (here: 2), F is the Faraday constant (96485.34 C mol^{-1} = 96485.34 J V^{-1} mol^{-1} 1^{-1}) (Haynes and Lide, 2011). Furthermore the Nernst equation shows that the reaction depends on the concentration of HONO and hydroxonium ions (protons; H_3O^+). Their concentration again is correlated which each other, since HONO is a weak Brønsted acid, but behaves amphoteric like water.

$$HONO + H_2O \rightleftharpoons H_3O^+ + NO_2^- \quad (R4)$$

$$HONO + H_3O^+ \rightleftharpoons H_2ONO^+ + H_2O \rightleftharpoons 2\,H_2O + NO^+ \quad (R5)$$

The strength of acidity is given by the negative logarithm of the acidy constant (K_a), the pK_a value.

$$K_a = \frac{[H_3O^+] \times [NO_2^-]}{[HONO]} \quad (2)$$

$$pK_a = -\log\left(\frac{[H_3O^+] \times [NO_2^-]}{[HONO]}\right) \quad (3)$$

Protonation and dissociation are temperature dependent processes, showing a pK_a value for HONO of about 3.16 at room temperature (da Silva et al., 2006).

$$K_a(T_2) = K_a(T_1) \times \exp\left(\frac{\Delta H_{dissociation}}{R} \times \left(\frac{1}{T_1} - \frac{1}{T_2}\right)\right) \quad (4)$$

With the pK_a value of HONO at 298 K and the dissociation enthalpy for HONO, $\Delta H_{dissociation}$(H-ONO) = 6.7 kJ mol^{-1} (da Silva et al., 2006), one can easily calculate the pK_a value of HONO for each temperature by using Eq. (4).

The addition of a strong acid to a NO_2^- solution yields in the formation of HONO and its protonated form, which eliminates water to form the nitrosyl cation (R5). The fate of the reactive molecule depends on the surrounding conditions, while the back reaction with water leads again to HONO, reactions with organic amines form alkyl- and aryldiazonium compounds (Fig.3).

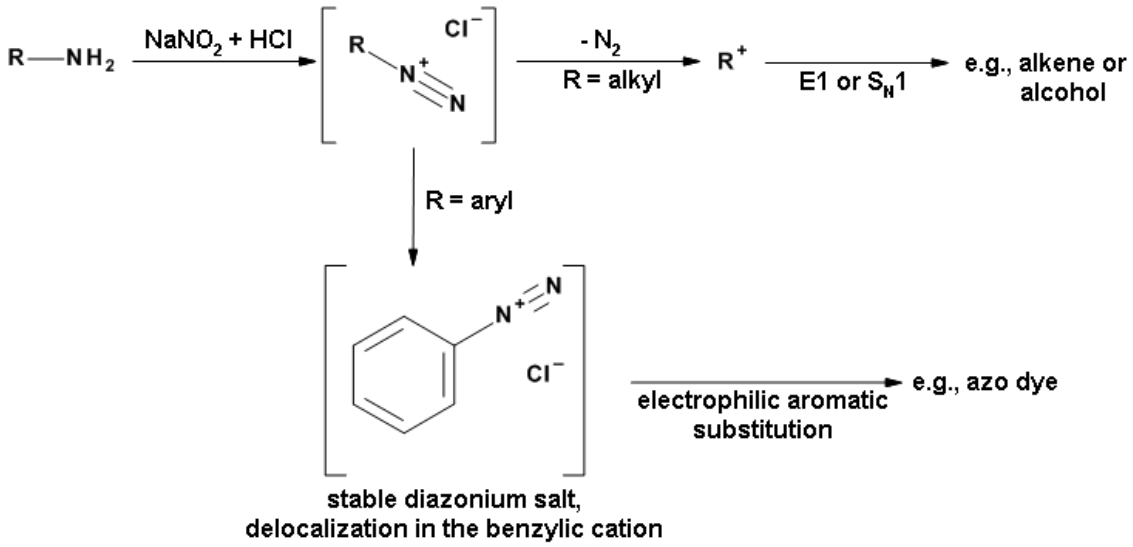

Figure 3. Reaction scheme of alkyl- and aryldiazonium compounds formation (adapted from Clayden, 2001).

Clayden (2001) state:

> *"Aryldiazonium salts are stable but alkyldiazonium salts are not: nitrogen gas is the world's best leaving group, and, when it goes, it leaves behind a carbocation." (p. 988)*

Alkyldiazonium salts decompose rapidly, releasing nitrogen (N_2). The formed carbocation undergoes further reaction (e.g., nucleophilic addition of a hydroxyl group). Aryldiazionum salts are quite stable and have nucleophilic character. Hence, they are able to react with electron rich aromatic compounds by electrophilic aromatic substitution forming mostly colorful products (reaction used for detecting HONO, see section 1.2).

Beside the reaction of HONO with organic molecules, there are several possibilities for HONO to form complex compounds with different metal atoms and ions. In the form of NO_2^-, it binds either with the central N yielding nitro-complexes or it binds with one of the terminal, equivalent oxygen yielding nitrito-complexes. The HONO coordination chemistry plays an interesting role in modern medicinal chemistry. It is recognized that enzymes like the Cytochrome P450s family (Estabrook, 2003) can alter the oxidation state of nitrogen (Roncaroli et al., 2007).

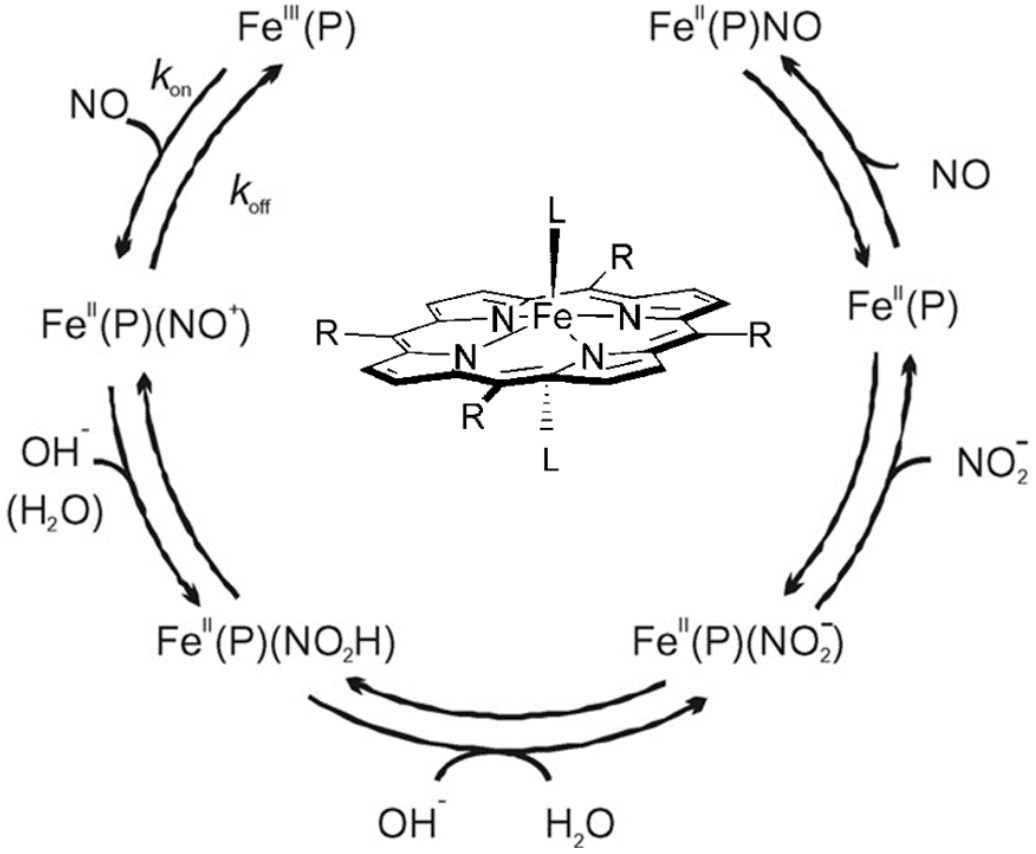

Figure 4. Coordination chemistry of HONO, NO_2^-, NO and NO^+ in dependency of pH and oxidation state of an iron porphorine complex system, like the enzyme Cytochrome P450 (adapted from Roncaroli et al., 2007).

In 1998 the Nobel Prize in Physiology or Medicine was awarded to R.F. Furchgott, L. J. Ignarro and F. Murad for the finding of the NO activity in the cardiovascular system (Source: www.Nobelprize.org.). One important feature of complex compounds like these, are the release of NO at certain circumstances (Fig.4). Recent investigations show that similar ruthenium complexes as in the P450 system are able to release NO by irradiating with UV-light (de Lima et al., 2005), comparable to the HONO photolysis (see (R12), section 1.1.3). Such compounds might be useful for exact local medication.

1.1.2 FIRE: Fuel and the combustion chemistry of nitrous acid

In 1976 Chan et al. suggested that homogeneous production of HONO in engine exhausts might be an important source for atmospheric HONO. Some years later Pitts et al. (1984) reported about the first measurement of HONO in the diluted exhaust of cars (Fig. 5). With a lower detection limit (LOD) for HONO of about 12 ppb they were able to observe HONO emissions by cars built before 1979, having no 3-way catalyst and running on leaded gasoline, while emissions from newer cars with a 3-way catalyst lay below the LOD. Highest emissions were detected during cold start of the engines (340 ppb HONO and 600 ppb NO_2).

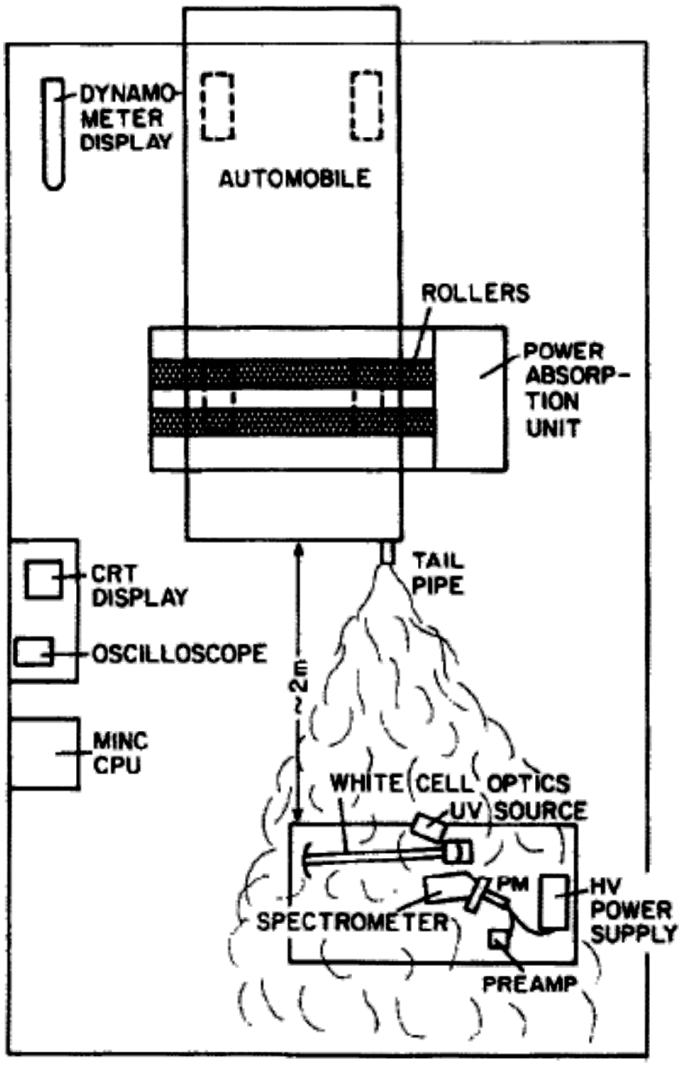

Figure 5. A sketch of the experimental setup of Pitts et al. (1984).

As it can be seen from the difference of exhaust emissions by cars with and without a 3-way catalyst, concentrations of reactive nitrogen in car exhaust has decreased with steady improvement of engines. Nevertheless, measurements of car exhaust fumes from fuel combustion processes and also from other vehicles like airplanes (e.g., Jurkat et al., 2011) are part of ongoing investigations concerning new reaction pathways of HONO formation (Aubin and Abbatt, 2007; Khalizov et al., 2010; Monge et al., 2010). Along with measurements, theoretical calculations based on molecular orbital theory give new insides in the reactive nitrogen chemistry during combustion. While the common reaction cascade comprises "only" HONO (Clothier et al., 1993a; Clothier et al., 1993b),

$$\text{Initiation: } \mathrm{Alk\text{-}O\text{-}NO_2} \rightarrow \mathrm{Alk-O + NO_2} \quad \text{(R6)}$$

$$\mathrm{NO_2 + RH \rightarrow HONO + R} \quad \text{(R7)}$$

$$\mathrm{HONO \rightarrow HO + NO} \quad \text{(R8)}$$

$$\text{Oxidation: } \mathrm{OH + RH \rightarrow ...} \quad \text{(R9)}$$

$$\text{Recycling: } \mathrm{2NO + O_2 \rightarrow NO_2} \quad \text{(R10)}$$

Chan et al. (2001) showed that the isomer of nitrous acid (see Fig. 2), the iso-nitrous acid, could play a role in the ignition response of fuels doped with organic nitrates. Within the reaction cascade OH is formed by HONO dissociation and is further important for the degradation of hydrocarbons (RH). In the reaction of HNO_2, there is no OH cleavage possible.

$$\mathrm{HNO_2 + O_2 \rightarrow HO_2 + NO_2} \quad \text{(R11)}$$

In the oxidation step, the peroxy hydroxyl radical (HO_2) may take the part of OH. However, organic nitrates as additives of fuel as a major global source of NO_x (Horowitz and Jacob, 1999) will become old-fashioned since globalization and industrialization increases the need for energy and hence, changes the expectations on fuel. Using renewable feedstocks, lowering emissions of insalubrious compounds and increasing performance of engines are just a few of these expectations (Mofijur et al., 2013; Chen et al., 2013).

Recently, paving stones containing titan dioxide (TiO_2) have been developed and become popular in cities, since they should decrease the amount of NO_2 in the air. The NO_2 from traffic is said to be oxidized to NO_3^- by the photocatalytic surface of the stones and subsequently washed out (braun-steine GmbH, 2014). However, several publications showed that TiO_2 surfaces convert NO_2 mainly to HONO, which is not totally stuck to the ground, but reenters the atmosphere and increases the reactivity of it (Asahi and Morikawa, 2007; Bedjanian and El Zein, 2012; El Zein and Bedjanian, 2012; Kebede et al., 2013).

1.1.3 AIR: Air chemistry of nitrous acid

During the last decades the knowledge of nitrous acid influencing atmospheric conditions has exponentially increased (Fig. 6). From the first detection of HONO in atmosphere (Nash, 1974), to the prove of importance of HONO being a photochemical source of OH via (R12) (Perner and Platt, 1979), it took five years.

$$\mathrm{HONO} \underset{k_{12}}{\overset{h\upsilon}{\rightleftharpoons}} \mathrm{OH+NO} \qquad \text{(R12)}$$

Perner and Platt (1979) also stated that the fast photolysis of HONO will yield in low daytime mixing ratios of maximal 10 ppt HONO. Increasing mixing ratios during nighttime have been attributed to the heterogeneous reaction of NO_2 on surfaces (for details see Finlayson-Pitts et al., 2003; De Jesus Medeiros and Pimentel, 2011). The DOAS technique measuring HONO was the state of art for the upcoming years. HONO regained interest with the curse of public schedule (Fig. 6) of monitoring active species influencing the acidification of rain (i.e. sulfur dioxide, SO_2, and HNO_3) and regulation of NH_3 emission budget for European countries. Along with these duties developments of new wet chemical instruments have emerged, measuring also HONO. Especially the EUROTRUC-1 (Borrell et al., 1997; Hov, 1997) program yielded in a rush of advanced wet denuder techniques. At the end of EUROTRUC-1 in 1995 and the alongside

ongoing improvement of the DOAS technique, it was possible to decrease the LOD and measure HONO mixing ratios also during daytime.

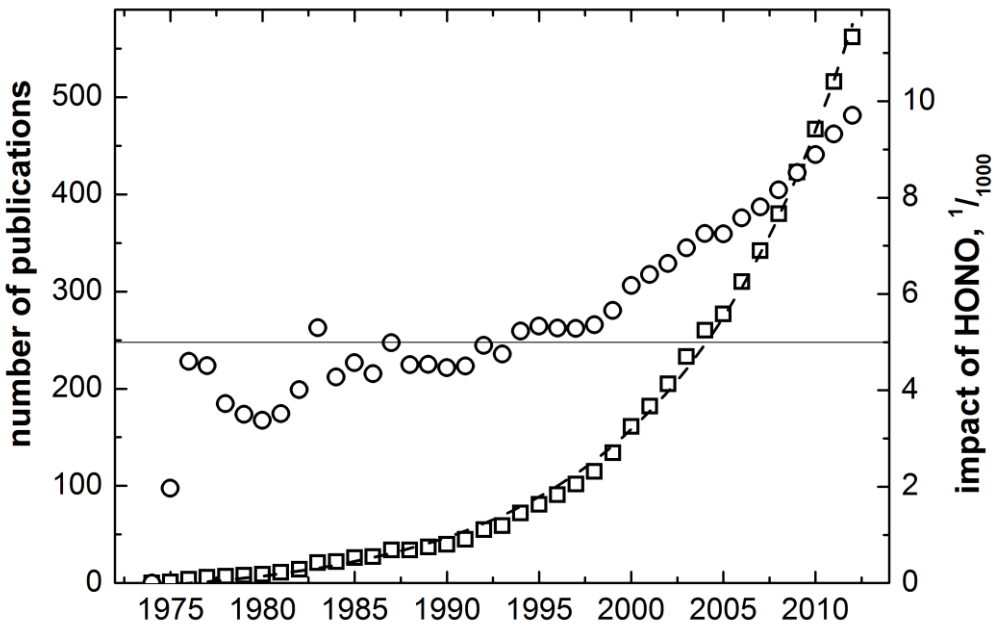

Figure 6. Importance of HONO to atmospheric science indicated by available publications. The number of publications containing the words HONO and atmospher* or HONO and tropospher* from 1974 till now (open squares) show an exponential increase (R^2 = 0.998). The impact of these publications is weighted by the number of publications containing the word troposphere (open circles).

The highly cited publications of Finlayson-Pitts and Pitts (1997) and Jacob (2000) mentioning the importance of HONO in tropospheric chemistry as well as reports about high daytime mixing ratios, which cannot be explained by known gas-phase reactions alone, focused the interest on missing sources of HONO (Fig. 6). Again an invention of a new wet chemical instrument measuring HONO, the long path absorption photometer (LOPAP) (Kleffmann et al., 2002), strengthened this finding (Kleffmann, 2007). Till now, a vast of possible reactions has been postulated to influence the HONO mixing ratios, especially during day (Table 1.1.3). However, understanding the atmospheric chemistry of HONO is an ongoing task.

Table 1.1.3 Atmospheric (a) sources and (b) sinks of nitrous acid. Reactions with reported rates or enthalpies are summarized.

(a)	Sources	Rates	Measurement	Reference
R12	$HO + NO + M \rightarrow HONO$	$k_{12} = 7.4 \times 10^{-31}$ cm^3 $molec.^{-1}$ s^{-1}	in N_2 at 298 K	(Atkinson et al., 2004)
R13	$HONO_2 + h\nu \rightarrow HONO + O(^3P)$	$\Delta H^0 = 305$ kJ mol^{-1}	$\lambda_{thres} = 393$ nm	(Atkinson et al., 2004)
R14	$HONO_2 + h\nu \rightarrow HONO + O(^3P)$	$\Delta H^0 = 495$ kJ mol^{-1}	$\lambda_{thres} = 242$ nm	(Atkinson et al., 2004)
R15	$HO_2 + NO_2 \rightarrow HONO + O_2$	$k_{15} = 5 \times 10^{-16}$ cm^3 $molec.^{-1}$ s^{-1}	at 298 K	(Tyndall et al., 1995)
R16	$NO + NO_2 + H_2O \rightarrow 2\ HONO$	$k_{16} = 1.0 - 13 \times 10^2$ M atm^{-2} s^{-1}	at 298 K	(Lee and Schwartz, 1981)
R17	$CH_3O + NO_2 \rightarrow CH_2O + HONO$	$k_{17} = 0.9 - 2.6 \times 10^{-13}$ cm^3 $molec.^{-1}$ s^{-1}	at 298 K	(McCaulley et al., 1985)
R18	$RH + NO2 \rightarrow R^{\cdot} + HONO$	$k_{18} = 1.4 - 960 \times 10^{-8}$ M^{-1} s^{-1}	at 298 K	(Pryor et al., 1982)
R19	o-nitrophenoles + $h\nu \rightarrow$ R + HONO	$J_{19} = 1.1 - 4.4 \times 10^{-5}$ s^{-1}	photolytic conversion rate at $J_{NO2} = 10^{-2}$ s^{-1}	(Bejan et al., 2006)
R20	$HA + NO_2 + h\nu \rightarrow A + HONO$	$P_{20} = 5 \times 10^{10}$ molec. cm^{-2}	production rate at 20 ppb NO_2 per reactive surface	(Stemmler et al., 2007)
R21	$HNO_3 + h\nu \rightarrow HONO + O(^3P)$	$J_{21} = 0.16 - 1.4 \times 10^{-5}$ s^{-1}	surface activated photolysis; in the range of RH from 0 to 80 %	(Zhou et al., 2003)
R22	$2\ NO_2 + H_2O \rightarrow HONO + HNO_3$	$k_{22} = 4 \times 10^{-2}$ ppb min^{-1} $ppm(NO_2)^{-1}$	HONO formation on surfaces at water vapor concentrations of 3.6×10^{17} cm^{-3}	(Finlayson-Pitts et al., 2003)

(b)	Sinks	Rates	Measurement	Reference
R12_2	HONO + hν → HO + NO	ΔH^0 = 207 kJ mol^{-1}	λ_{thres} = 578 nm	(Atkinson et al., 2004)
R23	HONO + hν → H + NO_2	ΔH^0 = 331 kJ mol^{-1}	λ_{thres} = 361 nm	(Atkinson et al., 2004)
R24	HONO + hν → HNO + $O(^3P)$	ΔH^0 = 442 kJ mol^{-1}	λ_{thres} = 271 nm	(Atkinson et al., 2004)
R25	$HONO_{ads}$ + HNO_3 $_{ads}$ → 2 NO_2 + H_2O	k_{25} = 1.55 x10^{-17} cm^3 $molec.^{-1}$ s^{-1}	at 300 K	(Kaiser and Wu, 1977)
R26	2 HONO → NO + NO_2 + H_2O	k_{26} = 1.5 x10^{-19} cm^3 $molec.^{-1}$ s^{-1}	at 293 K, 80 % and 50 % RH	(Ten Brink and Spoelstra, 1998)
R27	HONO + OH → NO_2 + H_2O	k_{27} = 7.05 x 10^{-12} cm^3 $molec.^{-1}$ s^{-1}	at 298 K	(Burkholder et al., 1992)
R28	4 HONO → N_2O + 2 HNO_3 + H_2O	k_{28} ≈ 0 to 5 ppm min^{-1}	promoted by sulfuric acid (H_2SO_4)	(Wiesen et al., 1995)

The mentioned sources and sinks of HONO all depend on certain parameters like solar irradiation, concentration of reactants, humidity, and so on. Therefore, two studies at different sites may not share the same significance of sources and sinks for HONO.

However, for many atmospheric processes it is important to know the solubility of HONO in water and the vapor pressure of HONO, respectively. The partitioning of HONO between the gas phase and liquid phase (water) is defined by Henry's law. The Henry's constant (K_H) is given by the ratio of concentration of HONO in water (c) and its partial pressure in the gas phase (p_i) (Seinfeld et al., 2006).

$$K_H = \frac{c}{p_i} \tag{5}$$

As mentioned before HONO is ampholytic; being protonated at low pH (R5) and deprotonating at higher pH (R4). These equilibria influence the partitioning of HONO and is taken into account as the effective Henry's constant ($K_{H,eff}$), defined with K_5 and K_a the acidity constants of (R5) and (R4), respectively (Kerbrat et al., 2010).

$$K_{H,eff} = K_H \, x \left(1 + \frac{K_a}{[H_3O^+]} + \frac{[H_3O^+]}{K_5}\right) \quad (6)$$

Acidification of water changes the solubility of HONO as Becker et al. (1996) and Becker et al. (1998) pointed out. The effective Henry coefficient ($K_{H,eff}$) decreases with decreasing pH, while showing the same temperature dependency until a certain level of acidity is achieved (Fig. 7). After that point $K_{H,eff}$ is increasing exponentially.

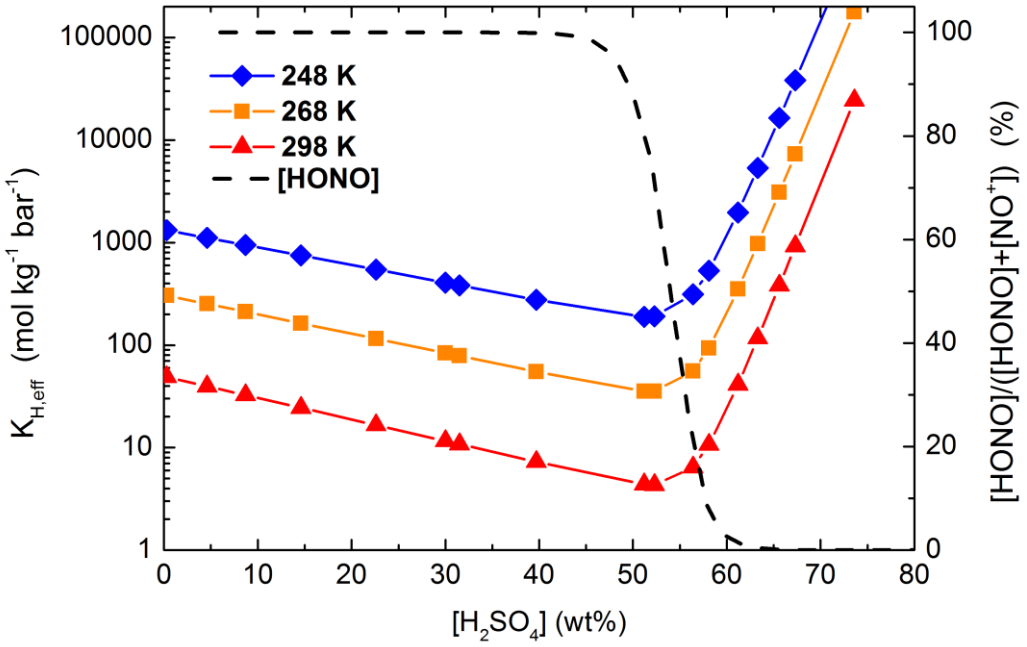

Figure 7. Influence of acidity on the effective Henry ($K_{H,eff}$) coefficient of HONO. The $K_{H,eff}$ (mol kg^{-1} bar^{-1}) depending on the concentration of sulfuric acid is shown for three different temperatures. Additionally the percentage of HONO concentration in liquid phase is given for 298 K (adapted from Becker et al. (1996) with data from Cook et al. (1975) and Park and Lee (1988).

The kink in the linear decrease of $K_{H,eff}$ can be explained by reaction R5. At very low pH HONO is completely transferred to the nitrosyl cation (NO^+) (dashed black line in Fig. 7) and, hence, is removed from the equilibrium of partitioning.

1.1.4 EARTH: Soil chemistry of nitrous acid

The chemistry of nitrous acid in soil reflects the chemistry in air and water, since chemistry in soil mainly processes in the pores of soil, which are occupied by air and water (Hillel et al., 1998). Additionally, the large surface availability within these pores increases the reactivity of HONO. Due to the acid base equilibrium the more stable NO_2^- is always a reservoir for HONO in soil. Beside, HONO and NO_2^- belong to the nutrients in soil solution essentially needed by microbes and plants. The general availability of nitrogen compounds in soil is strongly influenced by the metabolism of microbes (Fig.8) (Paul, 2007).

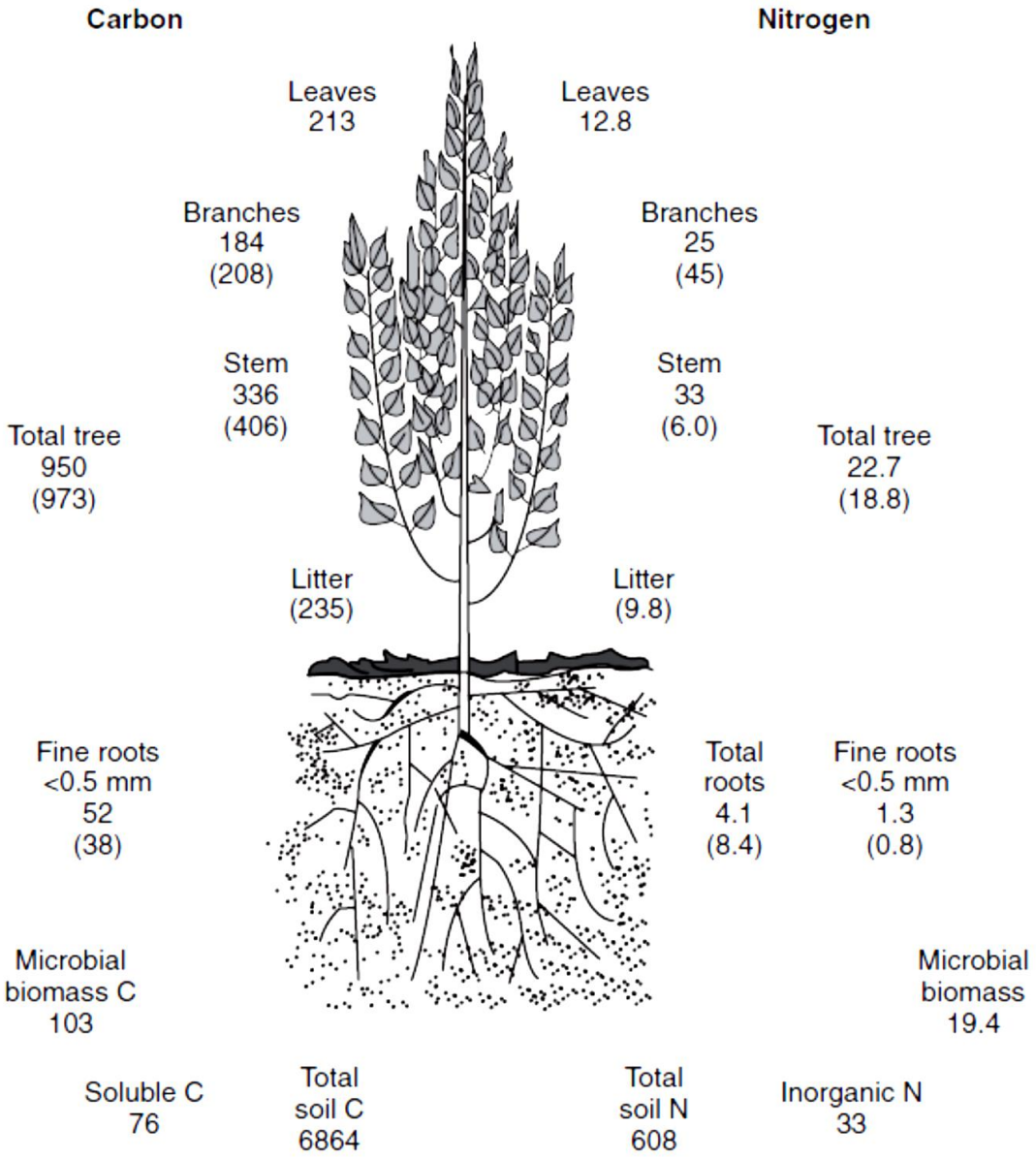

Figure 8. Importance of microbial activity on the availability of nitrogen can be seen from the distribution of C and N for a 2-year old hybrid poplar stand. The N in microbial biomass is nearly equal to N of the total tree. (taken from Paul, 2007)

Nitrogen transformation processes by soil microbes can be separated into two domains, anaerobic and aerobic conditions, i.e. absence and presence of oxygen, respectively.

Anaerobic conditions are preferred by denitrifying microbes, converting NO_3^- and NO_2^- into N_2 and NH_4^+ (Meixner and Yang, 2006), but also by anaerobic ammonium oxidation bacteria (ANAMMOX) (Canfield et al., 2010). Denitrification mainly occurs

in wetted soils, where pores of soil are blocked by water and diffusion into the soil is hindered (Fig.9, aeration limiting).

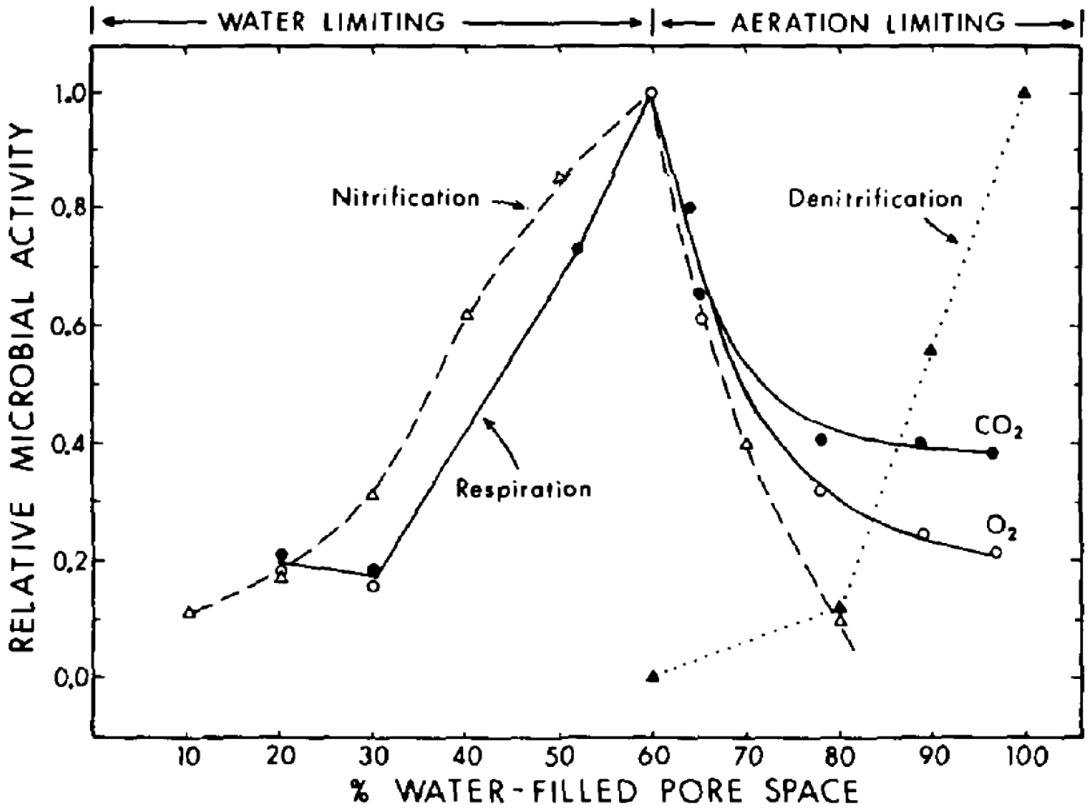

Figure 9. Relative microbial activity depends on the saturation of soil, expressed as % water-filled pore space. The dotted and dashed lines represent the relative activity of denitrifying and nitrifying microbes, respectively. (taken from Linn and Doran, 1984)

In contrast, nitrification takes place when the soil gets aerated, but relative microbial activity decreases with further drying out of soil (Fig. 9, water limiting). During nitrification NH_4^+/NH_3 is enzymatically oxidized to NO_2^- and further to NO_3^-. The first step in autotrophic nitrification needs two electrons.

$$NH_3 + 2H^+ + O_2 + 2\,e^- \xrightarrow{\text{ammonia mono-oxygenase}} NH_2OH + H_2O \qquad \text{(R29)}$$

These two electrons are re-gained by the second step in nitrification, during which HONO or commonly denoted in literature as $H^+ + NO_2^-$ is formed.

$$NH_2OH + H_2O \xrightarrow{NH_2OH\ \text{oxidoreductase}} HONO + 4\,H^+ + 4\,e^- \qquad \text{(R30)}$$

Therefore, reaction (R30) might be of major importance for HONO soil chemistry. The energy for bacterial growth is not gained by these to processes, but by a further reaction using the surplus of two electrons from reaction (R31).

$$2H^+ + \frac{1}{2}\,O_2 + 2\,e^- \xrightarrow{\text{terminal oxydase}} H_2O \qquad \text{(R31)}$$

The further oxidation of $HONO/NO_2^-$ is carried out by other bacteria, which is the reason why $HONO/NO_2^-$ is normally not accumulated in soil and very short-lived.

$$NO_2^- + H_2O \xrightarrow{\text{nitrite oxydoreductase}} NO_3^- + 2\,H^+ + 2\,e^- \qquad \text{(R32)}$$

Even the net reactions (R29 - 32) are well quantified the exact mechanisms are not completely understood. Especially, the intermediates and transition states need to be further analyzed. (Firestone and Davidson, 1989; Paul, 2007)

1.2 Technique used to detect nitrous acid

Several measurement techniques exist to measure HONO in the air phase as mentioned in section 1.1.3. For the work presented in this thesis two long path absorption photometer instruments, LOPAP instruments (Heland et al., 2001), were used. Hence, a short description of the technique is given.

Figure 10. Picture of the LOPAP instrument with external sampling unit (grey box at the right hand side) and a computer for data acquisition is shown. Technical parameters are adjustable at the front panel, like air and liquid flow rate (QUMA, 2006).

The LOPAP consists of two units, the 19" instrument and an external sampling unit, which is connected by a temperature-controlled isolated tubing (Fig. 10). In the external

sampling unit a stripping coil, which is also temperature controlled, is positioned. The sampling air gets pumped through the inlet of the stripping coil and gets in contact with reagent *R1* (Fig. 11), a solution of 0.06 M sulfanilamide in 1 M hydrochloric acid (HCl). HONO is irreversible adsorbed due to the formation of the nitrosyl cation, which reacts with sulfanilamide to form the stable diazonium salt (see Fig. 3). The solution containing the diazonium ion is transferred into the instrument by a liquid pump.

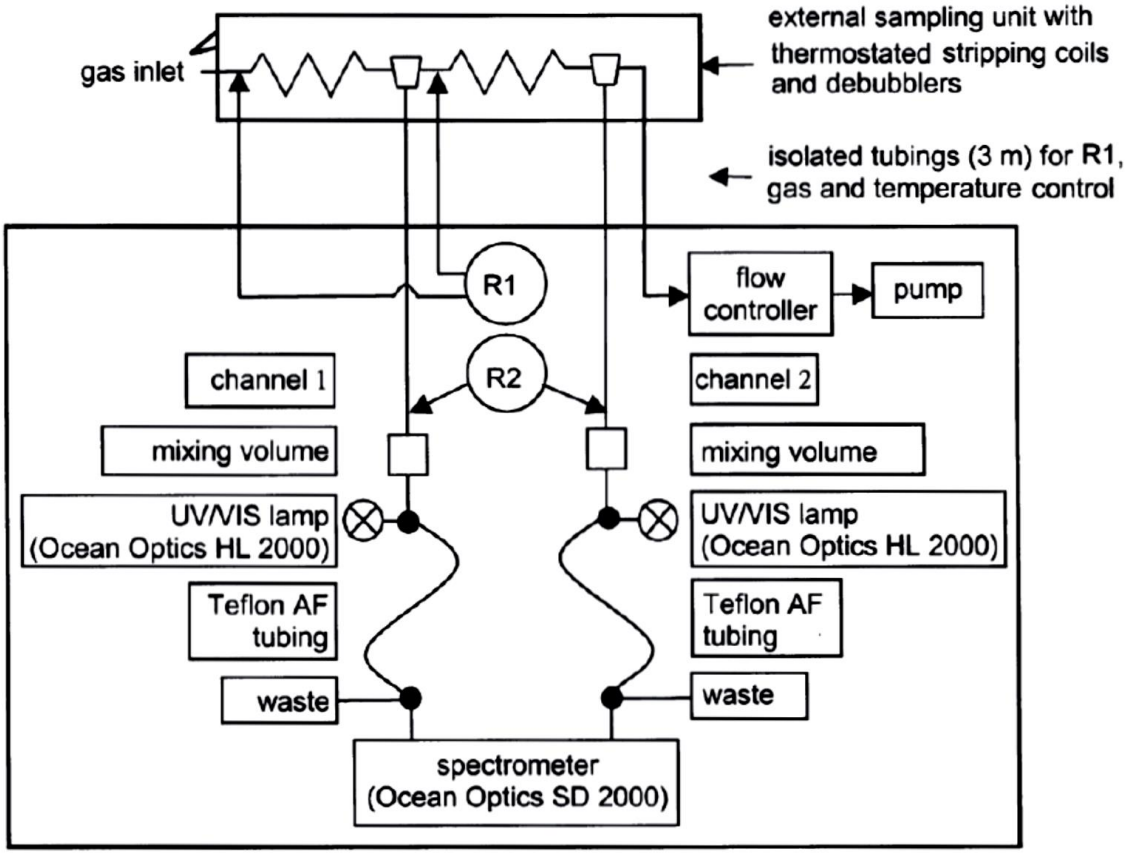

Figure 11. Scheme of the setup of the LOPAP instrument is shown (Kleffmann et al., 2002).

The reaction solution is mixed with reagent *R2*, a 0.8 mM n-(1-naphthyl)-ethylenediamine-dihydrochloride solution. In a small mixing volume the diazonium salt reacts further with *R2* to form an azo dye. The final solution of the azo dye is continuously pumped further through the Teflon AF tubing that acts as an absorption cuvette (absorption tubing). Light from an UV/VIS lamp (Ocean Optics HL 2000) is coupled by glass fibre into the absorption tubing. And at the opposite end of the absorption tubing the residual of light is collected again by a glass fibre. The absorption by the azo dye is quantified by a grating mini-spectrometer using a diode array detector

(OceanOptics, SD 2000). The concentration of the azo dye can be calculated according to Beer-Lambert law (Kleffmann et al., 2002).

$$abs = \log\left(\frac{I_{ref}}{I_{azo}}\right) = \varepsilon_{azo} \text{ x L x } [azo\ dye] + \text{const.} \quad (7)$$

The light intensities I_{azo} and I_{ref} are both measured after passing the same absorption tubing and refer to wavelengths at which the azo dye absorbs light (about 550 nm) and at which the azo dye does not absorb light (700 nm). From the ratio of intensities and the extinction coefficient of the azo dye, ε_{azo}, together with the absorption path length, L, the concentration of azo dye can be calculated. Since one molecule HONO reacts to form one molecule of azo dye, the concentration measured for the azo dye is proportional to the HONO concentration in the sampled gas phase. By considering the flow rates of liquid and air and the sensitivity of the absorption unit it is possible to calculate the concentration of HONO sampled in the gas phase.

A special feature of the LOPAP is the second stripping coil used in one row with the first stripping coil. The reagent solution of the second stripping coil is handled exactly like the reagent solution for the first one and parallel to this (Fig. 11). While about 99.7 % of gaseous HONO is collected by the first stripping coil, other trace gases (e.g. NO_2) leading to possible interferences are collected or react in similar amounts in the first and second stripping coil. Therefore, possible interferences with other molecules than HONO are quantified and get subtracted from the values of the first stripping coil.

The instrument can be adapted to the measurement conditions in several ways, depending on the required time resolution and instrument precision. While increasing the flow rate of liquid leads to a better time resolution, it increases the LOD due to dilution. By increasing the flow rate the LOD can be lowered again. A better time resolution can also be achieved by shortening the absorption tubings, which again leads to a higher LOD. In Table 1.2 two possible measurement conditions with corresponding adjustments of the LOPAP are given.

Table 1.2 Adjustments of the LOPAP instrument are shown for two possible applications. (adapted from Kleffmann et al., 2002)

Measurement condition	Emission (high concentrations)	Ambient (low concentrations)
Air flow rate	1 l min^{-1}	1 - 2 l min^{-1}
Liquid flow rate	1.3 ml min^{-1}	0.4 ml min^{-1}
Absorption tubing length	0.1 m	2.5 m
Range of wavelength used	540 - 600 nm	540 - 590 nm
Measurement range	200 - 2000 ppbv	0.005 - 10 ppbv
Sampling efficiency	99.8 %	99.8 - 98 %
Response time (10 - 90 % of full signal)	≈ 1.5 min	≈ 4 min
LOD	0.5 ppbv	0.001 - 0.002 ppbv

1.3 Motivation to study the formation and surface exchange of nitrous acid

1.3.1 Background

Next to health effects due to its toxicity (Pitts et al., 1978), HONO plays a major role in the formation of the OH radical in the atmosphere (Elshorbany et al., 2012). As mentioned in section 1.1.3 the understanding of HONO formation pathways in the atmosphere is a major challenge in atmospheric sciences. Especially, the mixing ratios of HONO during daytime are not fully explained by known reactions. Even in rural regions, where anthropogenic sources like car exhausts are of minor importance, elevated HONO mixing ratios were observed (Kleffmann, 2007; Su et al., 2008b; Sörgel et al., 2011a; Wong et al., 2012). Recent studies show that there is evidence for a ground based source (Harrison and Kitto, 1994; Sörgel et al., 2011a; VandenBoer et al., 2013).

1.3.2 Aim and progress of the PhD project

The aim of this PhD project was not only to study the formation of HONO, but especially to investigate the surface atmosphere exchange of HONO. While at the beginning it was planned to perform exclusively dynamic chamber experiments under controlled conditions in the laboratory, an opportunity to take part at a comprehensive field campaign was used to compare HONO formation below and above a canopy. Going back into the laboratory and performing measurements on soil samples yielded in a vast of new insights. With this a distinct direction established during the PhD project and led to following data sets:

In chapter 2, dynamic chamber experiments: First evidence for direct release of HONO by soil bacteria

In chapter 3, dynamic chamber experiments: Investigation of HONO formation in soil and the possible bidirectional exchange with the atmosphere

In chapter 4, field measurement: Simultaneously measured HONO mixing ratios at two heights during the field campaign HUMPPA-COPEC 2010

Chapters 2 to 4 are presented as reproductions of the published paper, draft manuscript and submitted paper, respectively.

2. HONO emissions from soil bacteria as a major source of atmospheric reactive nitrogen

This chapter is a reproduction of the article published as a report in Science in September 2013.

Authors: R. Oswald[1,2]†*, T. Behrendt[1,3]†, M. Ermel[1,2]†, D. Wu[1,4], H. Su[5], Y. Cheng[5], C. Breuninger[1], A. Moravek[1,6], E. Mougin[7], C. Delon[8], B. Loubet[9], A. Pommerening-Röser[10], M. Sörgel[1], U. Pöschl[5], T. Hoffmann[2], M.O. Andreae[1], F.X. Meixner[1] and I. Trebs[1*]

Affiliations:

[1] Biogeochemistry Department, Max Planck Institute for Chemistry, P.O. Box 3060, 55020 Mainz, Germany

[2] Institute for Inorganic and Analytical Chemistry, Johannes Gutenberg University Mainz,

55128 Mainz, Germany

[3] Institute for Geography, Johannes Gutenberg University Mainz, 55128 Mainz, Germany

[4] Key Laboratory of Agricultural Water Research, Center for Agricultural Resources Research, Institute of Genetic and Developmental Biology, The Chinese Academy of Sciences, 050021 Shijiazhuang, China

[5] Multiphase Chemistry Department, Max Planck Institute for Chemistry, P. O. Box 3060, 55020 Mainz, Germany

[6] Department of Micrometeorology, University of Bayreuth, 95447 Bayreuth, Germany

[7] Géosciences Environnement Toulouse (GET), Observatoire Midi-Pyrénées, Université de Toulouse, CNRS, IRD, 14 avenue Edouard Belin, 31400, Toulouse, France

[8] Laboratoire d'Aérologie, Université de Toulouse, Toulouse, France

[9] INRA, Unité mixte de Recherche INRA-AgroParistech, Environnement et Grandes Cultures, 78850 Thiverval-Grignon, France

[10] Department of Microbiology and Biotechnology, University of Hamburg, Hamburg, Germany

*Correspondence to: R. Oswald (robert.oswald@mpic.de)

and I. Trebs (i.trebs@mpic.de)

† These authors contributed equally to this work.

Abstract

Abiotic release of nitrous acid (HONO) in equilibrium with soil nitrite (NO_2^-) was suggested as an important contributor to the missing source of atmospheric HONO and hydroxyl radicals (OH). The role of total soil-derived HONO in the biogeochemical and atmospheric nitrogen cycles, however, has remained unknown. In laboratory experiments we found that for non-acidic soils from arid and arable areas, reactive nitrogen emitted as HONO is comparable to emissions of nitric oxide (NO). We show that ammonia-oxidizing bacteria can directly release HONO in quantities larger than expected from the acid-base and Henry's law equilibria of the aqueous phase in soil. This component of the nitrogen cycle constitutes an additional loss term for fixed nitrogen in soils, and a source for reactive nitrogen in the atmosphere.

Main text

Soil biogenic NO emissions account for about 20 % of the total NO sources to the atmosphere (IPCC, 2007) and vary as a function of microbial activity and physicochemical soil properties. NO is produced during nitrification, where soil microbes convert ammonium (NH_4^+) via NO_2^- to nitrate (NO_3^-), which both can accumulate in soil (Quastel, 1965; Jiang and Bakken, 1999). In addition, the reduction of NO_3^-, which is known as denitrification, can cause a release of NO. The two microbial processes are mainly influenced by temperature, soil water content, pH value, and mineral nitrogen availability in the soil (Ludwig et al., 2001; Gödde and Conrad, 1998; Naegele and Conrad, 1990). Previous studies have shown that HONO may also be emitted from soil; this release may originate from the transformation of soil NH_4^+ to NO_2^- (Kubota and Asami, 1985a) or from soil NO_2^- due to a chemical acid-base equilibrium (Su et al., 2011).

To estimate the contribution of soil HONO emissions to the total reactive nitrogen flux (HONO + NO) from the soil to the atmosphere and to elucidate the major processes

influencing HONO release from soil, we studied the relation of soil HONO emissions to biogenic soil NO emissions under controlled laboratory conditions using the dynamic chamber method (van Dijk et al., 2002). Earlier studies have shown that results using this technique are consistent with field measurements (Rummel et al., 2002; van Dijk et al., 2002; Remde et al., 1993). We investigated soils from various ecosystems around the world, covering a wide range of soil pH, organic matter and soil nutrient contents (Table S1). The soil samples were wetted to reach water holding capacity (WHC, see supplementary information) and placed into the chamber, which was then continuously flushed with purified air (free of HONO, NO_x, O_3, hydrocarbons and water vapor) leading to a slow drying of the soil sample during the course of the experiment. The gas phase mixing ratio of HONO released by the soil sample was measured at the chamber exit with a long path absorption photometer (LOPAP) (Kleffmann et al., 2002). Mixing ratios of NO and water vapor were also measured (Breuninger et al., 2012).

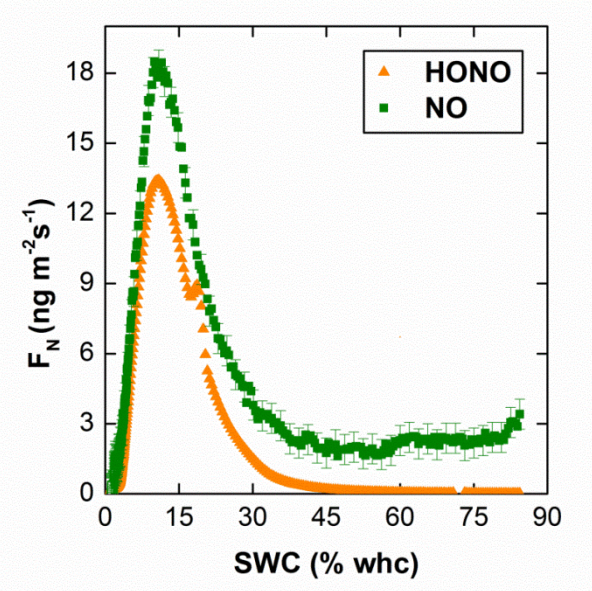

Figure 12. **Soil emissions of HONO and NO feature similar optimum curves.** Characteristic HONO (▲) and NO (■) emission fluxes (F_N, in terms of nitrogen mass) from soil sample S15 (jujube field, semi-arid, fertilized and irrigated, Mingfeng, Xinjiang, PR China) as a function of soil water content (SWC) expressed in % of water holding capacity (WHC). Experimental error bars (see supplementary information) are shown for every fourth data point for NO. Error bars of HONO fluxes have the size of the symbols and were omitted.

Figure 12 shows the characteristic moisture dependency of HONO and NO fluxes that is known from previous studies of soil biogenic NO emissions (Ludwig et al., 2001; van

Dijk et al., 2002; Pilegaard, 2013; Feig et al., 2008). We found that the maximal emission fluxes of HONO and NO (henceforth denoted as optimum fluxes; $F_{N,opt}$(HONO) and $F_{N,opt}$(NO)) are of comparable magnitude and occur at similar optimum soil water content (SWC,), i.e., within 10 % WHC of one another for all investigated samples.

Chemical acid-base equilibrium calculations predict that abiotic HONO emissions from soil nitrite should be largest for soils with low pH and high NO_2^- content (Su et al., 2011). The soil pH reflects a sum parameter, which depends on the amount of acidic and basic species in soil, and regulates the solubility of soil constituents and the protonation equilibria. These variables, however, also influence nitrifier and denitrifier activity in soil. In general, abundance and diversity of bacteria is positively correlated with pH (Rousk et al., 2010) and individuals mostly possess a maximum activity at a certain pH (Park et al., 2007). In contrast to expectations based on the acid-base equilibrium, the results from different soil samples presented in Fig. 13 do not show a decrease of HONO fluxes with increasing pH. In fact, the neutral soil sample S12, taken from a wheat field in Germany, features extremely high values for HONO and NO emissions ($F_{N,opt}$: 257.5 ± 0.1 ng m^{-2} s^{-1} HONO, 134.8 ± 0.6 ng m^{-2} s^{-1} NO). The second highest emission of HONO and NO was found for the alkaline, sodic soil represented by sample S17. Comparison with soil NO_2^- and NH_4^+ concentrations (Fig. 13) clearly demonstrates that high HONO and NO emissions are favored for soils with high nutrient content.

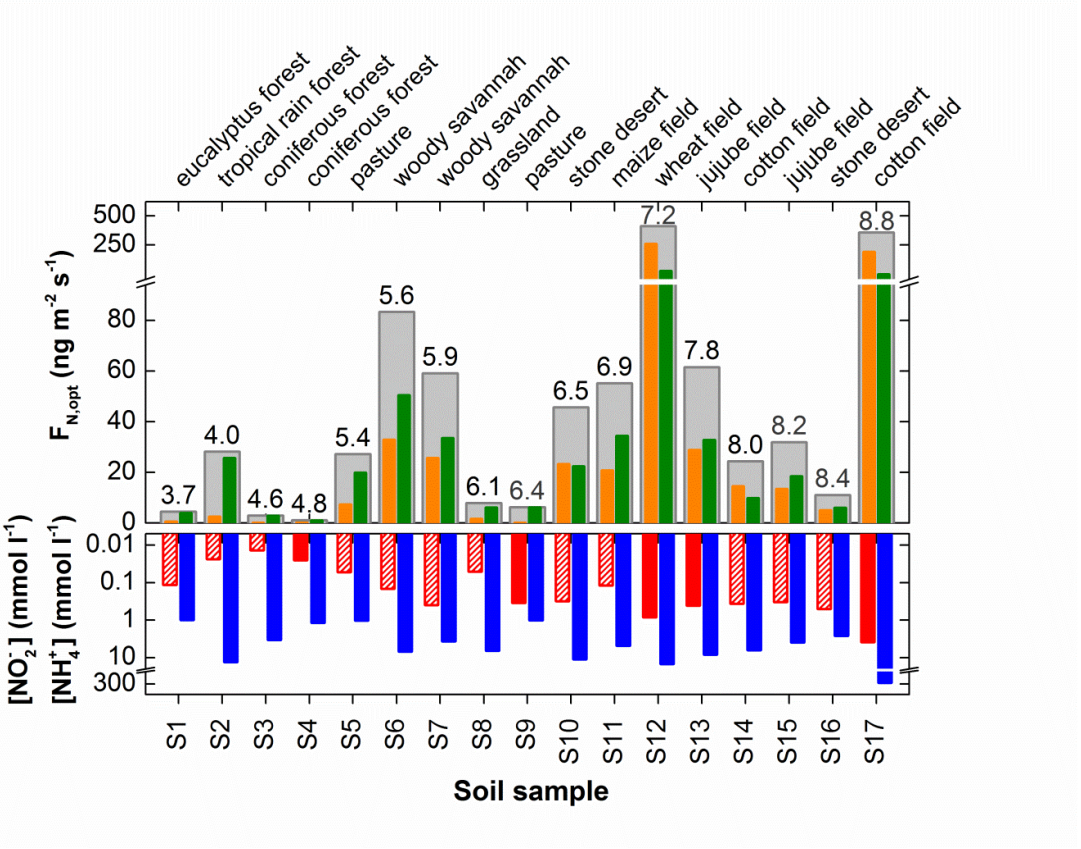

Figure 13. **Optimum emission fluxes of HONO are comparable to those of NO and are largest for NO_2^- rich, neutral to basic soils in arid and arable regions.** Upper panel: optimum emission fluxes of HONO (orange bars), NO (green bars) and their sum (grey bars) in terms of nitrogen for each soil sample (at 25 °C), arranged by increasing pH. Numbers on top of grey bars represent the soil pH. Land use of soil samples is shown on top axis. Lower panel: calculated concentrations of NH_4^+ (blue bars) and NO_2^- (red bars) in the soil solution at $F_{N,opt}$(HONO) ((see supplementary information), striped bars refer to theoretical NO_2^- values at the limit of detection, LOD).

The ratio of $F_{N,opt}$(HONO) to $F_{N,opt}$(NO) was found to be higher for arid and arable soils (on average 1.06 ± 0.44) than for non-arable soils of humid and temperate regions (on average 0.16 ± 0.12) (Fig. 34). For soil pH values higher than 7, the optimum HONO emission fluxes always exceed 5 ng m^{-2} s^{-1} (in terms of N), and even reached ~258 ng m^{-2} s^{-1} (at 25°C). We anticipate that HONO emissions are particularly relevant for arid and arable areas with neutral or alkaline soil pH, where they may significantly influence tropospheric chemistry. Potential HONO soil emission hot spots comprise for instance large areas of northern Africa, central / south-western Asia and North America as well as some regions around the Mediterranean Sea (Fig. 35), covering in total ~20 % of the terrestrial surface (excluding Antarctica). Given the high spatial variability of soil

properties (e.g., pH, nutrients) and our limited amount of soil samples, these hot spot areas may be even larger. This previously neglected ground source of reactive nitrogen may explain the unexpectedly high daytime HONO mixing ratios observed in many studies (Kleffmann, 2007). In addition, NO is produced on a time scale of ~30 minutes from the photolysis of HONO during daytime. Hence, soil HONO emissions in the identified hot spot areas (Fig. 35) may account for the observed discrepancies between soil emissions of reactive nitrogen estimated with global models using the Yienger and Levy algorithm and those derived from "top-down" approaches using nitrogen dioxide (NO_2) columns measured by satellites over arid ecosystems (Yienger and Levy, 1995; Steinkamp and Lawrence, 2011).

Biogenic NO emissions are known to depend strongly on soil temperature (Goedde and Conrad, 1999). We measured the temperature dependency of F_N(HONO) and F_N(NO) from soil sample S8 (an example for HONO is provided in Fig. 36). A temperature increase from 20 to 30°C yielded Q_{10} values (averaged over the whole SWC range) of 3.7 (±1.4) for HONO and 2.1 (±0.2) for NO, typical for soil respiratory systems (Davidson et al., 2006; Breuer et al., 2002; Feig et al., 2008). From an Arrhenius plot (Fig. 14A), we obtained similar activation energies for HONO (80 kJ mol^{-1}) and for NO (75 kJ mol^{-1}). These values are much lower than the activation energies reported for denitrification (202-250 kJ mol^{-1}) (Saad and Conrad, 1993), but are within the range reported for nitrification by ammonia-oxidizing bacteria (AOB) (25-149 kJ mol^{-1}) (Saad and Conrad, 1993; Jiang and Bakken, 1999), suggesting that the latter process governs the observed co-emission of HONO and NO.

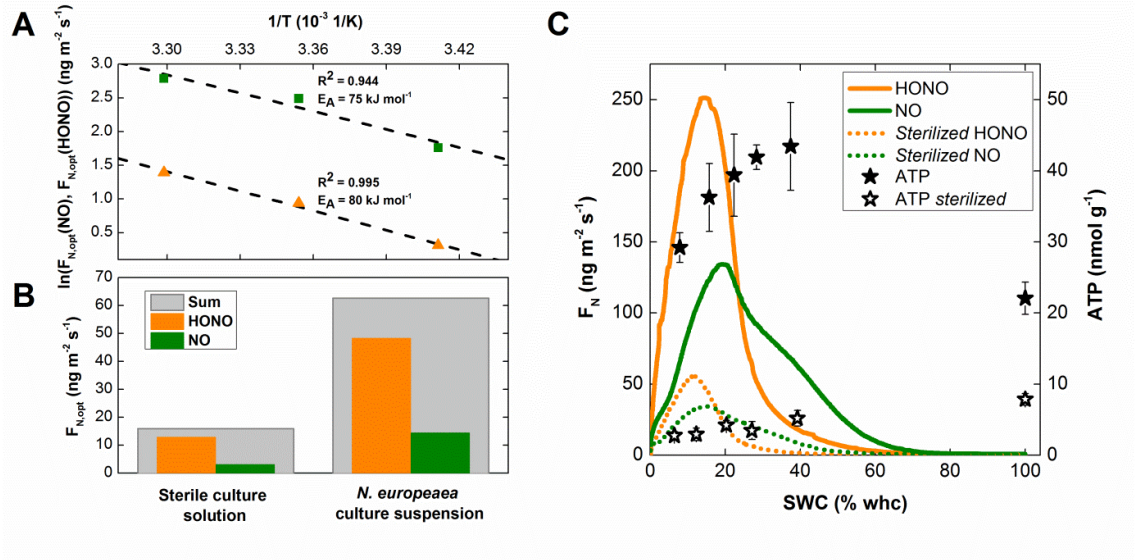

Figure 14. **Ammonia-oxidizing bacteria directly release HONO and cause high emissions from soil. A** Arrhenius plot of the optimum fluxes of HONO (▲) and NO (■) for soil sample S8. **B** Optimum fluxes of HONO, NO and their sum for a sterile AOB nutrient solution and a *Nitrosomonas europaea* culture suspension (activity equivalent to $1.1 \cdot 10^{-3}$ nmol ATP l^{-1}) applied to glass beads as a soil proxy. **C** Influence of bacterial activity on HONO and NO emissions for soil sample S12. Fluxes of HONO and NO for the untreated soil (solid orange and green line, respectively) and for a sterilized subsample (dotted orange and green line, respectively). ATP concentrations serve as indicator for bacterial activity during the dry out of the untreated sample (black filled stars) and the sterilized sample (black open stars). Error bars denote standard deviations of three replicates.

To test this hypothesis, we investigated a pure culture of *Nitrosomonas europaea*, a common and well-studied AOB (Koops and Pommerening-Röser, 2001). A suspension of the pure culture (buffered at pH = 8.2) was applied to glass beads serving as an inert soil-like matrix (Feig et al., 2008), and the model system was treated like a soil sample . Fig. 14B compares $F_{N,opt}$(HONO) and $F_{N,opt}$(NO) of the *N. europaea* culture suspension with the emissions using a sterile AOB nutrient solution additionally containing 0.14 mmol l^{-1} NO_2^-, which equals 0.5 mg kg^{-1} of NO_2^- (in terms of N) in soil. The NO_2^- added to the sterile solution equals the NO_2^- that would have been produced by the bacteria during the experiment and reflects the chemical contribution to the HONO emission from the model system, while the observed difference in $F_{N,opt}$(HONO) between the sterile solution and the culture suspension can be attributed to the direct emissions by the AOB. The *N. europaea* culture emits four times more HONO than the

sterile reference, demonstrating that AOB can indeed act as a strong direct source of HONO.

Measured adenosine triphosphate (ATP) concentrations during the dry out of S12 (Fig. 14C) show that soil microbes are active also under relatively dry conditions (% WHC < 20 %), where $F_{N,opt}$(HONO) is observed. Since ATP is an indicator for microbial activity in general, the maximum activity of AOB might not coincide with the maximal ATP concentration. We applied methyl iodide, a strong sterilization agent for soil (Stromberger et al., 2005) also targeting nitrification (Yan et al., 2013), to a subsample of S12 (Fig. 14C). Both HONO and NO emission fluxes are reduced by about 75 %, revealing a strong microbial source. This demonstrates that the findings from the model system in Fig. 14B are transferable to a real soil sample. The residual emissions can be largely attributed to the chemical source, as the ATP content and, hence, the microbial activity was reduced by about 92 % at the HONO emission optimum. These results explain the high HONO emissions from non-acidic soil samples.

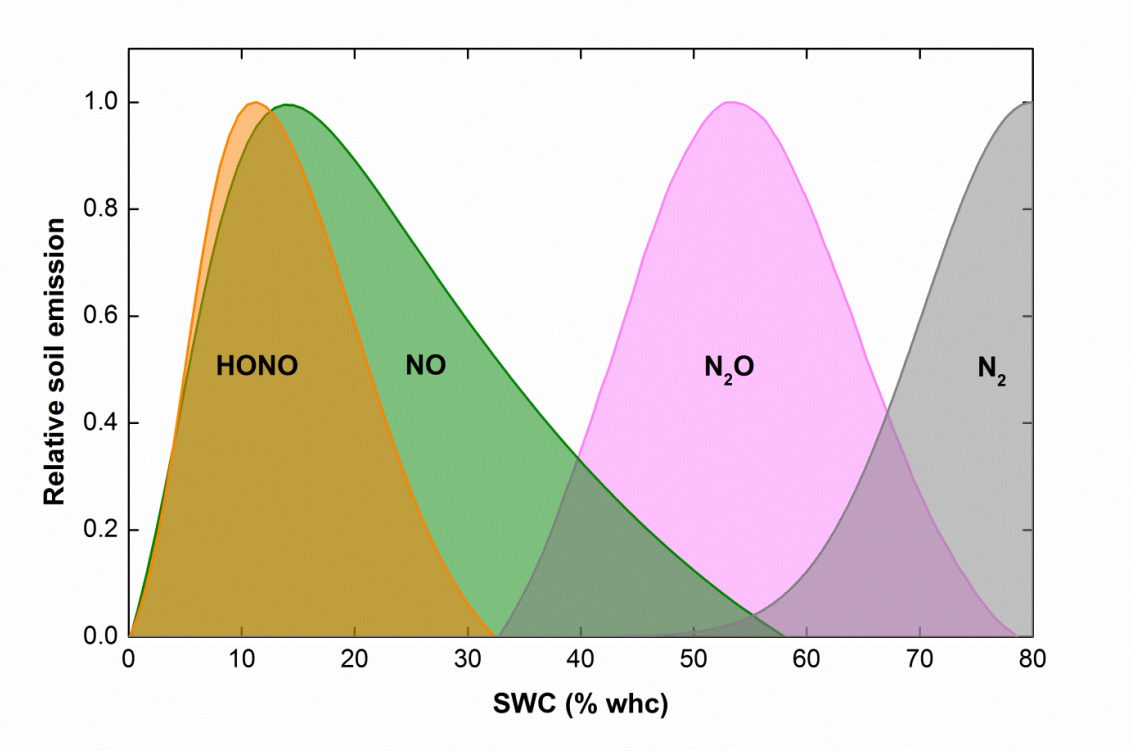

Figure 15. **HONO is a major component of nitrogen emissions from soil.** The conceptual model of soil nitrogen emissions as a function of SWC was adopted from Firestone and Davidson (Firestone and Davidson, 1989). The curves are based on measurements of HONO, NO and N_2O emissions from soil sample S12 (N_2 emissions were fitted from (Firestone and Davidson, 1989)).

The conceptual model in Fig. 15 shows that $F_{N,opt}$(HONO) and $F_{N,opt}$(NO) occur in the lower SWC range (~0-40 % WHC (Feig et al., 2008; Levine et al., 1996)), whereas at high SWC (~40-80 % WHC) nitrogen is released from soil mainly as the greenhouse gas N_2O. In general, substrate diffusion is limited at low SWC and gas diffusion is limited at higher SWC (Skopp et al., 1990). HONO is produced and emitted during nitrification, which predominates at low SWC (Gödde and Conrad, 1998). Samples from different soil and land-use types show their maximal release of the respective nitrogen compound at different optimum SWC (Pilegaard, 2013). The magnitude of the maximal emission of each compound varies depending on e.g., nutrient availability and abundance of soil bacteria.

Conclusions

We conclude that HONO emissions by AOB and possibly other types of bacteria represent an additional component for gaseous losses from the soil nitrogen pool to the atmosphere. Our survey of soils from different ecosystems indicates that HONO emissions may account for up to 50 % of the reactive nitrogen release from soil. This significant contribution of soil HONO emissions is currently not considered in model estimates of global soil reactive nitrogen emissions (IPCC, 2007) and may constitute one of the major uncertainties in this budget. Furthermore, these HONO emissions contribute to atmospheric chemistry by enhancing the oxidation capacity of the lower atmosphere.

Acknowledgments

This project was funded by the Max Planck Society. The work was supported by the Max Planck Graduate Center with the Johannes Gutenberg University Mainz (MPGC). We are grateful to S. Hohlmann, S. Müller, M. Welling, P. Stella, A. Held, B.L. Simmons, N. Mascher, C. Becker, A.C. and F. Hertel, and Z. Wu for supporting the experiments and helping to collect the soil samples, and to S. Böhnke for assistance in creating the global map. We thank K. Emde and team as well as the company Envilytix for analyzing chemical and physical soil properties. Soil sample S7 was collected in Mali at the Agoufou site belonging to the African Multidisciplinary Monsoon Analysis - Couplage de l'Atmosphère Tropicale et du Cycle Hydrologique (AMMA-CATCH) observatory (http://www.amma-catch.org/). The soil sample S11 from Grignon was collected within the framework of the European Commission project NitroEurope-IP (No. 017841). The work of Hang Su was supported by the European Commission within the framework of PEGASOS (No. 265148).

3. Influence of soil properties and ambient mixing ratios on HONO emission

This chapter is a reproduction of a draft manuscript for submission to Biogeochemistry in February/March 2014.

R. Oswald[1,2], T. Behrendt[1,3], M. Ermel[1,2], D. Wu[1,4], H. Su[5], Y. Cheng[5], C. Breuninger[1], A. Moravek[1,6],B. Loubet[7], U. Pöschl[5], T. Hoffmann[2], M.O. Andreae[1], F.X. Meixner[1], M. Sörgel[1], and I. Trebs[1*]

[1] Biogeochemistry Department, Max Planck Institute for Chemistry, P.O. Box 3060, 55020 Mainz, Germany

[2] Institute for Inorganic and Analytical Chemistry, Johannes Gutenberg University Mainz,

55128 Mainz, Germany

[3] Institute for Geography, Johannes Gutenberg University Mainz, 55128 Mainz, Germany

[4] Key Laboratory of Agricultural Water Research, Center for Agricultural Resources Research, Institute of Genetic and Developmental Biology, The Chinese Academy of Sciences, 050021 Shijiazhuang, China

[5] Multiphase Chemistry Department, Max Planck Institute for Chemistry, P. O. Box 3060, 55020 Mainz, Germany

[6] Department of Micrometeorology, University of Bayreuth, 95447 Bayreuth, Germany

[7] INRA, Unité mixte de Recherche INRA-AgroParistech, Environnement et Grandes Cultures, 78850 Thiverval-Grignon, France

[*] *now at: Centre de Recherche Public - Gabriel Lippmann, Department Environment and Agro-biotechnologies, 41 rue du Brill, L-4422 Belvaux, Luxembourg*

Correspondence to: R. Oswald (robert.oswald@mpic.de) and M. Sörgel (m.soergel@mpic.de)

Abstract

Recent studies showed that biogenic nitrous acid (HONO) emissions from soil can be as high as the relatively well known emission fluxes of nitric oxide (NO). The release of HONO into the troposphere potentially alters its chemical reactivity even stronger than biogenic soil NO emissions. This is due to its photolysis and hence production of the hydroxyl radical (OH) and also of NO during daytime. Our laboratory experiments determining HONO emission fluxes with a dynamic chamber system revealed a dependency on soil water content (SWC), pH and microbial activity. Here, we present new insights on the influence of physical and chemical soil properties on the emissions of HONO in comparison to those of NO. Furthermore, we investigated the uptake of HONO by soil, revealing that soil may act as a sink and source for HONO potentially causing bidirectional exchange fluxes. We calculated the compensation point mixing ratio (χ_{comp}) of HONO for a well characterised soil sample, which depends on SWC and showed a maximum value of about 12 ppb. For SWC above 60 % WHC soil acts as large sink for HONO with a chamber specific deposition velocity of 0.9 cm s^{-1}. Calculations of diffusion coefficients in soil reflect the importance of soil aeration on HONO emission fluxes, starting at the intercept of relative ion and gas diffusion coefficients in soil, in average being 4.3 x 10^{-2} at an average SWC of 57 % (~ 61 % WFPS).

3.1 Introduction

Trace gas emissions by soil have a large impact on atmospheric chemistry, especially in remote and rural regions where direct emissions from anthropogenic sources are absent. For example nitric oxide (NO) soil emissions contribute to about 20 % of total NO emission to the atmosphere (IPCC, 2007). Recent investigations show that biogenic nitrous acid (HONO) emissions by soils are comparable to the emission of NO and feature similar dependencies on soil properties (Su et al., 2011; Oswald et al., 2013). Since the photolysis of HONO forms NO and a hydroxyl radical (OH), known as the detergent of the atmosphere, the characterization and quantification of biogenic HONO

soil emission fluxes is highly relevant for understanding processes in atmospheric chemistry and climate change. While the first evidence for HONO emission by soil appeared in 1985 (Kubota and Asami, 1985b) and many studies on the role of nitrite (NO_2^-) in soil solution were made (Anthonisen et al., 1976; Shen et al., 2003; Russow et al., 2009), conclusive experimental results on the soil-atmosphere exchange of HONO are lacking. This paper presents new insights to the exchange of HONO between soil and atmosphere gained from laboratory studies using a dynamic chamber method. The relation of HONO emissions to soil properties (water holding capacity (WHC), loss on ignition (LOI), pH, nutrient concentration and gas and ion diffusion in soil) and ambient HONO mixing ratios is investigated.

3.1.1 Soil moisture and porosity of soil

Soil consists of the three phases; solid particles, water (soil solution) and air. The solid particles form a more or less rigid fabric depending on the type of particles. Within this fabric pores occur, which can be occupied either by water, dissolving soil solutes, or by air, containing reactive trace gases.

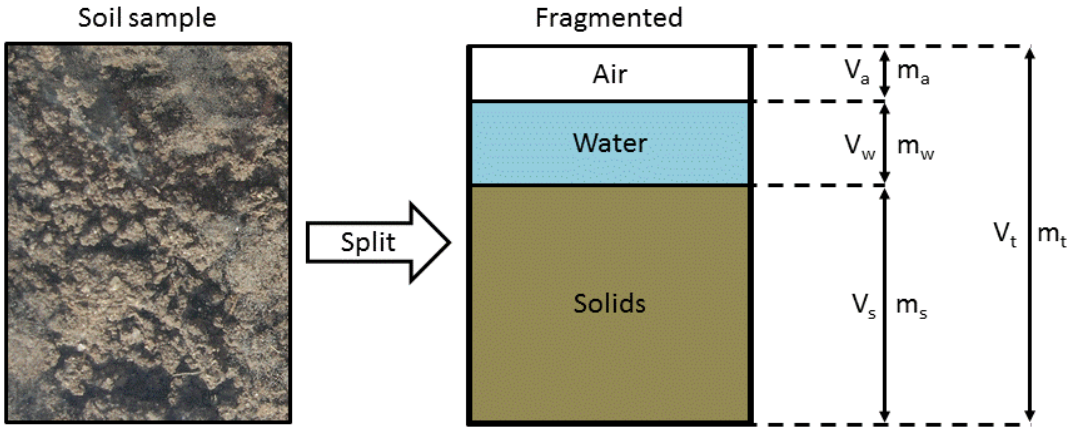

Figure 16. Simplified scheme of soil fractions, with V_a = volume of air, m_a = mass of air, V_w = volume of water, m_w = mass of water, V_s = volume of solids, m_s = mass of solids, V_t = total volume of soil, m_t = total mass of soil (edited from Hillel et al. (1998)).

The total porosity, Φ, describes the available pore volume in soil and, hence, is an important factor for its aeration. It is directly correlated to the bulk and particle density of soil (Hillel et al., 1998).

$$\phi = \frac{V_p\ (=V_a+V_w)}{V_t} = 1 - \frac{\rho_b}{\rho_s} \tag{8}$$

where V_p (m^3) is the volume of pores, which is equal to the sum of the volume of air, V_a (m^3), and the volume of water, V_w (m^3), ρ_s (kg m^{-3}) denotes the particle density and ρ_b the bulk density (kg m^{-3}), defined by the mass of solids, m_s (kg), divided by the volume of solids, V_s (m^3), and total volume, V_t (m^3), respectively. The fraction of pore volume occupied by air, V_a, to V_t is defined as the air-filled porosity, ε, which is a function of soil water content, SWC (%), (Skopp et al., 1990).

$$\varepsilon = \frac{V_a}{V_t} = \phi - \theta_V \tag{9}$$

The volumetric soil water content, θ_v (%), defined V_w, divided by V_t, can be computed from the gravimetric soil water content, θ_g (%), ρ_b and the density of water, ρ_w, (Hillel et al., 1998).

$$\theta_V = \theta_g \text{ x } \frac{\rho_b}{\rho_w} \tag{10}$$

Besides θ_v and θ_g, there are several other possibilities of expressing the soil moisture. To reduce potential measurement errors, the measured entity can be scaled with the maximum water holding capacity, WHC (%), also known as the field capacity of soil, fc, (Gödde and Conrad, 1998).

$$\text{"relative" SWC} = \frac{\theta_V \text{ x } 100}{\theta_V(\text{at WHC})} = \frac{\theta_g \text{ x } 100}{\theta_g(\text{at WHC})} = \text{value \% WHC} \tag{11}$$

The usage of the relative unit % WHC for comparing different soil types has the major advantage that it shows the status of soil moisture regardless of the soil type, e.g. sandy soil or soil with high organic content. Another relation to express the SWC that is more sensitive to effects like swelling of soil organics, is the water filled pore space, *WFPS* (%). It is closely related to θ_v and ε.

$$WFPS = \frac{V_w}{V_p} = \frac{\theta_V}{\Phi} = 1 - \frac{\varepsilon}{\Phi} \quad (12)$$

The *WFPS* is a linear function of θ_v and hence, linearly correlated to % WHC.

3.1.2 Biogenic HONO emission by soil

Soil microbes are able to gain energy by chemical transformation of organic and inorganic compounds in the soil solution. The oxidation of ammonia (NH_3) and its corresponding acid ammonium (NH_4^+) to NO_2^- and further to nitrate (NO_3^-) is known as nitrification (Meixner and Yang, 2006). The reverse process carried out by different soil microbes is called de-nitrification (Meixner and Yang, 2006). It was shown that during nitrification ammonia-oxidizing bacteria (AOB) and by the acid base equilibrium of NO_2^- in the soil solution HONO is produced, which is then released into air (Kubota and Asami, 1985b, a; Su et al., 2011; Oswald et al., 2013). According to the co-emission of HONO with NO from soil, dependencies on soil properties for the emission process might be the same (Naegele and Conrad, 1990; Skopp et al., 1990; Gödde and Conrad, 2000).

3.1.3 Diffusion of gases in air-filled pore space of soil and ions in water-filled pore space

The diffusion of gases and ions in soil depend on the composition of soil phases. The distribution and size of pores determines the free path of gas molecules. The total porosity (Eq. 8) describing the amount of pore volume of dry soil was used for calculating the diffusion of gases in soil (Penman, 1940; Marshall, 1959; Millington and Quirk, 1959). The influence of water on pore shape and pore size was first described by Currie (1961) and empirical models for calculating the diffusion of gases in wet soil

depending on the air-filled porosity (Eq. 9) were further investigated by Moldrup et al. (2000). They found the best correlation by adapting the model of Marshall (1959) for a linear reduction of pore space by water (WLR-Marshall).

$$D_{eff,gas}(T) = \mathrm{D}_{0,\mathrm{gas}}(T) \times \frac{\varepsilon^{5/2}}{\phi} \tag{13}$$

$D_{eff,gas}$ is the effective diffusion coefficient of a gas in soil ($m^2\ s^{-1}$) and $D_{0,gas}$ is the diffusion coefficient of the gas in free air ($m^2\ s^{-1}$). The model is recommended for application with sieved and repacked soils.

The ion diffusion in soil water (e.g., for NH_4^+ and NO_2^-) is depending on similar parameters like the gas diffusion in soil. The effective ion diffusion coefficient, $D_{ion,eff}$ ($m^2\ s^{-1}$), was calculated according to Moldrup et al. (1997) using the approach of Olesen et al. (1996) for predicting the water retention parameter, b:

$$D_{ion,eff}(T) = 0.45 \times \mathrm{D}_{0,\mathrm{ion}}(T) \times \left(\frac{\theta_V}{\phi}\right)^{0.3 \times \mathrm{b}} \tag{14}$$

$$\mathrm{b} = (0.303 - 0.093 \times \ln(\rho_\mathrm{b}) - 0.0565 \times \ln(\mathrm{CL}) + 3 \times 10^{-5} \times \mathrm{FS}^2)^{-1} \tag{15}$$

where $D_{0,ion}$ ($m^2\ s^{-1}$) is the standard ion diffusion coefficient in water, 0.45 is the impedance factor and θ_V is the volumetric soil water content (Eq. 10). The ratio of θ_V to Φ is equal to *WFPS* (Eq. 12). *WFPS* is closely related to ε, used for the effective gas diffusion (Eq. 13). The water retention parameter b can be calculated by Eq. 15 (Campbell, 1974; Olesen et al., 1996), with the gravimetric clay (CL; < 0.002 mm) and fine sand (FS; 0.02 to 0.2 mm) content of soil (in %).

3.2 Material and methods

3.2.1 Measurement setup

The dynamic chamber design was adapted from laboratory measurements of trace gas exchange fluxes between plants and the atmosphere (for more details see Breuninger et al., 2012). The chamber walls consist of Teflon foil (PFE). In contrast to the plant measurements, the bottom of the chamber was a hard disc with the same diameter as the chamber. A glass bowl (boro silicate) containing the soil sample was placed into the chamber for the measurement (Su et al., 2011; Oswald et al., 2013).

HONO concentrations were measured using a long path absorption photometer (Model LOPAP-03, QUMA, Germany; Kleffmann et al., 2002). To avoid artifacts by reactions on tubing walls the sampling unit of the LOPAP was mounted directly at the chamber and the inlet of the stripping coil penetrated the Teflon foil. NO and NO_x (sum of NO and nitrogen dioxide, NO_2) were measured at the chamber outlet with a chemiluminescence detector (Model 42C, Thermo Electron Cooperation, USA), that was equipped with a Blue Light converter (BLC, Droplet Measurement Technologies Inc.) to photolytically convert NO_2 to NO. Ozone, O_3, was monitored at the chamber outlet using a UV-absorption photometer (Model 49i, Thermo Electron Cooperation, USA). The temperature and humidity of the sampling air was measured online with a humidity probe (MP 103 A, Rotronic AG, Switzerland). The purging air flow rate was controlled by mass a flow controller (Model 1259CC, MKS instruments GmbH, Germany). Dry and clean air (T_{dew} ~ -15 °C, free of NO, NO_2, HONO, O_3) was produced by a pure air generator (PAG 003, ECOPHYSICS, Switzerland). A homebuilt control unit, V25, was used for data acquisition. Data of HONO mixing ratios were recorded separately by a computer connected to the LOPAP.

Calibrations of the MFC were conducted with a primary flow calibrator (Gilibrator 2, Sensidyne Inc., Deha GmbH, Germany). The humidity probe was calibrated with a portable dew point generator (Li-610, LI-COR, USA). The LOPAP calibration was

performed using a sodium nitrite standard solution (CertiPUR, ß(NO_2^- = 999 ± 5 mg/l), Merck KGaA, Germany). The NO/NO_x and O_3 analyzers were calibrated with a gas phase titration system (Sycos K-GPT, Ansyco GmbH, Germany) using a NO-standard gas (Crystal-mixture: 15 ppm NO in N_2, AIR-LIQUIDE GmbH, Germany).

For the experiment determining the HONO compensation point, a defined HONO mixing ratio has to be present in the purging air flow. Hence, a HONO source similar to Schimang et al. (2006) was used. A sodium nitrite solution was continuously mixed with a sulfuric acid solution in a temperature-controlled stripping coil, which was flushed by pure air. Dilution of this air stream yielded the desired HONO mixing ratio in the chamber headspace.

3.2.2 Soil samples

The investigated soil samples were previously described by Oswald et al. (2013) and were taken from the uppermost layer of the soil (5 cm).

Samples S1 (eucalyptus forest, Grose Valley, Australia, 33.61°S, 150.63°E), S5 (pasture, Hawkesbury River flood plain, Australia, 33.57°S, 150.77°E), S8 (grassland, Mainz-Finthen, Germany, 49.97°N, 8.16°E; (Plake and Trebs, 2013)), S11 (maize field, Grignon, France, 48.85°N, 1.97°E; (Stella et al., 2012)) and S12 (wheat field, Mainz-Finthen, Germany, 49.97°N, 8.16°E; (Su et al., 2011)) were dried at 40 °C for 24 h, sieved to 2 mm and stored at 4 °C in open plastic bags before measurement.

Soil samples S2 (tropical rain forest, Suriname, 05.08°N, 55.00°W), S3 (coniferous forest, Hohenpeißenberg, Germany, 47.80°N, 11.01°E), S4 (coniferous forest, Fichtelgebirge, Germany, 50.09°N, 11.52°E; (Sörgel et al., 2011b)) and S9 (pasture, Hohenpeißenberg, Germany, 47.79°N, 11.00°E; (Acker et al., 2006)) are characterized by high organic contents. These soils were sieved to 2 mm (S2) or 16 mm (S3, S4 and S9) (Bargsten et al., 2010) and measured directly after sampling.

All other soil samples, S6 (open woody savannah, Dahra, Senegal, 15.40°N, 15.43°W), S7 (open woody savannah, Agoufou, Mali, 15.34°N, 1.48°W; (Mougin et al., 2009)), S10 (stone desert, Ruta B 376, Chile, 23.48°S, 68.03°W), S13 (jujube field, Qiemo, China, 38.09°N, 85.55°E; (Mamtimin et al., 2011)), S14 (cotton field, Qiemo, China, 38.10°N, 85.55°E; (Mamtimin et al., 2011)), S15 (jujube field, Mingfeng, China, 37.05°N, 82.71°E; (Mamtimin et al., 2011)), S16 (stone desert, Sache, China, 37.69°N, 77.89°E; (Mamtimin et al., 2011)) and S17 (cotton field, Milan, China, 39.27°N, 88.91°E; (Mamtimin et al., 2011)) were already dry when sampled. They were sieved to 2 mm mesh size and stored at 4 °C in open plastic bags prior to measurement.

Physical and chemical properties of each soil sample were analyzed according to ISO or DIN standard procedures: bulk pH of soil according to ISO 10390, nitrite, nitrate and ammonium according to ISO/TS 14256-1, particle distribution according to ISO 11277, total C and N according to ISO 10649 and ISO 13878, loss on ignition according to DIN 19684-3 (Blume et al., 2000).

3.2.3 Measurement procedure

Standard procedure

Before each measurement, the soil sample was homogeneously spread into the glass bowl and wetted to reach WHC, which was gravimetrically determined before the experiment. The glass bowl was placed into the temperature-controlled chamber. The chamber was then closed, purged with purified air and was well mixed by a large fan (Breuninger et al., 2012). Since the chamber is set up in a climate cabinet the temperature can be adjusted and kept constant (± 0.5 °C). The soil sample dries out during the measurement. At the end of a measurement cycle the soil sample is weighed and its residual water content is determined (drying at 105°C/60°C to constant weight).

HONO compensation point mixing ratio

As previously suggested (Harrison and Kitto, 1994; Twigg et al., 2011; VandenBoer et al., 2013), the surface-atmosphere exchange of HONO might be bi-directional, which means that besides HONO production (emission) by the soil, HONO may simultaneously be deposited and consumed at the soil surface (Wong et al., 2012). In order to investigate that, we measured soil sample S11 in the same way as described in the sections above, but adjusted the inlet mixing ratio of HONO to 0 ppb (1) and to 10.3 ppb (2) in two different experiments. Accordingly, the HONO compensation point mixing ratio below the soil surface, at which production equals uptake (i.e. net flux equals zero), can be determined (Conrad, 1994).

3.2.4 Calculations

Soil water content

Since online measurements of the soil water content in the described chamber system is not possible, the gravimetric soil moisture content was determined by measuring the loss of water vapor during the measurement period and relating this temporal integral to the gravimetric soil moisture content observed at the start and end of the measurement (Bargsten et al., 2010).

$$\theta_g(t) = \theta_g(\mathrm{WHC}) - \theta_g(t_{max}) \times \frac{\int RH \times \mathrm{d}t}{\int_0^{t_{max}} RH \times \mathrm{d}t} \tag{16}$$

where θ_g is the gravimetric soil water content (%) at time t (s), θ_g(WHC) is the gravimetric soil water content at WHC, t_{max} is the total measurement time and RH is the relative humidity in the sampling air (%).

While the gravimetric soil water content is a useful quantity, e.g., to calculate concentrations of solutes, as mentioned in section 3.1.1, it is sometimes more appropriate to describe the spatial distribution of air and water in the soil by using Eqs. (9), (11) and (12). Therefore, we use SWC in % WHC in the following.

Net fluxes

Net fluxes of HONO and NO in terms of mass of nitrogen, F_N (ng m^{-2} s^{-1}), were calculated from the flat surface of the soil sample, i.e. the bottom area of the bowl, A (m^2), the purging flow rate, Q (m^3 s^{-1}), the inlet and outlet mixing ratios of the chamber, χ_{out} and χ_{in} (ppb), the molar mass of nitrogen (M_N = 14.01 g mol^{-1}) and the molar volume of air, V_m (m^3 mol^{-1}) (Pape et al., 2009),

$$F_N = \frac{Q}{A} \text{ x } \frac{M_N}{V_m} \text{ x } (\chi_{out} - \chi_{in}) \quad (17)$$

All values were calculated for the same temperature, T (K) and pressure, p (Pa). Uncertainties of F_N were calculated using Gaussian error propagation according to Oswald et al. (2013). The random error of χ_{out} (HONO) was calculated from the sum of the instrument noise at 0 ppb (3σ) and the accuracy of measurement (10 % of the measured value).

Compensation point mixing ratio

To calculate the compensation point mixing ratio for the performed chamber experiments, the linear regression of the outlet concentrations of HONO at different inlet concentrations of HONO is used (Breuninger et al., 2012).

$$y = m \text{ x } x + b \quad (18)$$

$$m = \frac{\chi_{out(2)} - \chi_{out(1)}}{\chi_{in(2)} - \chi_{in(1)}} \quad (19)$$

$$b = \chi_{out(1)} \quad (20)$$

$$\chi_{comp} = \frac{b}{1-m} = \frac{\chi_{out(1)}}{1 - \frac{\chi_{out(2)} - \chi_{out(1)}}{\chi_{in(2)} - \chi_{in(1)}}} \quad (21)$$

The indices $_{(1)}$ and $_{(2)}$ refer to the two experiments conducted with soil sample S11 as described above. Since $\chi_{in(1)}$ was set to 0 ppb (HONO), b equals $\chi_{out(1)}$.

Effective diffusion coefficient of HONO in soil

Since there is no study on the diffusion of HONO in soil, we used the relation of effective diffusion coefficient for NO and other trace gases described by Moldrup et al. (2000) (see Eq. 13).

$$D_{eff,HONO} = \mathrm{D}_{0,\mathrm{HONO}} \times \frac{\varepsilon^{5/2}}{\Phi} \quad (22)$$

The diffusion coefficient of HONO in air (1.54 10^{-5} m^2 s^{-1}) was taken from Ferm and Sjödin (1985). The effective diffusion coefficients of oxygen (O_2) and NO were calculated in the same way by using the diffusion coefficients of O_2 and NO in air (1.820 10^{-5} m^2 s^{-1} and 1.802 10^{-5} m^2 s^{-1}, respectively) from Massman (1998).

3.3 Results and discussion

The investigated soil samples cover a wide range of chemical properties like pH and nutrients as well as physical properties like texture (table 3.3).

Table 3.3 The chemical and physical properties of soil samples S1 - S17

Sample	pH	$N\text{-}NO_2^-$	$N\text{-}NO_3^-$	$N\text{-}NH_4^+$	C/N	ρ_b	WHC	Sand	Clay	LOI[I]
#		mg kg^{-1}	mg kg^{-1}	mg kg^{-1}	%	kg m^{-3}	%	%	%	%
S1	3.7	nd[II]	12.26	1.30	39.2	na[III]	40.7	77.4	8.7	4.4
S2	4.0	nd	4.88	83.40	13.8	na	58.9	na	na	18.2
S3	4.6	nd	3.48	36.64	18.9	305	65.4	na	na	37.1
S4	4.8	1.04	5.72	48.38	20.1	na	85.2	na	na	85.3
S5	5.4	nd	17.45	2.93	12.8	na	38.5	79.2	8.3	3.5
S6	5.6	nd	6.40	7.10	5.4	na	26.5	89.7	7.2	0.8
S7	5.9	nd	7.90	1.40	0.4	na	27.1	90.3	8.7	0.7
S8	6.1	nd	0.66	19.43	14.6	880	42.8	38.4	25.6	10.0
S9	6.4	1.56	14.60	4.60	10.6	778	53.7	17.2	32.9	18.3
S10	6.5	0.15	0.14	5.32	na	na	25.9	na	na	na
S11	6.9	0.15	25.26	6.04	11.7	1245	35.4	5.0	25.3	5.3
S12	7.2	1.03	77.71	18.06	10.5	1080	38.8	21.7	27.8	5.2
S13	7.8	0.21	37.78	4.20	42.2	1430	22.4	29.9	11.7	2.7
S14	8.0	0.15	41.50	2.60	41.5	1240	24.9	21.0	17.0	4.0
S15	8.2	0.15	14.19	1.78	98	1480	22.9	29.9	5.2	1.9
S16	8.4	0.15	4.18	0.78	82	1640	19.4	55.3	3.4	2.1
S17	8.8	1.09	691.67	82.98	40.6	1340	23.4	21.4	11.2	7.4

[I] LOI: loss on ignition; [II] nd: not detectable (< LOD); [III] na: not analyzed

3.3.1 Net HONO and NO flux under clean air conditions

Some of the measured soil properties change during a standard experiment. These changes are dominated by the dry out of the soil sample, i.e. the change in SWC. This leads to increasing aeration (Moldrup et al., 2000; Linn and Doran, 1984) and increasing concentration of solutes, while ion diffusion decreases (Olesen et al., 1996). This alters the microbial activity (Skopp et al., 1990) in the soil.

The standard measurement of soil sample S11 in Fig. 17 demonstrates that the emission fluxes of HONO and NO increase with decreasing SWC to reach a maximum. A further decrease in SWC leads to a more rapid decline of the emission fluxes (leading). The curves of HONO and NO emissions can be described by an optimum function, such as for instance a double sigmoidal function. Consequently, the maximum emission fluxes are denoted as optimum fluxes ($F_{N,opt}$) and the corresponding SWC as optimum soil water content, SWC_{opt} (%). For soils featuring higher SWC_{opt} the shape of the curve is vertically mirrored, meaning a stronger increase of emission fluxes with decreasing SWC, followed by a softer decrease of emission during dry out (tailing).

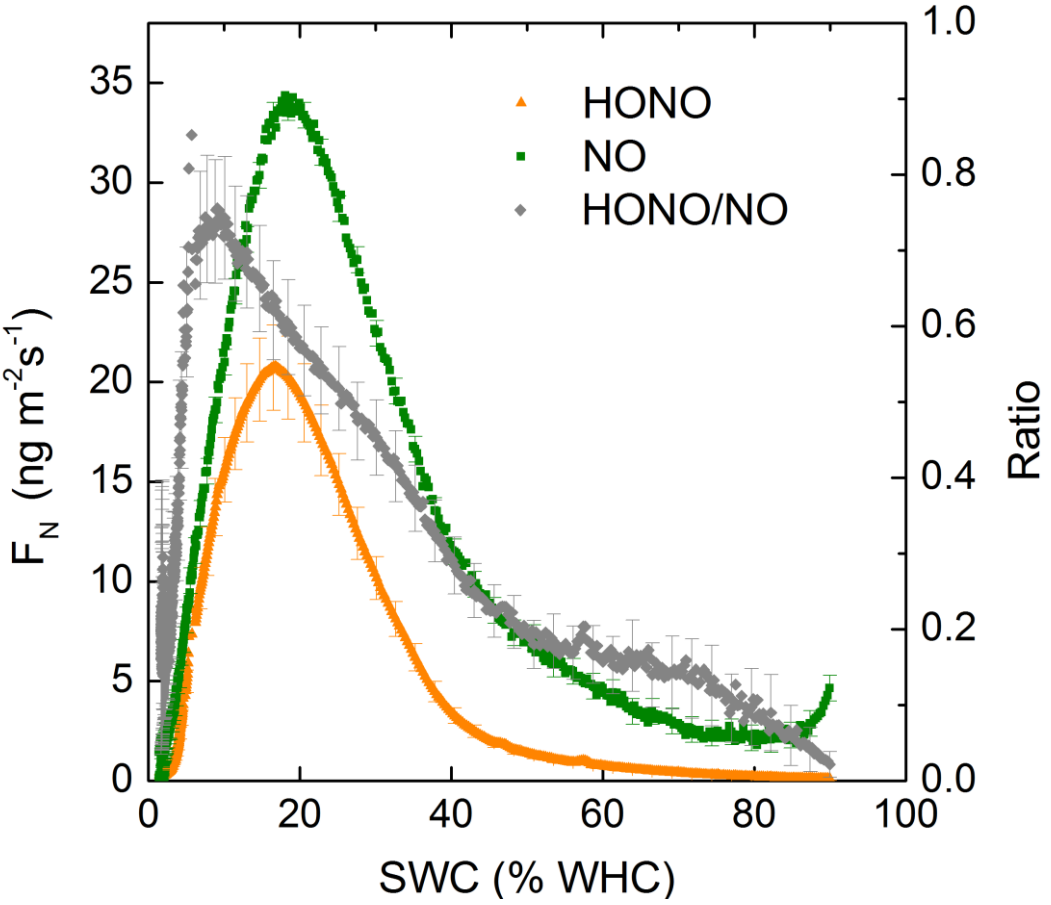

Figure 17. A standard measurement of soil sample S11; the chamber was flushed with clean air. On the left hand axis the calculated net fluxes (Eq. 17) for HONO (orange triangles) and NO (green squares) are shown in terms of N. The ordinate on the right hand side reflects the ratio of HONO to NO flux (grey diamonds). Every tenth error bar is presented.

The ratio of HONO to NO emission is not constant during the experiment. The NO emission increases already at higher SWC, while the HONO emission flux shows a narrower peak than the NO emission flux. This leads to low ratios at the beginning of the experiment that increase mainly due to the increase of HONO emission fluxes. The value of SWC_{opt}(HONO) with 16 % WHC is slightly lower than SWC_{opt}(NO) with 18 % WHC. Consequently, the ratio increases further after reaching the optima, $F_{N,opt}$(HONO) and $F_{N,opt}$(NO), until they approach each other and emission fluxes of HONO and NO decline towards zero. For each measured soil sample $F_{N,opt}$(HONO) and $F_{N,opt}$(NO) both occur within a range of 10 % WHC of one another (cf. Table 3.3.1).

Table 3.3.1 SWC at $F_{N,opt}$(HONO) for soil samples S1 - S17

sample	#	S1	S2	S3	S4	S5	S6	S7	S8	S9	S10	S11	S12	S13	S14	S15	S16	S17
SWC_{opt}(HONO)	% WHC	56.0	31.4	40.9	21.8	32.4	20.2	7.3	27.9	27.7	9.7	16.2	13.7	12.4	8.8	10.8	8.7	13.5
SWC_{opt}(NO)	% WHC	48.3	27.7	36.7	19.2	30.1	28.9	8.6	30.0	26.6	9.1	18.0	19.8	14.2	10.6	10.1	8.3	3.6

Repetition of experiments using two different subsamples of S8, S11, S12 showed good reproducibility for both SWC_{opt} and $F_{N,opt}$ with ΔSWC_{opt} of 0 to 3 % WHC and $\Delta F_{N,opt}$ of about 0.2 ng m^{-2} s^{-1}. While the difference of $F_{N,opt}$ is very small compared to the error of each measurement, $\Delta F_{N,opt}$ can be neglected, the difference of SWC_{opt} is larger compared to the error found by measurement procedure, e.g. precision of used balance. Therefore, we take 3 % WHC as the constant error of SWC in the following.

Influence of soil water content (SWC) and soil pH on the ratio of optimum emission fluxes of HONO to NO

We measured soils with a variety of WHCs. The capability of a soil to hold water depends on several factors, which influence the total porosity, the pore size distribution, the possibility of swelling and shrinking of soil. The amount of soil organic matter, SOM, has a positive effect on WHC. Fig. 18 (a) shows the dependency of WHC on the loss of ignition, LOI. We find an exponential increase of WHC with increasing LOI. During a standard experiment, the soil moisture is continuously decreasing and most soils show a typical double sigmoidal optimum function for HONO and for NO

emission fluxes (Fig. 17). SWC_{opt}(HONO) (Fig. 18 b) and SWC_{opt}(NO) (not shown) correlate linear with WHC.

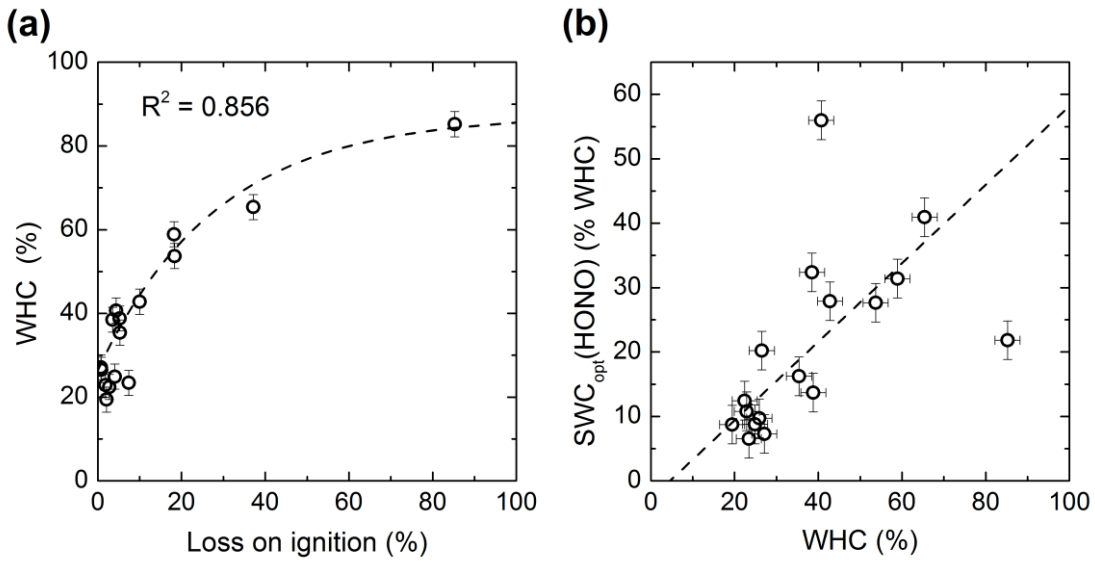

Figure 18. (a) WHCs of measured soil samples show an exponential increase with LOI $WHC = 87.4 - 61.0 \text{ x } \exp\left(-\frac{(LOI-1.9)}{28.4}\right)$. (b) The SWC at the optimum flux of HONO, SWCopt(HONO), depends linearly on the WHC of the soil. The used York linear fit yields in SWCopt(HONO) = (0.61 ± 0.05) x WHC – (2.8 ± 2.1).

With the correlations of Fig. 18 it is possible to estimate SWC_{opt}(HONO) from LOI via WHC or straight from WHC, which both can easily be determined. SWC_{opt}(HONO) itself influences the ratio of $F_{N,opt}$(HONO) to $F_{N,opt}$(NO) (Fig. 19 a), and, using the relationships from Fig. 18, it can thus be a first proxy for the strength of the HONO source when measurements of NO emission fluxes are available. The ratio of $F_{N,opt}$(HONO) to $F_{N,opt}$(NO) shows a negative correlation with increasing SWC_{opt}(HONO) (Pearson corr. -0.716).

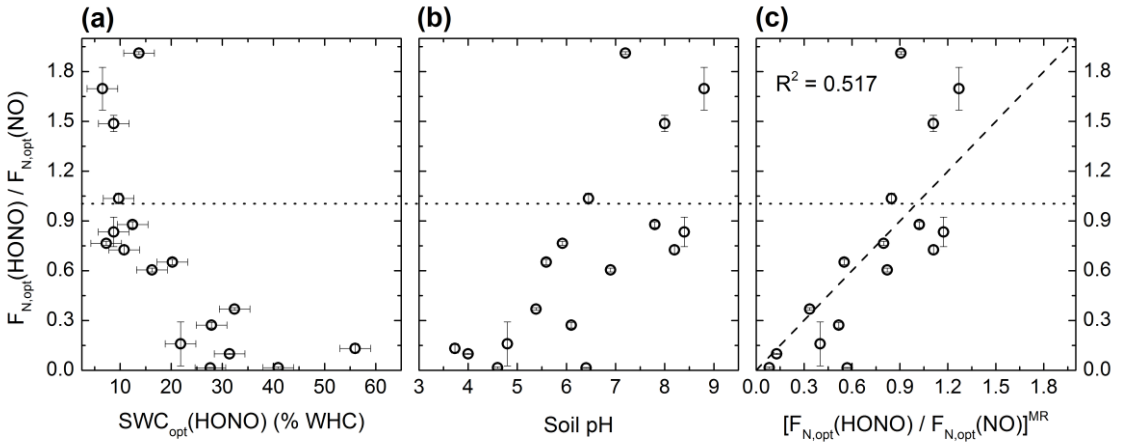

Figure 19. The ratio of $F_{N,opt}$(HONO) to $F_{N,opt}$(NO) is plotted versus, (a) SWC_{opt}(HONO), (b) the soil pH and (c) the multiple linear regression of (a) and (b).

Besides, the soil pH appears to correlate in addition to SWC_{opt}(HONO) with the ratio of the optimum fluxes (Pearson corr. 0.730) (Fig. 19 b). A multiple regression of both parameters, SWC_{opt}(HONO) and soil pH, results in a reasonable correlation (Fig. 19 c).

$$\left[\frac{F_{N,opt}(HONO)}{F_{N,opt}(NO)}\right]^{MR} = \text{-1.5 x } \frac{SWC_{opt}(HONO)}{100} + 0.16 \text{ x soil pH} - 0.04 \quad (23)$$

It is evident that the emission of HONO and NO by soil depends on more soil properties than just these two, but since those might influence emission fluxes of both trace gases in the same direction, the ratio is less affected. The pH might have a significant impact on the ratio due to the changing reactivity of HONO at different soil pH (protonation, deprotonation, disproportion, etc.) (Vancleemput and Baert, 1984; Van Cleemput and Samater, 1995). This could be additionally enhanced by the slower diffusion of HONO at higher SWC leading to lowest $F_{N,opt}$(HONO) to $F_{N,opt}$(NO) ratios at low soil pH with high SWC_{opt}(HONO) (Fig. 19 (a+b), Eq. 22). As mentioned above, the LOI is correlated with SWC_{opt}(HONO). Additionally, SOM might react with HONO, and, furthermore, decrease the ratio of the fluxes (Allison, 1963).

Comparison of optimum HONO emission flux to optimum NO emission flux

The emission of HONO and NO is related to chemical and microbial transformation of nitrogen compounds in soil. There is evidence that HONO is emitted from soil nitrite by

a reversible acid-base reaction and partitioning between air and the aqueous phase of humid soil (Su et al., 2011), while chemodenitrification of HONO or NO_2^- is said to produce NO (Islam et al., 2008). On the other hand, HONO emission mainly occur during nitrification (Oswald et al., 2013), which also produces NO (Ludwig et al., 2001). Our results underline the correlation of the emission fluxes of these two reactive nitrogen species.

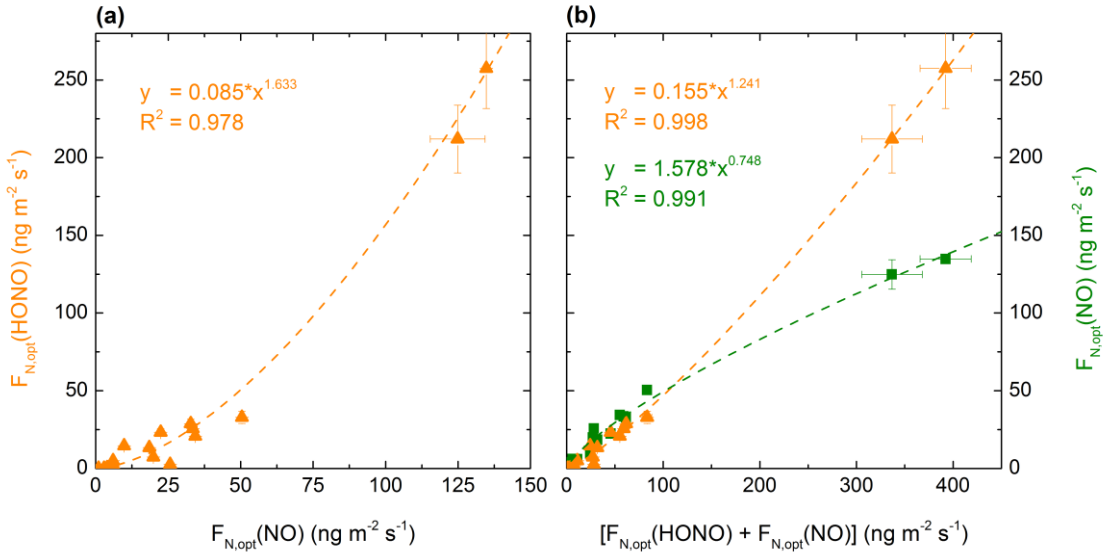

Figure 20. (a) $F_{N,opt}$(HONO) (orange triangles) is positively correlated to $F_{N,opt}$(NO) (allometric fit function) and (b) hence, also positively correlated to their sum, $F_{N,opt}$(HONO) + $F_{N,opt}$(NO), while $F_{N,opt}$(NO) (green squares) shows negative allometry when correlated with $F_{N,opt}$(HONO) + $F_{N,opt}$(NO).

The allometric fit function seems to be more appropriate for the correlations with the sum of $F_{N,opt}$(HONO) and $F_{N,opt}$(NO) (Fig. 20). This is reasonable in case the two emission fluxes are competing and depend on the same precursor. Oswald et al. (2013) proposed that nitrification, during which NH_3 is oxidized to NO_2^- by AOB, is responsible for the emission of HONO. The produced NO_2^- is further oxidized to NO_3^- by nitrite-oxidizing bacteria (NOB). Hence, NH_3 is the main precursor and its availability is expected have an influence on the emission fluxes. Fig. 21 shows the ratio of $F_{N,opt}$(HONO) to $F_{N,opt}$(NO) plotted versus the soil pH as in Fig. 19 (b), but with the relative activity of AOB and NOB using the correlation with pH derived by Park et al. (2007).

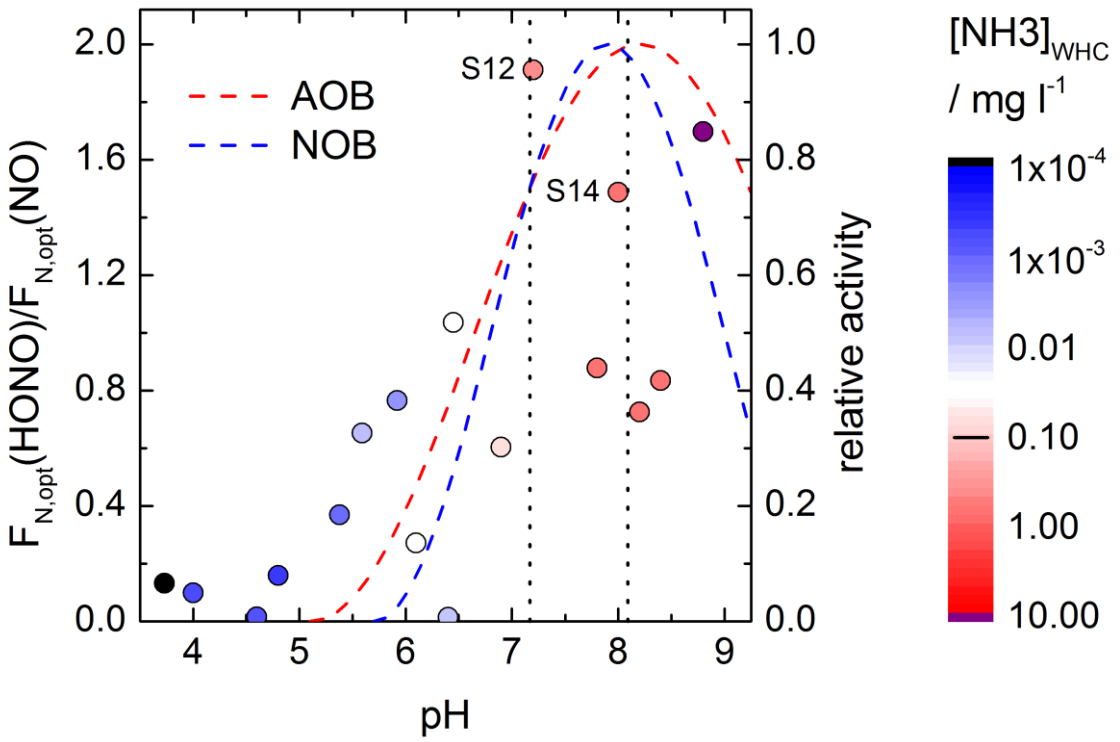

Figure 21. The ratio of $F_{N,opt}$(HONO) to $F_{N,opt}$(NO) plotted versus soil pH (coloured dots). The colour-code of the dots represents the calculated concentration of free ammonia at WHC, calculated by acid-base equilibrium. The dashed lines show the relative activity of AOB (red) and NOB (blue), while the vertical dotted lines refer to point where the relative activity of AOB equals the relative activity of NOB.

The ratio of $F_{N,opt}$(HONO) to $F_{N,opt}$(NO) is lowest for acidic soils and increases with the relative activity of AOB and NOB. At the first intersection of the two relative activity curves (pH = 7.2) the ratio of $F_{N,opt}$(HONO) to $F_{N,opt}$(NO) is maximal. Close to the second intersection only one of four soil samples feature a ratio higher than unity (Fig. 21). Sufficient NH_3 is required for nitrification to take place, but concentrations beyond a certain limit can also inhibit both AOB and NOB activities due to toxicity of NH_3. The threshold lies between 0.1 and 1.0 mg l^{-1} of NH_3 for NOB, while AOB are inhibited at values above 10 mg l^{-1} of NH_3 (Anthonisen et al., 1976). All soil samples with a soil pH above 7 show concentrations of NH_3 above 0.1 mg l^{-1} at WHC. Soil sample S12, providing the highest ratio of $F_{N,opt}$(HONO) to $F_{N,opt}$(NO), contains 0.4 mg l^{-1} NH_3 and soil sample S14 contains 0.7 mg l^{-1} NH_3 (Fig. 21). Both concentrations are already within the range for inhibition of NOB. Soil samples S13, S15 and S16, show a lower flux ratio than S14, but contain similar NH_3 concentrations as S14 at WHC. Since the

soil samples are not identical and differ not only by NH_3 concentrations, other factors may play an important role (see above). Higher NH_3 concentrations might lead to higher ratios of $F_{N,opt}$(HONO) to $F_{N,opt}$(NO) due to better availability of nutrients and the subsequent increase of the AOB activity. On the other hand, an inhibition of NOB leading to accumulation of NO_2^- may also increase the ratio of $F_{N,opt}$(HONO) to $F_{N,opt}$(NO). However, based on our results we are not able to draw final conclusions on this and further measurements are required to discover the influence of NH_3 on HONO emission fluxes in more detail.

3.3.2 Net HONO flux at elevated HONO mixing ratio

Under environmental conditions HONO mixing ratios can reach several ppb even in rural regions (Lammel and Cape, 1996). So far, we investigated the net fluxes from soil samples at 0 ppb HONO headspace mixing ratio, which correspond to potential daytime fluxes at ambient HONO mixing ratios below 200 ppt. To investigate the effect of elevated HONO mixing ratios on the net flux, we set the headspace concentration χ_{in}(HONO) to 10.3 ppb, which exceeded the maximal observed χ_{out}(HONO) of the standard experiment with zero air (Fig. 22). The uncertainty of $\chi_{in(2)}$ was calculated from the noise (3σ) of the HONO source (~ 1 ppb).

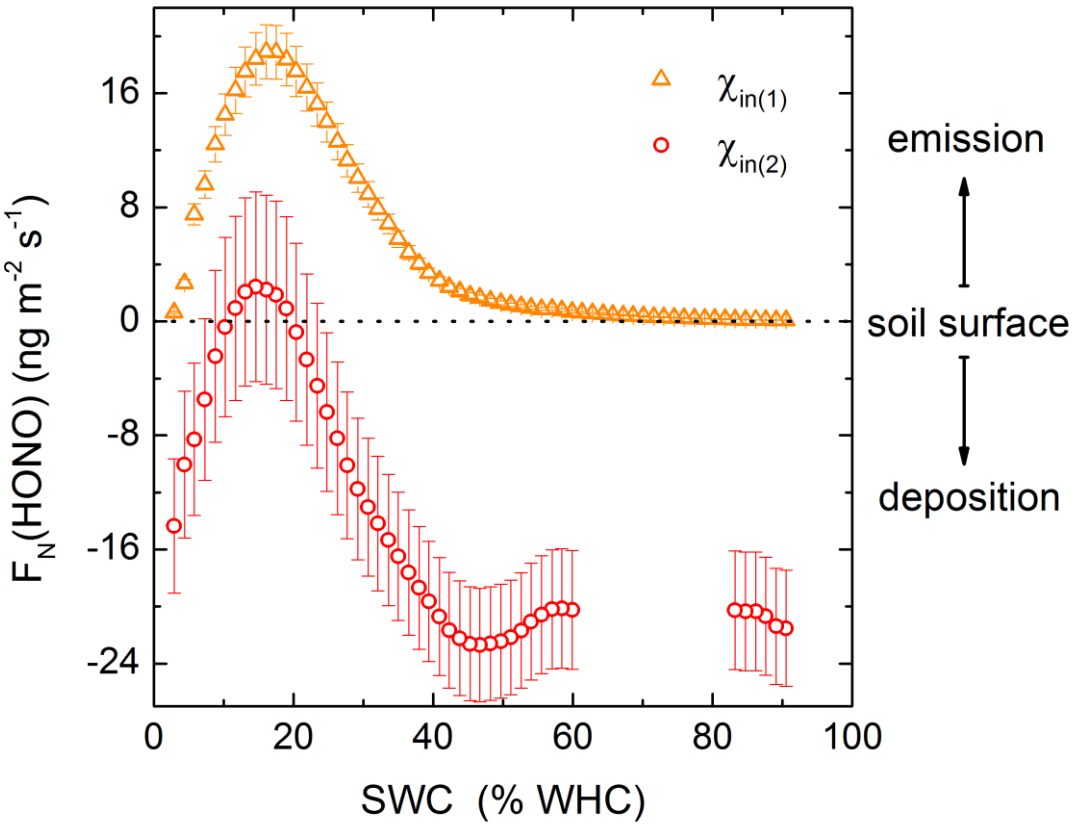

Figure 22. Comparison of two experiments for soil sample S11 (maize field, Grignon, France) conducted with different inlet mixing ratios of HONO at changing SWC. F_N(HONO) at 0 ppb ($\chi_{in(1)}$) is the standard experimental run (orange triangles) and the representative case for very low ambient HONO mixing ratios during daytime, while the measurement with elevated HONO mixing ratio at 10.3 ppb ($\chi_{in(2)}$) reflects the opposite case for high ambient HONO mixing ratios in polluted areas (or during nighttime) (red circles).

The comparison of F_N(HONO) at $\chi_{in(2)}$, $F_N(HONO)_{(2)}$, to F_N(HONO) at $\chi_{in(1)}$, $F_N(HONO)_{(1)}$, reveals that nearly all HONO is taken up by soil sample S11 at elevated inlet mixing ratios, resulting in a negative flux (deposition rate) (Fig. 22). Only close to SWC_{opt}, which remained the same within the uncertainties for the two experiments, the flux becomes positive and HONO is emitted. The missing values at the beginning of the experiment (2) are due to a temporary malfunction of the liquid flow pump of the HONO source. However, it can be assumed that the flux is stable for that period, since there is no change of $F_N(HONO)_{(1)}$ and the same value of $F_N(HONO)_{(2)}$ appear at both ends of the interruption. At SWC below 60 % WHC the flux decreases to become

minimal at around 46 % WHC. With a further decline of SWC $F_N(HONO)_{(2)}$ increases and becomes positive before decreasing again when the soil completely dried out.

Fig. 23 (a) shows the measured mixing ratios during the two experiments. Comparing the measured outlet mixing ratio $\chi_{out(2)}(HONO)$ with the corresponding inlet mixing ratio $\chi_{in(2)}$, it is obvious that more HONO is deposited than emitted from the soil. Interestingly, the shape of the curve is nearly the same as for the standard experiment with 0 ppb HONO inlet mixing ratio. This implies that the process of HONO formation in soil is not essentially altered by adding HONO to the purging air flow.

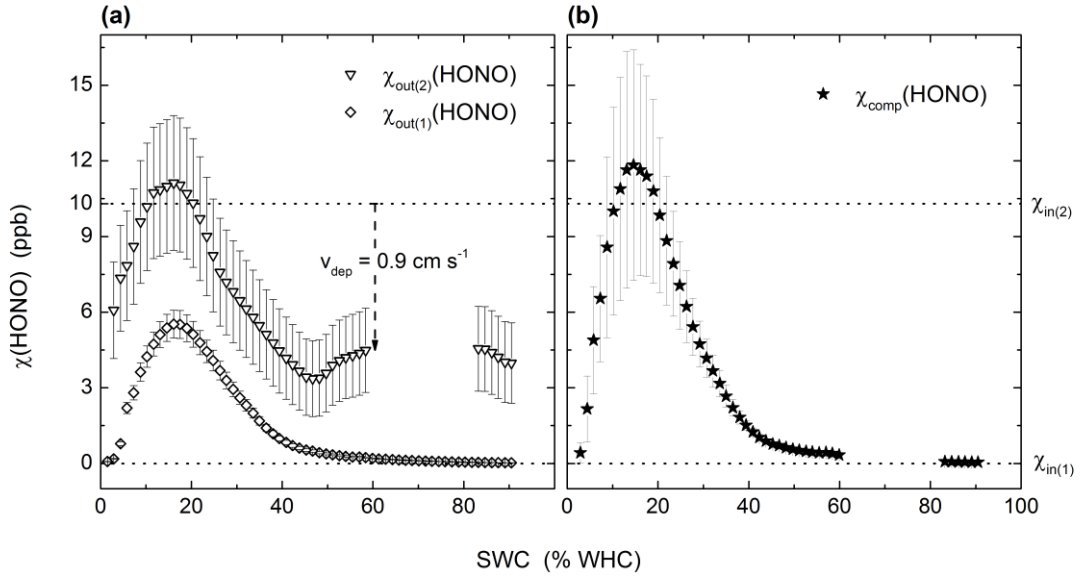

Figure 23. (a) HONO mixing ratios $\chi_{out(1)}(HONO)$ (open diamonds) and $\chi_{out(2)}(HONO)$ (open triangles) are plotted versus SWC for sample S11. The dotted lines represent the respective inlet mixing ratios at each experiment, $\chi_{in(1)}$ = 0 ppb and $\chi_{in(2)}$ = 10.3 ppb. (b) The compensation point mixing ratio of HONO, $\chi_{comp}(HONO)$, as a function the SWC is shown (filled stars).

$F_N(HONO)_{(2)}$ two times equals 0 ng m^{-2} s^{-1} (Fig. 7) and $\chi_{out(2)}(HONO)$ two times equals $\chi_{in(2)}$ (Fig. 23 a), which means that $\chi_{comp}(HONO)$ of 10.3 ppb is reached at about 20 and 10 % WHC. By using Eq. 21, $\chi_{comp}(HONO)$ can be calculated for the entire measured SWC range (Fig. 23 b). Since $\chi_{comp}(HONO)$ reflects the mixing ratio in the chamber headspace and in the soil air, it is possible to calculate the concentration of nitrous acid in the soil solution by applying Henry's law. Accordingly, the maximum concentration of HONO in the soil solution equals (1.6 ± 0.05) mg l^{-1}, which is below the threshold for

inhibition of NOB by nitrous acid (Anthonisen et al., 1976). The constant uptake of HONO at wet soil (SWC > 60 %) shows a chamber specific deposition velocity of about 0.9 cm s^{-1} (Breuninger et al., 2012).

3.3.3 Diffusion limitations

We discussed the influence of SWC on F_N(HONO), F_N(NO) and their ratio in section 3.3.1. We mentioned previously that diffusion is influenced by SWC, which is the possible reason for the existence of an optimum SWC. Linn and Doran (1984) showed that microbial activity is limited by soil aeration at high SWC and limited by water at low SWC. Skopp et al. (1990) further stated that an optimum curve for microbial activity exists, which is limited by oxygen diffusion and substrate diffusion in the soil, as suggested by Linn and Doran (1984). They postulated that soil respiration is highest at *WFPS* of around 60 %. This value was obtained by non-linear regression of soil respiration data, using a function derived from the simplification of an aerobic respiration activity formula. This depends on several variables, but the diffusion of oxygen in soil and the diffusion of substrate in the soil solution should have the main influence. Using the fluxes presented in Fig.17 and adding the negative logarithm of the relative gas diffusion coefficient, $-\log(D_{eff,gas}/D_{0,gas})$ (denoted as pD_{gas}), and the negative logarithm of relative ion diffusion coefficient, $-\log(D_{eff,ion}/D_{0,ion})$ (denoted as pD_{ion}), to Fig. 24, the two functions form the shape of the curve found by Skopp et al. (1990).

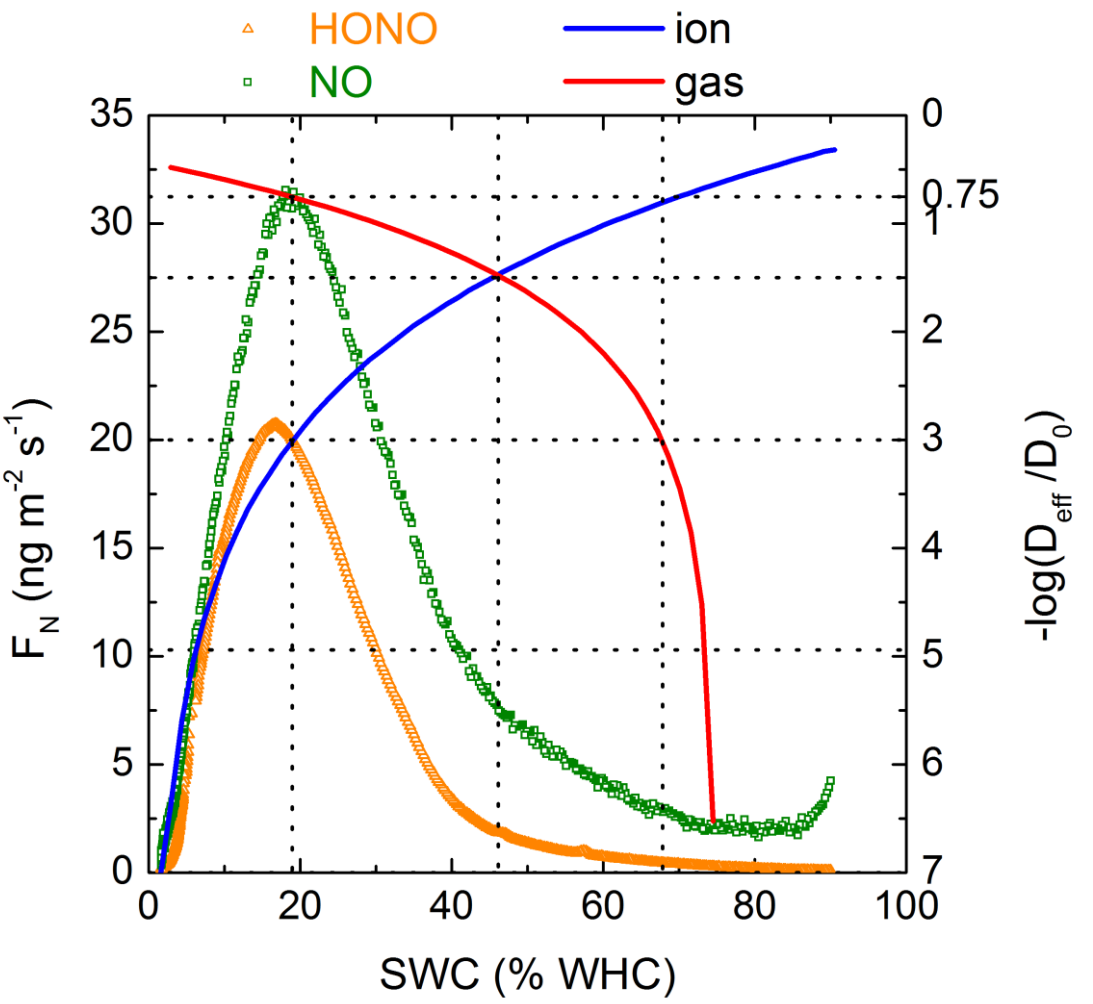

Figure 24. Fluxes of HONO (orange triangles) and NO (green squares) for soil sample S11 calculated from Eq. (17) are plotted versus SWC and the negative logarithm of relative diffusion coefficients for gas (red line) and ions (blue line) are shown.

Using pD instead of D_{eff} has the major advantage that it is identical for every compound (e.g. $D_{eff,HONO}/D_{0,HONO} = D_{eff,NO}/D_{0,NO} = D_{eff,O2}/D_{0,O2}$) and the values can be computed easier.

The dotted lines in Fig. 24 indicate the boundaries for the emission fluxes. Starting at wet soil (right hand side) the first threshold seems to be at $pD_{gas} = 3$ ($D_{eff}/D_0 = 10^{-3}$), which equals a four times smaller pD_{ion} of about 0.7. F_N(HONO) and F_N(NO) start to increase at this point, which should be mainly limited by gas diffusion. With decreasing SWC the two lines of pD approach each other. Skopp et al. (1990) state that the intercept of the gas diffusion function with the ion diffusion function determines the maximum microbial activity. In Fig. 24 the intercept of pD_{gas} and pD_{ion} at SWC of 46 %

WHC is close to the values found in their study (46 % WHC equals 61% WFPS for S11). At this point the value of pD_{gas} and pD_{ion} is 1.5, two times the pDion and half the pDgas at the first boundary. The emissions of HONO and NO strongly increase from this intercept onwards with decreasing SWC until the optimum is reached. At this maximum the next boundary is found with pD_{ion} of 3 and pD_{gas} of 0.75 like at the first boundary, but vice versa. F_N(HONO) and F_N(NO) decrease rapidly during further drying out of the soil. The effective gas and ion diffusion coefficients were also calculated for soil samples S8, S12, S13, S14, S15, S16 and S17. On average the intercept of pD_{ion} and pD_{gas} was at (61 ± 10) % WHC or expressed in *WFPS* (57.2 ± 3.1) %, with a mean value of 1.37 ± 0.7. The optimum emission occurred on average for pD_{ion} of 3.35 ± 0.76.

These findings may partly explain the measured fluxes in the dynamic chamber, e.g. the increased uptake of HONO between 47 and 57 % WHC in Figs. 22 and 23 (a), corresponding to the range between the first and second boundary of pD_{gas} and pD_{ion}. However, unexpectedly the intercept reflecting the maximal microbial activity (Skopp et al., 1990) and the maximum of soil aspiration, does not determine the SWC of $F_{N,opt}$(HONO) and $F_{N,opt}$(NO). While pD_{ion} seems to fit quite well to the shape of emission fluxes at low SWC (< 20 % WHC), pD_{gas} does not. In order to fit the shape of the curve we used effective diffusion coefficient of HONO, NO or O_2.

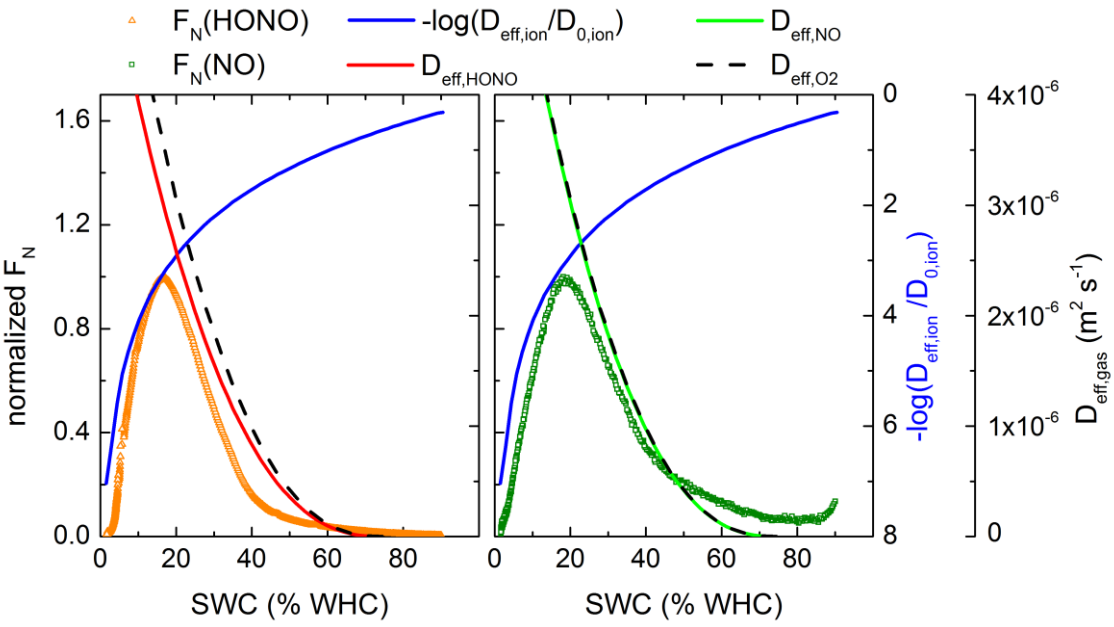

Figure 25. The normalized flux of HONO (orange triangles) and NO (green squares) are plotted versus SWC. In addition, the negative logarithm of relative ion diffusion coefficient (blue line) the corresponding effective gas diffusion coefficient is shown ($D_{eff,HONO}$ (red line), $D_{eff,NO}$ (green line) and $D_{eff,O2}$ (black dashed line)) for soil sample S11.

The aeration of soil is most important for the production and release of HONO. The effective diffusion coefficients of HONO, NO and O_2 increase with decreasing SWC and simultaneously the emission flux of HONO increases (Fig. 25). Besides the diffusion of oxygen into the soil initiating nitrification by microbes, also carbon dioxide (CO_2) might be needed by autotrophic bacteria. Moreover, HONO and NO also need to diffuse out of the soil to be finally emitted. Therefore, we may not clearly distinguish which diffusion process is more important. Nevertheless, each curve of D_{eff} can describe the shape of increase of the emission fluxes. The optimum of the emission is on the other hand, also restricted to sufficient SWC. Microbial activity is limited to ion diffusion in soil, necessary for nutrient transport. The effective diffusion coefficient for NH_3 and NO_2^- in soil show a vertically mirrored response to decreasing SWC compared to the effective gas diffusion coefficients in soil and the values of $D_{eff,ion}$ are about four orders of magnitude smaller compared to $D_{eff,gas}$ at 46 % WHC. Hence, the comparatively slow diffusion of ions is still sufficient for microbial release of HONO and NO, which then shows an immediate decrease after reaching a certain threshold of $D_{eff,ion}$. Schmidt et al. (2004) showed that AOB start to produce NO_2^- after a certain

internal concentration of NH_4^+ is reached. This accumulation might be accelerated by an increasing concentration of NH_4^+ in the soil solution during the dry out of the soil sample and may explain the low SWC values at the optimum microbial release of HONO and NO.

3.4 Conclusions

We have measured biogenic HONO soil emission fluxes (simultaneously with NO emission fluxes) for a broad range of soil samples using a state of the art laboratory dynamic chamber system. The emission fluxes of HONO and NO as a function of SWC feature a distinct optimum curve. The SWC at optimum HONO emission (SWC_{opt}) ranges between 6.5 and 56.0 % WHC. We found that SWC_{opt} is strongly related to WHC and loss on ignition, which is a proxy for the organic matter content in the soil. SWC_{opt} can be computed for each soil from these two quantities. The value of SWC_{opt} has a strong influence on the ratio of HONO to NO emission fluxes. This can be described by a multiple regression function of SWC_{opt} and soil pH, which similarly influence the HONO to NO emission flux ratio. This influence might be due to the activity of ammonia-oxidizing bacteria (AOB) and nitrite-oxidizing bacteria (NOB), whose metabolism depend on soil pH.

Besides acting as a source for HONO, soil may also be a strong sink, which was shown by an experiment with increased HONO mixing ratios in the dynamic chamber. The HONO production process was obviously unaffected by the increased HONO mixing ratio. A HONO compensation point mixing ratio of (11.8 ± 4.6) ppb for SWC_{opt} of 15 % WHC (20 % *WFPS*), (4.5 ± 2.1) ppb at 6 and 30 % WHC (8 and 40 % *WFPS*) and below (1 ± 0.08) ppb at 45 % WHC (60 % *WFPS*) was calculated for a soil sample from a maize field (Grignon, France). Therefore, soil can be a sink for HONO under conditions with higher mixing ratios e.g. above 1 ppb and a SWC above 30 % WHC or at completely dry state.

Further analysis of effective diffusion coefficients for gases and ions in soil reveal the strong influence of SWC on the production, uptake and emission of HONO. We showed

that gas and ion diffusion in soil constitute the boundaries for HONO and NO emission and increased uptake.

Acknowledgements

This project was funded by the Max Planck Society. The work was supported by the Max Planck Graduate Center with the Johannes Gutenberg University Mainz (MPGC). We are grateful to S. Hohlmann, M. Welling, P. Stella, A. Held, B.L. Simmons, N. Mascher, C. Becker, A.C. and F. Hertel, and Z. Wu for supporting the experiments and helping to collect the soil samples. We thank K. Emde and team as well as the company Envilytix for analyzing chemical and physical soil properties. Soil sample S7 was collected in Mali at the Agoufou site belonging to the African Multidisciplinary Monsoon Analysis - Couplage de l'Atmosphère Tropicale et du Cycle Hydrologique (AMMA-CATCH) observatory (http://www.amma-catch.org/). The soil sample S11 from Grignon was collected within the framework of the European Commission project NitroEurope-IP (No. 017841). The work of Hang Su was supported by the European Commission within the framework of PEGASOS (No. 265148). We thank E. Mougin, C. Delon for collecting the soil samples S6 and S7.

4. Comparison of HONO budgets for two measurement heights at a field station within the Boreal Forest (SMEAR II – HUMPPA-COPEC-2010)

This chapter is a reproduction of the article submitted to Atmospheric Chemistry and Physics in February 2014.

R. Oswald[1,2], M. Ermel[1,2], K. Hens[3], A. Novelli[3], H. G. Ouwersloot[3,4], P. Paasonen[5], T. Petäjä[5], M. Sipilä[5], P. Keronen[5], R. Königstedt[3], Z. Hosaynali Beygi[3], H. Fischer[3], , B. Bohn[6], D. Kubistin[3], H. Harder[3], M. Martinez[3]J. Williams[3],T. Hoffmann[2], I. Trebs[1#], and M. Sörgel[1]

[1] Biogeochemistry Department, Max Planck Institute for Chemistry, P.O. Box 3060, 55020 Mainz, Germany

[2] Institute for Inorganic and Analytical Chemistry, Johannes Gutenberg University Mainz,

55128 Mainz, Germany

[3] Airchemistry Department, Max Planck Institute for Chemistry, 55128 Mainz, Germany

[4] Meteorology and Air Quality, Wageningen University, Wageningen, The Netherlands

[5] Dept. Phys., P.O. Box 64. 00014 University of Helsinki, Finland

[6] Institut für Energie- und Klimaforschung IEK-8: Troposphäre, Forschungszentrum Jülich GmbH, 52428 Jülich, Germany

[*] now at: University of Wollongong, School of Chemistry, Wollongong, Australia

[#] now at: Centre de Recherche Public - Gabriel Lippmann, Department Environment and Agro-biotechnologies, 41 rue du Brill, L-4422 Belvaux, Luxembourg

Correspondence to: m.soergel@mpic.de

Abstract

Atmospheric concentrations of nitrous acid (HONO), one of the major precursors of the hydroxyl radical (OH) in the troposphere, normally exceed by far the values predicted by the assumption of a photostationary state (PSS) during daytime. Therefore, additional sources of HONO were intensively investigated in the last decades. Here, we present budget calculations of HONO based on simultaneous measurements of all relevant species including HONO and OH at two different measurement heights, i.e. 1 m above ground and about 2 to 3 m above canopy (24 m above ground), conducted in Boreal forest environment. We observed mean HONO concentrations during daytime of about 6.5 x 10^8 molecules cm^{-3} (26 ppt), more than twenty times higher than expected from the PSS, 0.2 x 10^8 molecules cm^{-3} (1 ppt). To close the budgets in both heights a strong additional source term during daytime is required. This unidentified source is maximal at noon (up to 1.1 x 10^6 molecules cm^{-3} s^{-1}, 160 ppt h^{-1}) and in general up to 2.3 times stronger above the canopy than close to the ground. The insignificance of known gas phase reactions and also other processes like dry deposition or advection compared to the photolytic decomposition of HONO at this measurement site was an ideal prerequisite to study possible correlations of this unknown term to proposed HONO sources. But neither the proposed emissions from soils nor the proposed photolysis of adsorbed HNO_3 contributed substantially to the unknown source. However, the unknown source was found to be perfectly correlated to the unbalanced photolytic loss of HONO.

4.1 Introduction

Since the first unequivocal detection of HONO in the atmosphere by Perner and Platt (1979), its formation and fate as well as its contribution to primary OH production has been intensively studied (Lammel and Cape, 1996; Kleffmann, 2007). Recently, the importance of HONO in atmospheric chemistry and its implications has been demonstrated using a global chemistry transport model (Elshorbany et al., 2012). While

the fate of HONO is mainly determined by the photolytic decomposition producing OH, the major uncertainty in modelling studies results from the lack of understanding the HONO formation pathways. Budget calculations of the postulated sources and sinks (Kleffmann et al., 2005; Su et al., 2008c; Sörgel et al., 2011a) have usually been used to quantify the magnitude of the missing source term. Only a few source estimates derived from flux measurements have been published up to now (Zhang et al., 2012; Zhou et al., 2011; Ren et al., 2011). The current status of HONO formation and loss pathways, important for atmospheric chemistry is as follows.

The major sink during daytime for HONO is the homolytic cleavage of the O-N single bond by radiation ($\lambda < 400$ nm), determined by the photolysis frequency, J(HONO).

$$HONO \xrightarrow{h\nu} OH + NO \qquad \text{(R12\_2)}$$

Since OH is produced, this reaction is of primary importance to atmospheric photochemistry. J(HONO) shows a similar wavelength dependency as the photolysis frequency of nitrogen dioxide (NO_2), J(NO_2) (Kraus and Hofzumahaus, 1998). Therefore J(HONO) can be linked to J(NO_2) by using the approach of Trebs et al. (2009):

$$J(HONO) = 0.17 \times J(NO_2) \qquad (24)$$

The back reaction of (R12_2) in presence of a third body, reaction (R12), can reform HONO with a rate constant (k_{12} at 298 K and 1013 hPa) of (7.4 ± 1.3) x 10^{-12} cm^3 $molecules^{-1}$ s^{-1} (Sander et al., 2011).

$$OH + NO \xrightarrow{M} HONO \qquad \text{(R12)}$$

While the gas phase reaction of OH with NO forms HONO, OH may also react with HONO and reform NO_x.

$$HONO + OH \rightarrow NO_2 + H_2O \qquad \text{(R27)}$$

Due to the in general low concentrations of HONO and OH compared to NO this reaction is less important than reaction (R12) even with a similar reaction rate constant (k_{27} at 298K and 1013 hPa) of about 6.0 x 10^{-12} cm^3 $molecules^{-1}$ s^{-1} (Atkinson et al., 2004) and constitutes typically less than 5 % of the total HONO loss (Su et al., 2008c; Sörgel et al., 2011a).

A surface reaction of NO_2 and H_2O was suggested as another formation pathway for HONO. Finlayson-Pitts et al. (2003) proposed a mechanism, whereby NO_2 after dimerization is dissolved in a humid surface film. The formed N_2O_4 rearranges into the mixed anhydride of nitrous acid and nitric acid ($ONONO_2$), which rapidly dissolves into HONO and nitrate.

$$2NO_2(g)+H_2O(l)\rightarrow HONO(g)+H^+(aq)+NO_3^-(aq) \quad \text{(R22)}$$

Yabushita et al. (2009) and De Jesus Medeiros and Pimentel (2011) further investigated the mechanism with focus on the NO_2 uptake and the kinetics of the initial hydrolysis. The reaction rate constant of reaction (R22) is difficult to determine in the field, but can be estimated with the approach of Alicke et al. (2002).

$$k_{22}^{\mathrm{dark}} = \frac{[HONO]_{max} - [HONO]_{sunset}}{(t_{max} - t_{sunset}) \times \overline{[NO_2]}_{t_{sunset}}^{t_{max}}} \quad (25)$$

After sunset the concentration of HONO, $[HONO]_{sunset}$, increases and reaches a maximum, $[HONO]_{max}$. The difference between $[HONO]_{max}$ and $[HONO]_{sunset}$ divided by the product of the elapsed time (t_{max}-t_{sunset}) and the average NO_2 concentration during that time, $\overline{[NO_2]}_{t_{sunset}}^{t_{max}}$, determines the rate of heterogeneous HONO formation during the night. The reaction rates found for nighttime conversion range from 0.4 (Kleffmann et al., 2003) to 2.0 ppb(HONO) x ppb$(NO_2)^{-1}$ x h^{-1} (Sörgel et al., 2011a). This approach is only valid, if the heterogeneous dark reaction (R22) is the dominant source of HONO during night.

Beside the dark reaction of NO_2, ortho-nitrophenols, o-NPs, can photolytically decompose to form HONO as a side product (Bejan et al., 2006).

$$\text{o-NPs} \xrightarrow{h\nu} [\text{products}]^* + HONO \quad \text{(R19)}$$

The authors propose parts of the reaction mechanism, but since they could not measure the main products, the exact and complete mechanism is not yet clarified. It is further stated that this source might be of primary interest for the atmosphere under urban conditions, where possibly 1 ppb of o-NPs occurs. Since the o-NPs absorb light in a similar wavelength range as NO_2, one can estimate the photolysis by an upper limit approach (Bejan et al., 2006),

$$J(\text{o-NPs}) = 2.5 \times 10^{-3} \times J(NO_2) = 1.4 \times 10^{-2} \times J(\text{HONO}) \quad (26)$$

In addition to the reaction of NO_2 with surface adsorbed water (R22), Stemmler et al. (2006) and (2007) found that a surface film or aerosol of humic acid (HA) can act as photosensitizer when irradiated and reduces NO_2 to HONO.

$$\begin{aligned} \text{HA} &\xrightarrow{h\nu} A^{red} + X^{ox} \\ A^{red} + X^{ox} &\rightarrow \text{HA}' \\ A^{red} + NO_2 &\rightarrow \text{HA}'' + \text{HONO} \end{aligned} \quad (R20)$$

HA naturally occurs in the environment for example in soil. Hence, soil might act as a source for HONO under irradiation in the UV and exposure to NO_2 (Stemmler et al., 2006). Other reactants than A^{red} in reaction (R21) might also be reductive. E.g. fresh soot particles are supposed to reduce NO_2 and form HONO. This source is only important for high NO_2 concentrations and environments with freshly emitted soot (Aubin and Abbatt, 2007; Monge et al., 2010).

It was shown by several studies (Kubota and Asami, 1985b; Twigg et al., 2011; Su et al., 2011; Oswald et al., 2013) that soils can emit HONO. Decreasing soil water content and hence drying out of soil leads to an increase in soil aeration with emission of trace gases, namely N_2O, NO and HONO. Due to the complexity of soil emission fluxes, depending on biological, physical and chemical processes and properties of soil, it is not straight forward to calculate the source strength, although observed NO emissions might serve as a proxy for HONO emission fluxes (Oswald et al., 2013).

Surface adsorbed nitric acid $HNO_{3(ads)}$ either deposited or directly formed during the reaction cascade of (R22), is proposed to be photolytically sensitive and might decompose to HONO in the UV (Zhou et al., 2011).

$$\begin{aligned} HNO_{3(ads)} &\xrightarrow{h\nu} \left[HNO_{3(ads)}\right]^* \\ \left[HNO_{3(ads)}\right]^* &\rightarrow HONO_{(ads)} + O\left(^3P\right)_{(ads)} \\ HONO_{(ads)} &\rightleftharpoons HONO_{(g)} \end{aligned} \quad (R21)$$

The production of HONO by photolysis of $HNO_{3(ads)}$ depends on the physicochemical state of the surface. While for dry surfaces (relative humidity (RH) = 0%) NO_x is the

major product, relative humidity of about 20 % suffices to increase the HONO yield (Zhou et al., 2003). According to Goodman et al. (2001), at 20 % RH there should be at least a monolayer of water present on the surface. Zhou et al. (2003) further propose that $NO_{2(ads)}$ formed during the photolysis of $HNO_{3(ads)}$ may also react further via reaction (R22), which not only forms HONO, but also recovers parts of HNO_3. Later Zhou et al. (2011) suggested that the formed NO_2 is reduced to HONO via the mechanism of reaction (R21) and (R20) proposed by Stemmler et al. (2006). However, the rate of HONO formation depends on the amount of HNO_3 available on irradiated surfaces and the photolysis frequency of HNO_3, $J(HNO_3)$, which is enhanced by adsorption to surface compared to gas phase photolysis (Zhu et al., 2008; Zhu et al., 2010). Depending on the type of surface the enhancement factor varies; Zhou et al. (2003) found an enhancement of about 2 orders of magnitude by HNO_3 adsorption on borosilicate glass (see also Ramazan et al., 2004), while Baergen and Donaldson (2013) calculated an enhancement of about 4 orders of magnitude by HNO_3 adsorbed to grime.

Other loss terms than reactions (R12_2) and (R27) include the dry and wet deposition of HONO. The dry deposition of HONO depends on the ambient mixing ratio of HONO, on turbulent mixing within the planetary boundary layer and the ability of terrestrial surfaces to take up HONO. With a Henry coefficient of 49 M atm^{-1} (Park and Lee, 1988), wet deposition of HONO is quite efficient. After a rain event mixing ratios of HONO strongly decrease (Sörgel et al., 2011b).

Assuming only the known gas phase reactions R12, R12_2 and R27 contribute to the HONO formation, a photostationary state should be established (Kleffmann et al., 2005),

$$\frac{d[HONO]_{PSS}}{dt} = k_{12}[NO][OH] - J(HONO)[HONO]_{PSS} - k_{27}[OH][HONO]_{PSS} = 0 \quad (27)$$

$$\Rightarrow \quad [HONO]_{PSS} = \frac{k_{12}[NO][OH]}{J(HONO) + k_{27}[OH]} \quad (28)$$

This equilibrium can only explain a minor portion of gas phase HONO observed at remote and rural sites (Kleffmann, 2007; Su et al., 2008b; Sörgel et al., 2011a; Wong et al., 2012), but may play an important role for measurement results obtained in urban areas (Lee et al., 2013). The budget calculations of Sörgel et al. (2011a) and Li et al. (2012) showed that including heterogeneous reactions of NO_2 (R22) only slightly

improves the discrepancy between $[HONO]_{PSS}$ and measured HONO mixing ratios. In this study, we present the results of the field campaign HUMPPA-COPEC 2010 (Hyytiälä United Measurement of Photochemistry and Particles in Air – Comprehensive Organic Precursor Emission and Concentration study) related to HONO chemistry and we provide a detailed overview of its sources and sinks using a budget calculation for two measurement heights, i.e. below and above a boreal forest canopy. We explicitly analyse additional source terms, like HONO emission by soil and the formation of HONO by photolysis of $HNO_{3(ads)}$.

4.2 Experimental

The HUMPPA-COPEC-2010 was a comprehensively instrumented intensive field measurement campaign, performed from 12 July until 12 August at the SMEAR II site (Station for Measuring Ecosystem-Atmosphere Relation; 61.846°N, 24.295°E) located in the Boreal forest in Hyytiälä (Williams et al., 2011).

HONO was measured using two Long Path Absorption Photometer instruments (LOPAP, QUMA Elektronik & Analytik, Wuppertal, Germany). A detailed description of the instrument has been given by Kleffmann et al. (2002) and Heland et al. (2001). Briefly, an acidic solution of sulfanilamide is used to sample HONO with a stripping coil. HONO is transformed rapidly into a diazonium salt, the precursor of diazotation, carried out in sequence. The concentration of the azodye formed is equivalent to the concentration of HONO in the sampled air and is measured by a VIS-photometer. The intercomparison of both LOPAP instruments used in this study has been described in detail by Sörgel et al. (2011b) and showed a good agreement (within 12 % relative error) under dry conditions (no rain or fog). The inlets of the two instruments were positioned at about 1 m and 24 m above ground (canopy top height 20 to 21 m).Both instruments ran with a response time of below 10 min and lower limit of detection ranging from 0.2 to 1.3 ppt during campaign.

A laser induced fluorescence (LIF) instrument to measure the atmospheric concentration of the hydroxyl radical, OH, based on the fluorescence assay by gas expansion technique (FAGE) (Hens et al., 2013; Novelli et al., 2014) measured OH above the

canopy at a height of about 24 m, while a chemical ionization mass spectrometer (CIMS; Petäjä et al., 2009) measured OH near to the ground at about 1 m. The two different systems were compared under field conditions, measuring at 1 m above ground level and showed reasonable agreement (Hens et al., 2013). Lower detection limits of LIF and CIMS were about 9 x 10^5 molecules cm^{-3} and 5 x 10^4 molecules cm^{-3}, respectively.

NO and NO_x were monitored by high resolution and high sensitivity chemiluminescence detectors, a TEI 42C TL (Thermo Fisher Scientific, US) with a limit of detection of about 75 ppt positioned at 4 m, and a modified (Hosaynali Beygi et al., 2011) CLD 790 SR with a detection limit of about 16 ppt (ECO-Physics, Switzerland) positioned at 24 m above ground. Both instruments use a blue light converter for efficient and selective transformation of NO_2 to NO. In addition ozone, O_3, was measured by a UV-absorption photometer above canopy.

The photolysis rates of NO_2 and O_3, $J(NO_2)$ and $J(O^1D)$, respectively, were measured using filter radiometers (Meteorologie consult, Königstein, Germany; Bohn et al., 2008). Two $J(NO_2)$ sensors were positioned at 2 m and 24 m above ground, and one $J(O^1D)$ sensor was placed at 24 m. Each measured the downwelling radiation.

Relative humidity, temperature, wind direction, wind speed and other meteorological parameters were monitored routinely by the SMEAR II station (Junninen et al., 2009; http://www.atm.helsinki.fi/smartSMEAR/).

Evaluation of the boundary layer height was determined by radiosondes, measuring relative humidity, temperature, pressure and altitude. From this data vertical profiles of the potential temperature and the specific humidity were gained and hence the height and type of boundary layer have been inferred (Ouwersloot et al., 2012).

A soil sample was taken in June 2012 at the measurement site and was measured under controlled conditions in the laboratory according to Oswald et al. (2013) to investigate NO and HONO emission fluxes from soil.

4.3 Results

During the measurement period of HUMMPA-COPEC 2010 from 12 July to 12 August 2010, not all instruments were running continuously. Beside specific instrument malfunctions, several power disruptions caused by thunderstorms often interrupted the measurement. From 17 July until 5 August, the two LOPAP instruments were running about 30 % of the time simultaneously. The dataset of other measurements is close to complete for this period, except for the OH measurement above the canopy and the $J(NO_2)$ measurement below the canopy (see Fig. 26). The same situation is found for J(HONO) below the canopy, hence it was calculated from $J(NO_2)$ according to Eq. (24).

4.3.1 Overview of measurements and general description

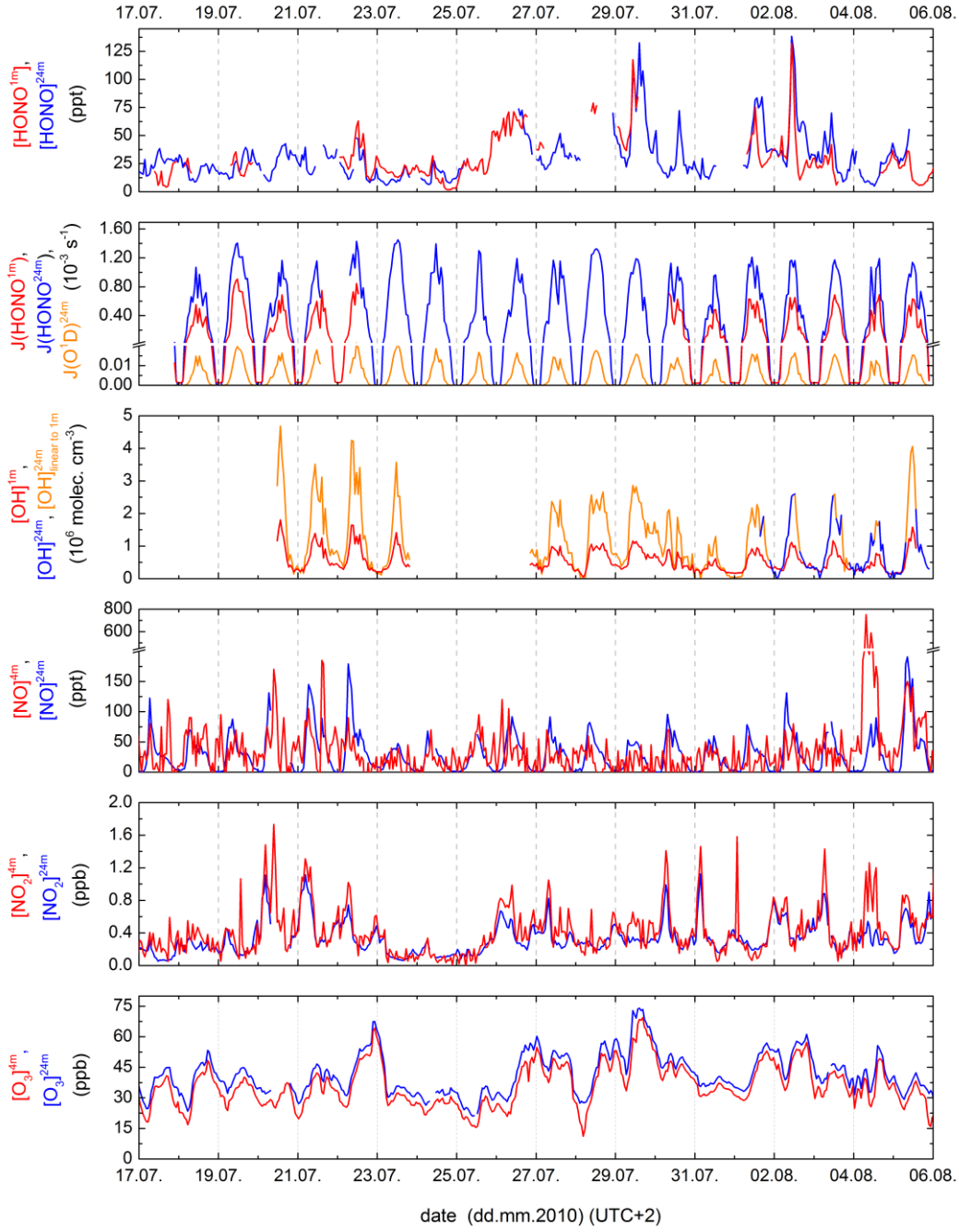

Figure 26. Overview of the measured concentration of different trace gases and the photolysis frequencies J(HONO) and J(O^1D). The linearly connected data points represent 60 min average values. Mixing ratios or concentrations are shown for the period where HONO was measured at both heights. $[OH]^{24m}_{\text{linear to 1m}}$ was used to fill the gaps in OH measurements above the canopy (see Fig. 27 a).

Aside from a linear relationship found between OH measured at the forest floor and above canopy (Fig. 27 a), the exponential relationship of $J(NO_2)$ at 2 m above ground and $J(NO_2)$ at 24 m above ground, was used to interpolate OH above the canopy and $J(NO_2)$ below the canopy to extend the data basis for PSS calculations.

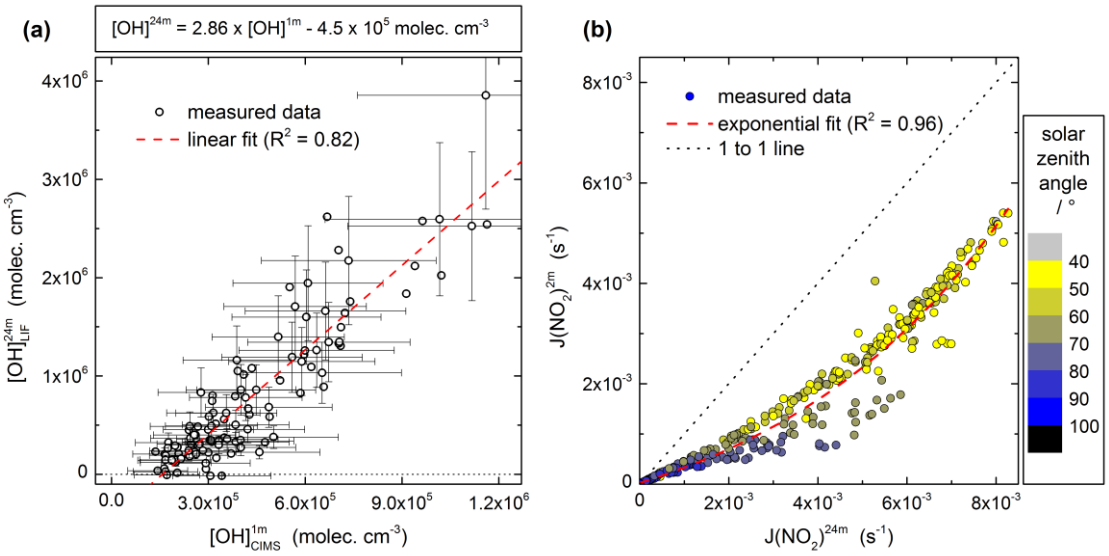

Figure 27. (A) The linear correlation of OH concentration below and above the canopy was used for interpolating data of OH concentration above the canopy. Error bars are representatively shown for 85 data points. (B) Similar to (A) the exponential correlation of measured photolysis frequency below and above the canopy was used to interpolate data of $J(NO_2)$ below the canopy. Color code of dots represents the solar zenith angle. Additionally the 1 to 1 line is shown as dashed line.

4.3.2 Diel variation of HONO

In the clean environment of Hyytiälä diurnal variations of HONO were observed with mean daytime concentrations of 6.6 x 10^8 molecules cm^{-3} (27 ppt) at 1 m height and 6.5 x 10^8 molecules cm^{-3} (26 ppt) at 24 m height and mean nighttime concentrations of 9.1 x 10^8 molecules cm^{-3} (37 ppt) at 1 m height and 9.2 x 10^8 molecules cm^{-3} (37 ppt) at 24 m. Maximum values reached 3.2 x 10^9 molecules cm^{-3} (132 ppt) at 1 m and 3.4 x 10^9

molecules cm^{-3} (138 ppt) at 24 m at 22:30 in the late evening of 2 August. The concentrations reached a minimum after a short and strong rain event in the morning of the 25 July with values below 2 ppt close to the detection limit. The concentrations of HONO were calculated according to Eq. (28) by assuming a PSS, only valid for conditions with short photolytic lifetime of HONO. In agreement with Kleffmann et al. (2005) and Sörgel et al. (2011a) the box plots in Figure 28 obviously show that for both heights the calculated concentrations are often more than one order of magnitude lower than the measured concentration of HONO. While the PSS calculation shows a peak in the morning (6:30) at 1 m height and around mid-morning (8:30) at 24 m height, the daytime measured values peak at noon (11:30).

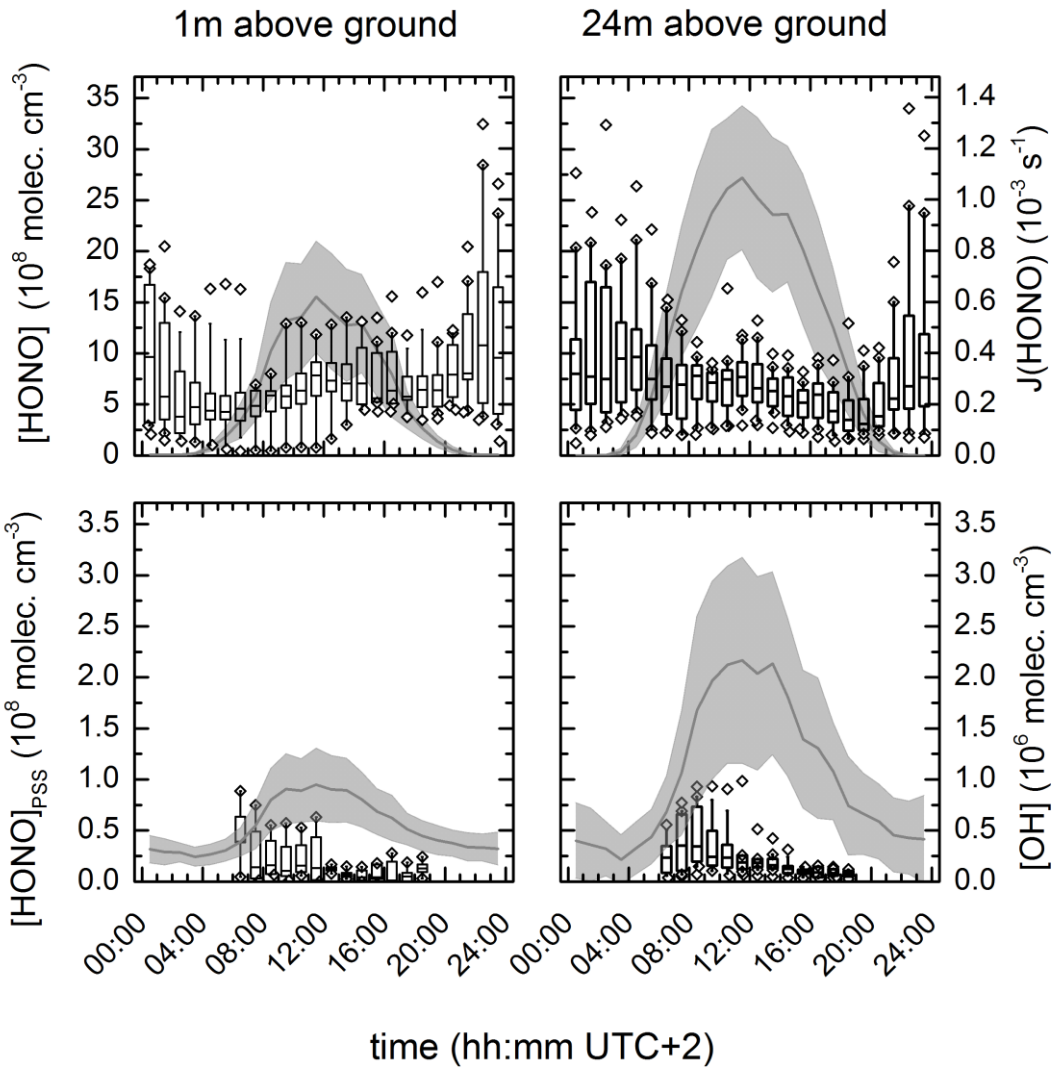

Figure 28. Upper panels show box plots of the diel cycle of HONO measured at 1 m and 24 m, respectively and the average corresponding J(HONO) with standard deviation (grey shaded line). Lower panels show box plots for the calculated PSS concentration of HONO for the heights of 1 m and 24 m, respectively, during daytime (lifetime of HONO below 4 h) where PSS is possibly attained. Additionally, the average concentration of OH with standard deviation (grey shaded line) for the two respective heights is presented. The boxes represent the 25 to 75 percentile, the line within the box is the median, the bars show the 10 to 90 percentile and outliers are marked as open diamonds.

Sörgel et al. (2011a) stated that $[HONO]_{PSS}$ correlates best with measured [NO] and found neither a correlation to measured [OH] nor to measured J(HONO). The correlation between $[HONO]_{PSS}$ and [NO] was strong also in our data (Fig. 29). The

reasonable correlation of $[HONO]_{PSS}$ to measured [NO] might serve as a proxy for $[HONO]_{PSS}$ in general, since the ratio seems to be quite constant.

$$\frac{[HONO]_{PSS}}{[NO]} = \frac{k_{12\_2}[OH]}{J(HONO)+k_{27}[OH]} \cong 0.02 \tag{29}$$

J(HONO) at PSS shows values of about 2 orders of magnitude higher than k_{12} or k_{27} multiplied with the [OH]. Since OH formation is strongly linked to radiation (Rohrer and Berresheim, 2006), its concentration positively correlates with J(HONO). Therefore, NO drives the variability of the PSS.

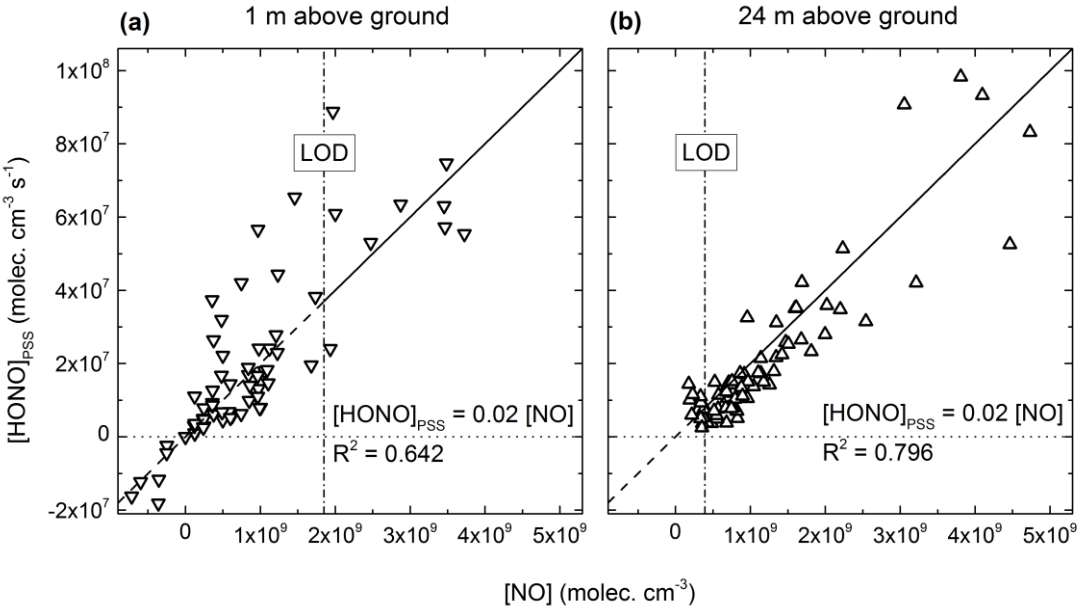

Figure 29. The PSS concentration of HONO, $[HONO]_{PSS}$, at 1 m measurement height (a) and at 24 m measurement height (b) is plotted against the concentration of NO at the corresponding heights. The dashed-dotted vertical line reflects the lower limit of detection (LOD) for each NO measurement. The linear fit using a fixed slope of 0.02 and no offset leads to a reasonable correlations between $[HONO]_{PSS}$ and [NO] in both cases.

4.3.3 HONO budget calculations

The two gas phase reactions (R12) and (R27) together with the photolysis fail to explain the observed HONO concentrations. The comparison of observed changes in HONO concentrations with calculated values considering further sources and sinks leads to a more complete understanding of HONO cycling.

$$\underbrace{\frac{\Delta[\mathrm{HONO}]}{\Delta t}}_{observed} = \underbrace{Sources - Sinks}_{calculated\ budget} \tag{30}$$

If the calculated difference in sources and sinks equals the observed value, the budget would be closed. As mentioned before, normally this is not the case and an unknown source is missing, which can be calculated according to Su et al. (2008c) and Sörgel et al. (2011a) with the following equation:

$$P_{unknown} = \underbrace{\frac{\Delta[\mathrm{HONO}]}{\Delta t}}_{observed} - \underbrace{k_{12}[NO][OH]}_{\text{R12: } P_{NO+OH}} - \underbrace{k_{22}^{dark}[NO_2]}_{\text{R22: } P_{het}} + \underbrace{J(HONO)[HONO]}_{\text{R12\_2: } L_{phot}}$$
$$+ \underbrace{k_{27}[OH][HONO]}_{\text{R27: } L_{HONO+OH}} + \underbrace{\frac{v_{dep}}{h_{BL}}[HONO]}_{\text{dry deposition: } L_{dep}} \underbrace{\pm T_h \pm T_v}_{\text{horizontal and vertical transport}} \tag{31}$$

The resulting $P_{unknown}$ shows, that for most of the day there is still a large source missing (Fig. 30), at least for the period from 6:00 in the morning to 20:00 in the evening where HONO lifetimes are below 30 min. This source is dominated by the photolytic loss of HONO that forms the major sink for HONO and which exceeds the considered sources by far.

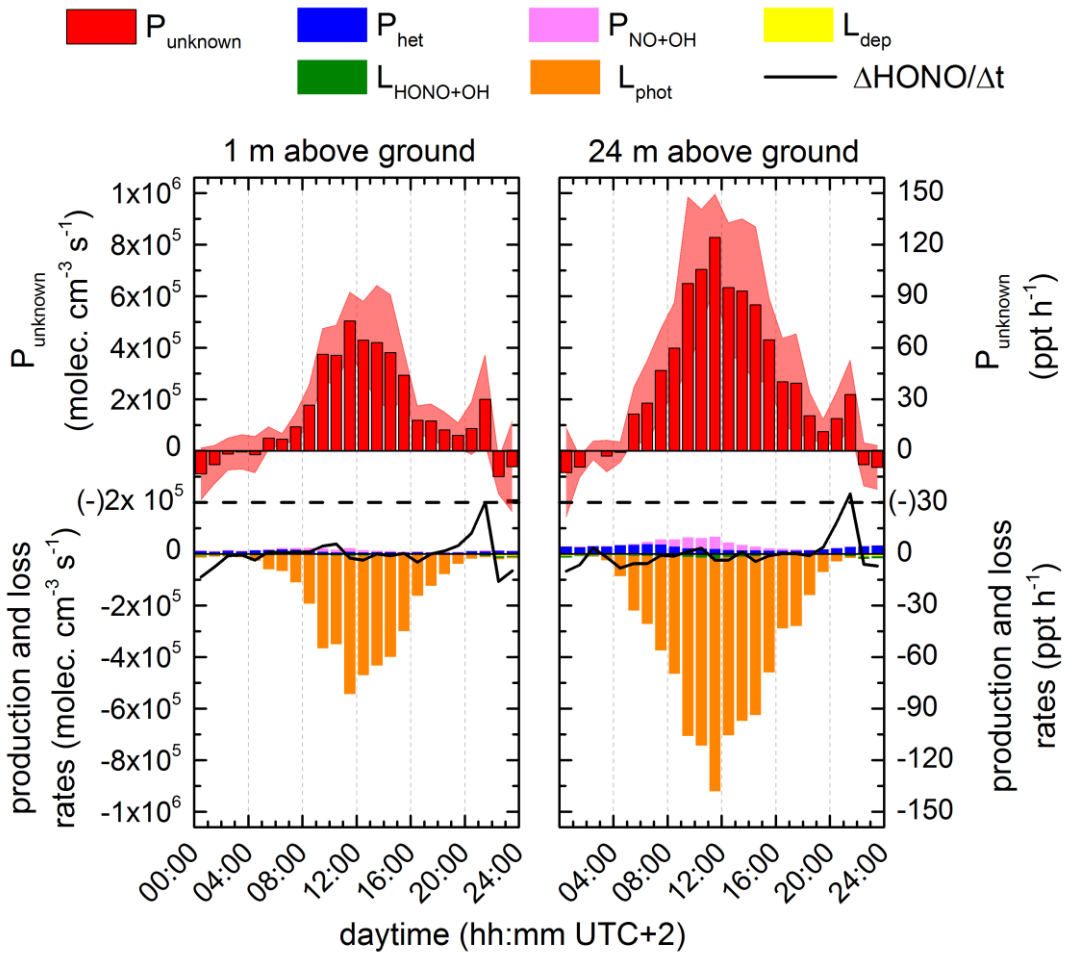

Figure 30. The diel variation of $P_{unknown}$ (red bars, upper panel) with standard deviation (red shade) and single production and loss terms (lower panel) for the two heights are shown. The scales and units at the left and right hand y-axis are valid for both measurement heights and were chosen for an easy comparison with other publications.

Not only the known sources seem to be small compared with the photolytic loss rate, also the other sinks are negligible. E.g. with a deposition velocity for HONO of 2 cm s^{-1} (Harrison et al., 1996; Su et al., 2008a), a mean daytime HONO concentration of 6.6 x 10^8 molecules cm^{-3} and a typical boundary layer height at midday of about 1000 m, the deposition rate is 1.3 x 10^3 molecules cm^{-3} s^{-1}, i.e. 1.9 ppt/h and thus 1 to 2 orders of magnitude less than the photolytic loss. The very low contribution of the dry deposition to HONO loss has already been reported for other measurement campaigns (Su et al., 2008c; Sörgel et al., 2011a).

Horizontal transport, T_h, can strongly influence budget calculations in urban regions (Lee et al., 2013). However, Hyytiälä is surrounded by uniform Boreal forest with up to

95 % of the area within 5 km radius being forested, mostly by Scots pine and Spruce trees (Williams et al., 2011) representing a homogenous fetch. Furthermore, with an average J(HONO) of about 6.7 x 10^{-4} s^{-1}, corresponding to a HONO lifetime of about 25 min and an average horizontal wind speed of 2 m s^{-1} (maximum 7 m s^{-1}), direct emissions of HONO will be transported about 3 km (maximum 10 km) within one lifetime. As most of the surrounding is covered by forest and the next city Tampere, being nearly 50 km away there are no significant emission sources within the fetch, thus horizontal advection of direct emissions will have little influence on the HONO concentration during day. Therefore, the measurement site of SMEAR II, with its homogeneous fetch is well suited to analysing the behaviour of $P_{unknown}$, because all processes disturbing the analysis like horizontal transport and direct emissions can be neglected.

The contribution of vertical transport, T_v , to surface loss of HONO was estimated to be about 50 to 60 % (Wong et al., 2013), thus being the dominant loss process for HONO close to the ground. Vertical mixing acts as a sink close to the surface and as an additional, yet unaccounted, loss term at elevated levels. Hence, depending on the concentration gradient of HONO and the ratio of photolysis, vertical transport can lead to reciprocal changes in $P_{unknown}$ above canopy and below canopy when using the budget approach.

4.3.4 Tracing the missing source

Influence of J(NO_2) on $P_{unknown}$

Reactions (R19-22) and (R25) comprise several mechanisms of HONO formation from photolytic dissociation of ortho-nitrophenols or light induced conversion of NO_2 on different reductive surfaces, which are thought to be possible major sources for HONO during daytime (Stemmler et al., 2006). The wavelength range for the proposed reactions is mostly covered and well described by J(NO_2). Therefore, a source corresponding to these reactions should correlate to J(NO_2) and especially the light

induced conversion of NO_2 should correlate even better with $P_{unknown}$ scaled to the NO_2 concentration (Fig. 31) (Sörgel et al., 2011a).

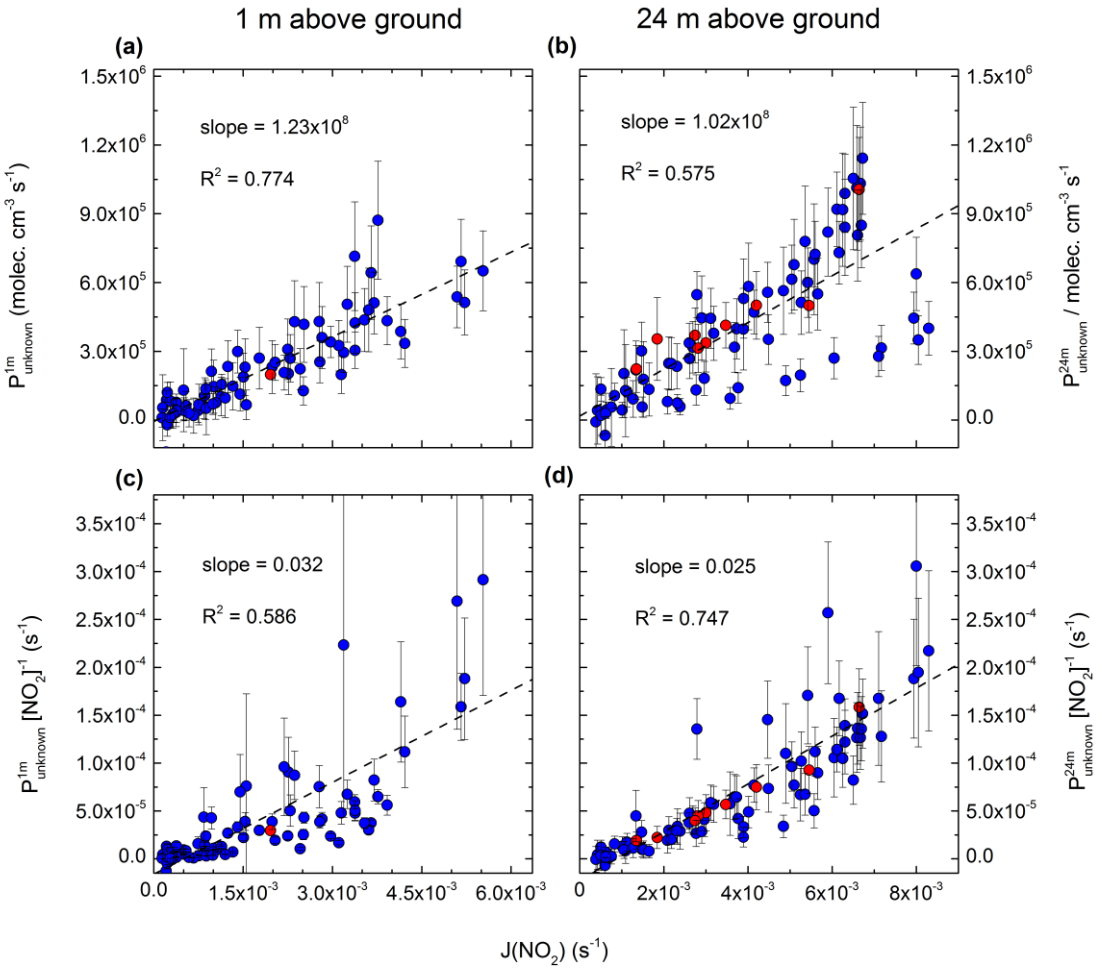

Figure 31. In the upper panels, (a) and (b), $P_{unknown}$ for both measurement heights is linearly correlated with corresponding $J(NO_2)$. In the lower panels, (c) and (d), $P_{unknown}$ is scaled by the NO_2 concentration and still linearly correlated with $J(NO_2)$. Blue dots denote budget data availability at both heights, whereas red dots are available only at the respective measurement height. Linear fits refer to total data available (blue and red),

Scaling $P_{unknown}$ with the concentration of NO_2 on the ground leads to higher scattering of data points, which might be caused by the higher noise levels of NO_2 data on ground. On the contrary, the correlation above canopy is improved with similar scaling (figure 31 panels b and d). The data points most affected belong to a period of rather cold and very clean conditions with low NO_2 concentration of 1.6 to 2.9 x 10^9 molecules cm^{-3}

(65 - 118 ppt) at the 23 July (Williams et al., 2011). Since scaling $P_{unknown}$ above the canopy with corresponding NO_2 concentration increases the correlation with $J(NO_2)$, leads to the assumptions that either NO_2 plays a direct role in HONO formation or that in general NO_2 is a tracer for reactive nitrogen (other potential HONO precursors) in the atmosphere. The fact that the correlation between $P_{unknown}$ and $J(NO_2)$ below the canopy descends by scaling $P_{unknown}$ with NO_2 concentrations can be either due to data scattering as mentioned above, due to HONO deposition on the forest floor (Sörgel et al., 2014) or due to different pathways of HONO and NO_2 formation below canopy. NO_2 below canopy is formed by shifted PSS below canopy and additional NO soil emissions oxidized by O_3 (Rummel et al., 2002). Opposed, due to low OH and NO values below canopy, the shift in the $[HONO]_{PSS}$ by reduced radiation below canopy has minor influence on HONO values (Fig. 28).

With our data set it is not possible to rule out that photolytic conversion of ortho-nitrophenols is a possible pathway, since there were no measurements of these species. However, from Eq. 26 one can estimate that the concentration of o-NPs has to exceed the concentration of HONO by a factor of about 70 in order to compensate the photolytic loss of HONO. Taking the average daytime mixing ratio of HONO above canopy, the resulting mixing ratio of o-NPs would be about 1.8 ppb. Based on earlier studies (Bejan et al., 2006; Kourtchev et al., 2013), the concentration in clean environment such as Hyytiälä should be much lower and thus insignificant for HONO formation.

Another possible $J(NO_2)$ depending source for HONO is the photolytic activation of organic surface reactants (R21, R20, R25) to reduce NO_2 and form HONO (Stemmler et al., 2006). But as before, due to the lack of in-situ measurements of all parameters, this contribution could not be quantified. Obviously, there are many possibilities for humic acids or similar compounds to occur in the highly organic surrounding of the Boreal Forest. A strong hint on such a source might be the merging effect on the correlation of the $P_{unknown}$ with $J(NO_2)$ by scaling with the concentration of NO_2 above the canopy. On the other hand, an increase in correlation by scaling $P_{unknown}$ with the NO_2 concentration, which is anticorrelated to $J(NO_2)$, might just reflect the reaction of the final products of NO_2 photolysis, NO and OH (R12).

Indirect influence of J(NO_2) on $P_{unknown}$

Besides the activation or the photolytic reaction of molecules by J(NO_2), the radiation influences also other parameters. One of these is the temperature of soil. The temperature of soil surface changes stronger and faster than in deeper layers of soil and is driven by radiative heating and cooling. Nitrification and denitrification by microorganisms takes place at the uppermost layer of soil and produces reactive nitrogen gases (Conrad, 1996). The rate of reactive nitrogen formation depends on many parameters like soil water content (SWC), pH, nutrient availability and, important in this context, the temperature of soil (Skopp et al., 1990; Oswald et al., 2013). Therefore, radiation can accelerate the formation of HONO by soil.

Since we did not measure the potential emission of HONO by soil in the field, a soil sample was taken afterwards and measured in the laboratory under controlled conditions according to Oswald et al. (2013). Concentrations of nutrients were quite low with ammonium being (1.60 ± 0.56) mg kg^{-1} N-NH_4^+, while nitrate and nitrite were not measureable/below detection limit (below 2 mg kg^{-1} and 0.07 mg kg^{-1}, respectively). The soil pH was very low with a value of about 3.0. The measurement of the soil sample showed no significant emission fluxes of HONO being below the limit of detection (0.08 ng m^{-2} s^{-1} = 0.288 μg m^{-2} h^{-1}) and emission fluxes of NO scattering around the limit of detection (1 ng m^{-2} s^{-1} = 3.6 μg m^{-2} h^{-1}). This is in good agreement with Oswald et al. (2013) and Maljanen et al. (2013), who both found that acidic forest soils tend to low emission fluxes of HONO. Maljanen et al. (2013) measured a maximum HONO flux of about 2 μg m^{-2} h^{-1} in terms of N. This would equal a source-strength of 7.1 x 10^3 molecules cm^{-3} s^{-1} (1 ppt h^{-1}) considering a boundary layer height of 1000 m and hence is negligible.

HONO formation by nitric acid photolysis

Adsorbed HNO_3 on humid surfaces (R21) seems to be more rapidly photolyzed than HNO_3 in the gas phase or in aqueous solution (Zhou et al., 2003; Abida et al., 2012). Therefore, leaves and needles loaded with nitric acid could be a major source of HONO in clean environments (Zhou et al., 2011). This mechanism has also been postulated as significant for the Boreal forest by Raivonen et al. (2006) to explain light induced NO_y

(NO, NO_2, HONO, HNO_3, peroxy acyl nitrate) emissions. To estimate the strength of this source we used a constant surface loading of HNO_3 of (8.3 ± 3.1) x 10^{-5} mol m^{-2} (Zhou et al., 2011). The gas phase photolysis frequency for HNO_3 was parameterized using $J(NO_2)$ and $J(O^1D)$ (Sander et al., 2011). By adsorbing to the surface the absorption cross-sections of HNO_3 increases (Zhu et al., 2010; Abida et al., 2012), which is typically considered by the use of an empirical enhancement factor for natural systems (Zhou et al., 2011; Li et al., 2012). For Figure 32 we used the enhancement factor of 43 (Zhou et al., 2003; Zhou et al., 2011).

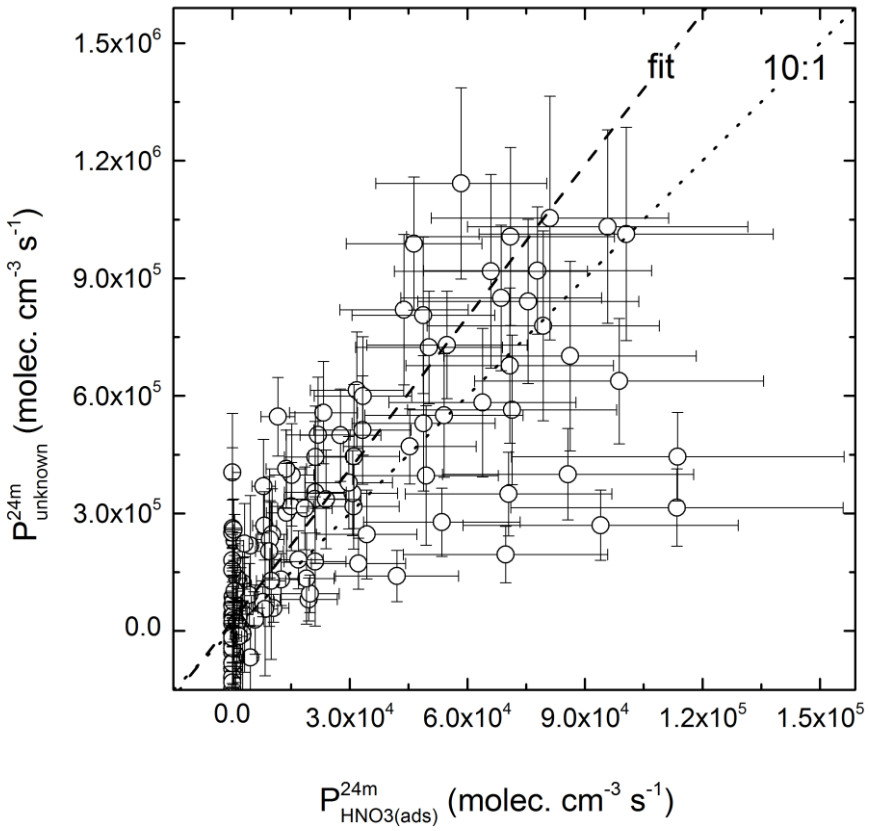

Figure 32. $P_{unknown}$ at the measurement height of 24 m during daytime is plotted against the production of HONO from photolysis of adsorbed HNO_3 on leaf surfaces, $P_{HNO3(ads)}$. With an enhancement factor of 43 and a surface loading of (8.3 ± 3.1) x 10^{-5} mol m^{-2} it might explain up to 10 % of $P_{unknown}$, indicated by the 10 to 1 line (dotted line). The York linear fit (York et al., 2004) yields in $P_{unknown}$ = (12.9 ± 1.0) x $P_{HNO3(ads)}$ + (2.4 ± 1.1) x 10^4 molecules cm^{-3} s^{-1}.

The photolysis rate of surface adsorbed HNO_3 needs to be more than 400 times enhanced compared to the photolysis in gas phase to explain $P_{unknown}$ of HONO

(Fig. 32). The error of $P_{HNO3(ads)}$ was calculated by using the standard error of the surface loading of HNO_3 (Zhou et al., 2011). $J(HNO_3)$ constitutes the only variable of $P_{HNO3(ads)}$ and is closely correlated to $J(NO_2)$ and $J(O^1D)$. This leads to a similar correlation of $P_{unknown}$ with $P_{HNO3(ads)}$, like seen before with $J(NO_2)$ (Fig. 31). An additional correlation might derive from the mechanism of HNO_3 photolysis, which is not fully understood by now. Zhou et al. (2011) proposed that formed NO_2 during HNO_3 photolysis reacts further with organics on the surface to form HONO (R20) as proposed by Stemmler et al. (2006).

4.3.5 Direct comparison of $P_{unknown}$ determined for two different heights

The ratio of $J(NO_2)$ at 24 m to $J(NO_2)$ at 2 m tracks the ratio of direct and diffuse radiation penetrating the canopy. In the early morning the ratio increases, due to increasing direct sunlight at the upper height. With the rising sun more direct sunlight penetrates the canopy and a rather constant ratio develops which seems to be influenced by light patches. The ratio of $P_{unknown}$ at 24 m to $P_{unknown}$ at 1 m during daytime is mainly above unity, except for the first value where $P_{unknown}$ at both heights were still negative (Fig. 30). It strongly decreases from values above 4 in the morning hours before it gets more stable with values around 2, but still decreases until 2 hours after reaching the minimum of solar zenith angle (~43°). This diel pattern can be explained by a combination of two processes; the change of the photolysis frequency and the change of the concentration gradient (Fig. 8 a). The product of both, the concentration and the photolysis frequency equals the photolytic loss rate, L_{phot}, which is the unbalanced sink that determines $P_{unknown}$ (see Fig.30, Fig. 33 panels b and c). This is at least valid from 8:30 to 17:30 where the contribution of other source and sink terms is less than 20 %. The HONO concentrations above the canopy are higher than below the canopy in the morning (values over unity in Fig 33a). The gradients vary around zero from late morning to noon and in the afternoon the concentrations below the canopy are higher. This closely resembles the pattern found by Sörgel et al. (2011b) for a different

forest ecosystem and might therefore be typical for forests in general. Sörgel et al. (2011b) showed that this could be attributed to different sources and sinks and the extent of the vertical exchange between the forest and the atmosphere above. However, the variability of the ratios is smallest at minimum solar zenith angle, which is the maximum of J(HONO). In a strict sense this is the only period where the budget could be used for the determination of $P_{unknown}$ as the assumptions like well mixed conditions (i.e. no concentration gradients), stationarity due to low lifetime and potentially establishment of a PSS are fulfilled. During this period it could be questioned if a budget below canopy makes sense as the portion below canopy where J(HONO) and thus L_{phot} is reduced is very small compared to the whole boundary layer and recombination of NO and OH below canopy has been found to play a minor role (section 4.3.3).

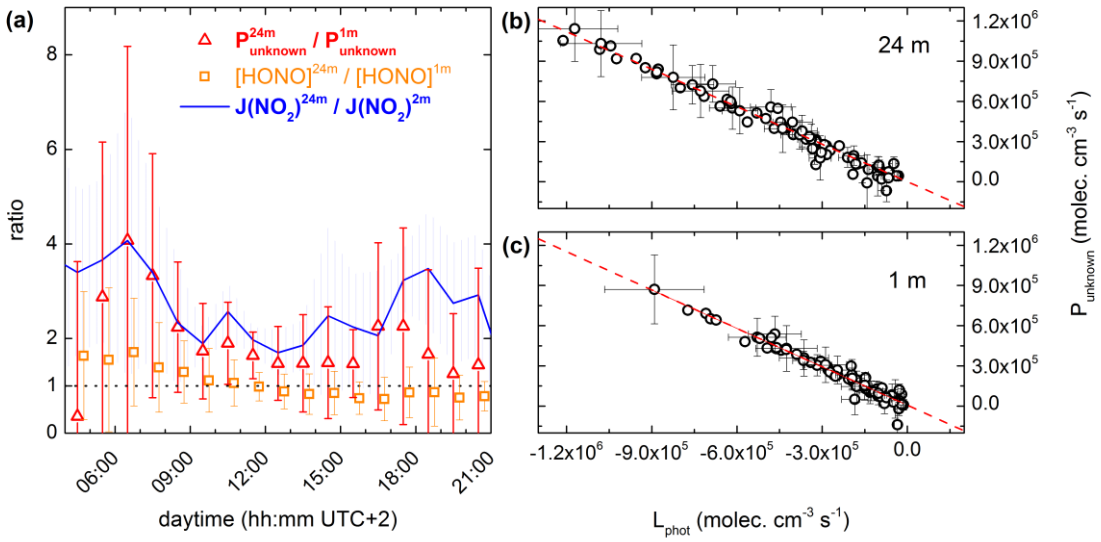

Figure 33. (a) The average ratio of $P^{24m}_{unknown}$ to $P^{1m}_{unknown}$ (red triangles), the average ratio of $[HONO]^{24m}$ to $[HONO]^{1m}$ (orange squares) and the average ratio of $J(NO_2)^{24m}$ to $J(NO_2)^{2m}$ (blue line) change during daytime (lifetime of HONO < 4 h). For clarity a second x-coordinate for the ratio of $[HONO]^{24m}$ to $[HONO]^{1m}$ is used with a shift of +15 min, but is not shown. (b) $P^{24m}_{unknown}$ and (c) $P^{1m}_{unknown}$ are plotted against the photolytic loss rate of HONO at 24 m and 1 m above ground, respectively. The York linear fit (York et al., 2004) of $P^{24m}_{unknown}$ with L^{24m}_{phot} and $P^{1m}_{unknown}$ with L^{1m}_{phot} yields in $P^{24m}_{unknown} = -(0.93 \pm 0.05) \times L^{24m}_{phot} + (0.9 \pm 14.2) \times 10^3$ molecules cm^{-3} s^{-1} and $P^{1m}_{unknown} = -(0.96 \pm 0.08) \times L^{1m}_{phot} + (0.6 \pm 11.9) \times 10^3$ molecules cm^{-3} s^{-1}, respectively.

Impressively, $P_{unknown}$ correlates much better with L_{phot} (Fig. 33 b and c) than with $J(NO_2)$ or with the ratio of $J(NO_2)$ to concentration of NO_2 (Fig. 31). This correlation is not disturbed by any environmental condition, like the different regimes of stressed and normal Boreal and even more astonishing it is not disturbed by the wild fire pollution plumes transported from Russia (Nölscher et al., 2012), since the corresponding data points are included. The almost perfect correlation of $P_{unknown}$ with L_{phot} is caused by the low contribution to the budget of all other processes (sources and sinks) considered so far. Even including the parameterized HNO_3 photolysis would not change much as it is only around 10 % of $P_{unknown}$. Therefore, the unknown source is a process that exactly balances HONO photolysis or the sink itself is erroneous. Nevertheless, this unbalanced photolysis term ($P_{unknown}$) has been found by applying different techniques for HONO detection such as LOPAP (e.g., Kleffmann et al., 2005; Sörgel et al., 2011a), denuder (Acker et al., 2006), differential optical absorption spectroscopy (Alicke et al., 2002; Wong et al., 2012) and recently by using chemical ionization mass spectroscopy (VandenBoer et al., 2013). Additionally, recent flux measurements reported strong daytime upward fluxes of HONO (Zhou et al., 2011, Ren et al., 2011), thus confirming a ground source of HONO.

4.4 Conclusions

Concentrations of HONO during daytime exceeded in average the expected values calculated by the PSS by a factor of about 20 and thus lead to an imbalanced budget above and below canopy. To balance the budget an additional yet unknown source is required. However, photolysis of ortho-nitrophenols is likely of minor importance under the clean environment of the Boreal Forest. A laboratory measurement of a soil sample in a dynamic chamber shows that direct soil emissions of HONO are insignificant for the humid temperate region, featuring low soil nutrient content and low soil pH. However, the photolytically active radiation has a major influence on the budget of HONO, since the missing source resembles the photolytic loss of HONO by day. It was

not possible to clearly identify the most important, but a tendency for a possible coupling of different processes is most likely. E.g. the photolytic dissociation of HNO_3 adsorbed on humid surfaces and the conversion of NO_2 on photolytically activated surfaces, like humic acids, might occur simultaneously. However, the almost perfect correlation of $P_{unknown}$ with L_{phot} is caused by the low contribution of the considered processes to the budget and hence, the unknown source is a process that exactly balances HONO photolysis. Further investigations in the field are needed to understand daytime HONO chemistry and its implication to the budget. Especially the role of vertical mixing needs to be analysed in more detail.

Acknowledgements

This project was funded by the Max Planck Society. The work was supported by the Max Planck Graduate Center with the Johannes Gutenberg University Mainz (MPGC). The entire HUMPPA-COPEC team is grateful for the support of the Hyytiälä site engineers and staff. We like to thank for the support of the European Community Research Infrastructure Action under the FP6 "Structuring the European Research Area" Programme, EUSAAR 15 Contract No RII3-CT-2006-026140. The campaign measurements and analyses were supported by the ERC Grant ATMNUCLE (project No 227463), Academy of Finland Center of Excellence program (project No 1118615), The European Integrated project on Aerosol Cloud Climate and Air Quality Interactions EUCAARI (project No 036833-2), the EUSAAR TNA (project No 400586), and the IMECC TA (project No 4006261). We also wish to thank C. Breitenberger, J. Crowley, T. Klüpfel, U. Parchatka, M. Rudolf, L. Ganzeveld for their support during HUMPPA-COPEC-2010. We are further grateful to S. Hohlmann, M. Welling, D. Plake, A. Moravek, E. Falge, T. Behrendt, D. Mogensen for supporting the measurements and for the fruitful discussions.

5. Conclusions and outlook

This thesis can be separated into two parts; laboratory measurements of HONO emission by soil using a dynamic chamber system and field measurements of HONO investigating HONO formation pathways at two different measurement heights.

During the first part of this thesis a dynamic chamber system was successfully adapted and applied to trace gas exchange fluxes between soil and atmosphere under controlled conditions in the laboratory. By attaching a LOPAP (long path absorption photometer) to the chamber, it was possible to measure the soil emission fluxes of HONO. Measurements of a survey of soils from different ecosystems indicated that HONO emission fluxes may account for up to 50 % of the reactive nitrogen release from soil. These emissions may be attributed to ammonia-oxidizing bacteria (AOB) and possibly other types of bacteria. HONO emission by soil represents an additional component for gaseous losses from the soil nitrogen pool to the atmosphere, which is currently not considered in model estimates of global soil reactive nitrogen emissions and may constitute one of the major uncertainties in this budget. Furthermore, these HONO emissions contribute to atmospheric chemistry by enhancing the oxidation capacity of the lower atmosphere. Further, it has been shown that the emission fluxes of HONO and NO are a function of soil water content (SWC) and feature a distinct optimum curve. The value of SWC at maximum emission (SWC_{opt}) has a strong influence on the ratio of HONO to NO emission fluxes. Hence, the knowledge of this property is of major importance, in order to estimate the source strength of HONO emission fluxes compared to NO, e.g., for use in modeling HONO emissions. Analysis of effective diffusion coefficients for gases and ions in soil reveal the strong influence of SWC on the emission of HONO and NO. In general, gas and ion diffusion in soil constitute the boundaries for HONO and NO emission fluxes. An exact analysis of the diffusion regulation of HONO emission fails due to the lack of measurements of HONO diffusion in soil. Besides acting as a source for HONO, soil may also be a strong sink, which was shown by an experiment with increased HONO mixing ratios in the purging air flow. The HONO production process was unaffected by the increased HONO mixing ratio,

which means that AOB activity was not influenced by the increased level of HONO. Compensation point mixing ratios of HONO were calculated for the soil sample from a maize field in Grignon, France. At this maize field the measurement campaign PHOTONA took place (Stella et al., 2012), where HONO upward fluxes have been observed. It is part of the ongoing research to compare the results found in the laboratory with direct flux measurements in the field. Here, the presented dynamic chamber system for HONO could serve as a potential technique for the determination of in-situ exchange fluxes. In addition, the chamber system setup is the basis for two follow-up doctoral theses on the exchange of HONO from pure bacterial culture suspensions and atmosphere as well as further soil process studies.

In a second part of the thesis, HONO was simultaneously measured at two heights during the field campaign HUMPPA-COPEC 2010 at the SMEAR II site in Finland. With one LOPAP instrument positioned close to the ground at approximately 1 m above ground and the other LOPAP instrument positioned above the canopy at about 24 m above ground, it was the aim to analyse possible differences in HONO formation pathways and the exchange of HONO between the two heights. The observed mixing ratios of HONO during daytime exceeded on average the expected values calculated via the photo-stationary state by a factor of about 20 at both heights. Similar to other publications an additional yet unknown source ($P_{unknown}$) is required to balance the calculated budget of HONO. The ratio of $P_{unknown}$ at 24 m to $P_{unknown}$ at 1 m was above unity during daytime. However, neither HONO emission by soil nor photolytic dissociation of HNO_3 adsorbed on humid surfaces nor the light-induced conversion of NO_2 on surfaces, seem to have a significant impact on $P_{unknown}$. A very good correlation of $P_{unknown}$ with the photolytic loss of HONO was observed for both heights and is caused by the low contribution of the considered processes to the budget. Hence, $P_{unknown}$ is a process which exactly balances HONO photolysis. It is questionable if a source of the strength of HONO photolysis is missing or if the photolysis of HONO itself is erroneous. Since field measurements employing different HONO measurement techniques showed that a possible source is missing leads to the final conclusion that either $P_{unknown}$ exists or the photolysis frequency is overestimated and that HONO mixing ratios are quantified accurately enough. Many studies on the absorption cross-section of HONO are available, but only two studies (Cox et al., 1976; Wall et al., 2006)

deal with the quantum yield of NO and OH production. The quantum yield is assumed to be unity at radiation wavelength below 400 nm, but measurements of the quantum yield under realistic conditions, i.e. including the effects of relative humidity and aerosol particles, which might stabilize HONO by cluster formation and adsorption, are lacking. Measurements of the quantum yield of HONO photolysis over the whole wavelength range could possibly give new insights into the HONO pathways in the atmosphere.

Appendix A: Supplementary Material

HONO emissions from soil bacteria as a major source of atmospheric reactive nitrogen

R. Oswald*, T. Behrendt, M. Ermel, D. Wu, H. Su, Y. Cheng, C. Breuninger, A. Moravek, E. Mougin, C. Delon, B. Loubet, A. Pommerening-Röser, M. Sörgel, U. Pöschl, T. Hoffmann, M.O. Andreae, F.X. Meixner and I. Trebs*

Corresponding authors: robert.oswald@mpic.de (R.O.); i.trebs@mpic.de (I.T.)

Published 13 September 2013, *Science* **341**, 1233 (2013)

DOI: 10.1126/science.1242266

Materials and methods

Soil samples

All soil samples were taken from the uppermost layer of the soil (5 cm). Samples S1 (eucalyptus forest, Grose Valley, Australia, 33.61°S, 150.63°E), S5 (pasture, Hawkesbury River flood plain, Australia, 33.57°S, 150.77°E), S8 (grassland, Mainz-Finthen, Germany, 49.97°N, 8.16°E) (Plake and Trebs, 2013), S11 (maize field, Grignon, France, 48.85°N, 1.97°E) (Stella et al., 2012) and S12 (wheat field, Mainz-Finthen, Germany, 49.97°N, 8.16°E) (*8*) were dried at 40 °C for 24 h, sieved to 2 mm and stored at 4 °C in open plastic bags before measurement.

Soil samples S2 (tropical rain forest, Suriname, 05.08°N, 55.00°W), S3 (coniferous forest, Hohenpeißenberg, Germany, 47.80°N, 11.01°E), S4 (coniferous forest, Fichtelgebirge, Germany, 50.09°N, 11.52°E) (Sörgel et al., 2011b) and S9 (pasture, Hohenpeißenberg, Germany, 47.79°N, 11.00°E) (Acker et al., 2006) are characterized by high organic contents. These soils were sieved to 2 mm (S2) or 16 mm (S3, S4 and S9) (Bargsten et al., 2010) and measured directly after sampling.

All other soil samples, S6 (open woody savannah, Dahra, Senegal, 15.40°N, 15.43°W), S7 (open woody savannah, Agoufou, Mali, 15.34°N, 1.48°W) (Mougin et al., 2009), S10 (stone desert, Ruta B 376, Chile, 23.48°S, 68.03°W), S13 (jujube field, Qiemo, China, 38.09°N, 85.55°E) (Mamtimin et al., 2011), S14 (cotton field, Qiemo, China, 38.10°N, 85.55°E) (Mamtimin et al., 2011), S15 (jujube field, Mingfeng, China, 37.05°N, 82.71°E) (Mamtimin et al., 2011), S16 (stone desert, Sache, China, 37.69°N, 77.89°E) (Mamtimin et al., 2011) and S17 (cotton field, Milan, China, 39.27°N, 88.91°E) (Mamtimin et al., 2011) were already dry when sampled. They were sieved to 2 mm mesh size and stored at 4 °C in open plastic bags prior to measurement.

Physical and chemical properties of each soil sample were analyzed according to ISO or DIN standard procedures: bulk pH of soil according to ISO 10390, nitrite, nitrate and ammonium according to ISO/TS 14256-1, particle distribution according to ISO 11277,

total C and N according to ISO 10649 and ISO 13878, loss on ignition according to DIN 19684-3 (Blume et al., 2000).

Measurements

The prepared soil samples were homogenously spread in a borosilicate glass dish to 5 mm thickness and wetted with purified water to water holding capacity (whc, Eq.35). After that, the glass dish was placed into the Teflon (PFE) chamber (volume 0.047 m^3) (*8*). Complete mixing of the chamber headspace volume was achieved by a fan. Dried and purified air was purged through the chamber at a flow rate of $1 \cdot 10^{-4}$ m^3 s^{-1} and mixing ratios of HONO, NO (NO_2), O_3 and H_2O were measured at the chamber outlet. The chamber was placed in a thermostatic cabinet to control the temperature of the experiment (accuracy ± 0.1 °C). All measurements were conducted in the dark to exclude photosensitized reactions found by Stemmler et. al (Stemmler et al., 2006). Additionally, potential interferences from background HONO formation can be excluded, as flushing the empty chamber with NO did not lead to HONO production. The inlet concentration of the purging air flow was measured regularly and was below the detection limits of the trace gas analyzers. A pure air generator (PAG 003, ECOPHYSICS, Switzerland) continuously provided dry air (dew point of about -15 °C).

HONO was measured by a long path absorption photometer (LOPAP) (QUMA Elektronik & Analytik GmbH, Wuppertal, Germany; limit of detection (LOD) ≈ 5 ppt) (*13*). NO (and NO_2) were detected by a gas phase chemiluminescence detector equipped with a blue light converter (Model 42C, Thermo Electron Corporation, USA; LOD_{NO} ≈ 120 ppt and LOD_{NO2} ≈ 300 ppt) (*14*). Additionally, the headspace concentration of O_3 was monitored using an UV-absorption analyzer (Model 49i, Thermo Electron Corporation, USA; LOD ≈ 0.5 ppb). The loss of soil water during the experiments was determined by measuring temperature and relative humidity at the outlet of the dynamic chamber (Model MP 103 A, Rotronic Messgeräte GmbH, Ettlingen, Germany).

For the measurement of the pure culture of *Nitrosomonas europaea*, the measurement of S2 and S12, including the ATP assays and the sterilization, the experimental setup was slightly modified. A smaller Teflon chamber (volume 0.008 m^3) was used and the

Thermo NO_x instrument was replaced by a more sensitive chemiluminescence analyzer (CLD 780TR, ECOPHYSICS, Switzerland, $LOD_{NO} \approx 35$ ppt and $LOD_{NO2} \approx 120$ ppt). The water vapor difference between the inlet and outlet of the chamber was measured with an infrared gas analyzer (LI-7000, Li-Cor Biosciences GmbH, Germany). An intercomparison was performed using a constant source of NO_2, which yielded the same emission fluxes for both setups (not shown). During the experiment, a flow of $1 \cdot 10^{-4}$ m^3 s^{-1} was purged through the chamber containing the glass bead sample (0.25 – 0.50 mm diameter, Carl Roth, Germany) or the soil samples, respectively. To ensure sterile conditions, the chamber inlet was equipped with a sterile air filter (MILEX®-FG Vent Filter 0.2 µm, 50 mm diameter, Millipore, France). The glass beads and glass bowl were sterilized by washing with ethanol (70 %, absolute for analysis, Merck, Germany). Sterility of the setup was checked by an ATP assay for a sample of sterile AOB nutrient solution. For each experiment 50 g of glass beads were used and wetted either with sterile AOB nutrient solution (Krümmel and Harms, 1982; Koops et al., 2006) or AOB culture suspension to reach whc. *Nitrosomonas europaea* was cultured as described by Krümmel and Harms (Krümmel and Harms, 1982) and the purity of the cultures was checked by microscopy. ATP was measured using a commercial ATP kit (BacTiterGlo, PROMEGA GmbH, Germany) combined with a luminometer (GloMax 20/20, PROMEGA GmbH, Germany). To sterilize sample S12 the soil was placed into a desiccator, along with 1 ml methyl iodide (99% Reagent Plus, SIGMA-ALDRICH Chemie GmbH, Germany) in a separate bowl. The desiccator was evacuated and the soil sample was exposed to a high partial pressure of methyl iodide for 24 hours. The sample was measured directly after this procedure.

Calculations

Fluxes of HONO, NO and NO_2 were calculated using the following formula:

$$F_N = \frac{Q}{A} \cdot (\chi_{out} - \chi_{in}) \cdot \frac{M_N}{V_m} \tag{32}$$

with F_N the flux of trace gas in terms of N (ng m^{-2} s^{-1}), the purging flow rate Q (m^3 s^{-1}), the headspace mixing ratio at outlet and inlet of the chamber χ_{out} and χ_{in} (ppb), the area

of soil A (m^2), the molar volume of air V_m (m^3 mol^{-1}) and the molar mass of nitrogen M_N (g mol^{-1}).

The uncertainties of the fluxes (ΔF_N) were calculated using Gaussian error propagation, neglecting the potential error of V_m. For the inlet and outlet mixing ratios (χ_{in} and χ_{out}) the errors are identical since $\Delta\chi$ was set to the noise of the instrument at the limit of detection (LOD):

$$\Delta F_N = \pm\sqrt{\left(\left[\left(\frac{\partial F_N}{\partial Q}\right)_{A,\chi_{in/out}}\cdot\Delta Q\right]^2+\left[\left(\frac{\partial F_N}{\partial A}\right)_{Q,\chi_{in/out}}\cdot\Delta A\right]^2+\left[2\cdot\left(\frac{\partial F_N}{\partial \chi}\right)_{A,Q,\chi_{in}}\cdot\Delta\chi_{out}\right]^2\right)} \quad (33)$$

The area of the soil was calculated from the radius of the dish, which had an error of approximately 2 mm. The error of the purging air flow rate Q was calculated from the noise (3σ) of the measured flow rate. All measured values of χ_{out} that were not significantly different from χ_{in} were rejected.

We calculated the loss of water during the experiment from weighing the soil sample before and after the experiment and from the humidity measurements in the sample air, and subsequently derived the soil water content (normalized by the water holding capacity, see table S1):

$$SWC(t) = \left(1 - \frac{m(\text{loss of water})}{m(\text{dry soil})}\cdot\frac{\int_{t=0}^{t} RH(t)\cdot dt}{\int_{t=0}^{t_{max}} RH(t)\cdot dt}\cdot\frac{100}{whc}\right) \quad (34)$$

where SWC(t) is the soil water content (%) at time t (s), m(loss of water) is the mass of water (kg) evaporated from the soil during dry out, m(dry soil) is the mass of dry soil (kg), RH(t) is the relative humidity in the sample air (%) at time t and whc is the water holding capacity (%), defined as:

$$whc = \frac{m_{sat}(\text{water})}{m(\text{dry soil})}\% \quad (35)$$

where m_{sat}(water) is the mass of water in soil at field capacity (kg).

The NO_2^- and NH_4^+ concentrations at optimum SWC were calculated using the following equations:

$$\left[NO_2^-\right] = \frac{\rho(\text{water})}{SWC \cdot whc} \cdot \frac{\%\text{m}\left(NO_2^-\right)}{\text{M}(\text{N})} \tag{36}$$

$$\left[NH_4^+\right] = \frac{\rho(\text{water})}{SWC \cdot whc} \cdot \frac{\%\text{m}\left(NH_4^+\right)}{\text{M}(\text{N})} \tag{37}$$

where $[NO_2^-]$ and $[NH_4^+]$ are the concentrations (mmol l^{-1}), ρ(water) is the density of water (kg l^{-1}), M(N) is the molecular mass of nitrogen (g mol^{-1}) and $\%m(NO_2^-)$ and $\%m(NH_4^+)$ are the nutrient contents of dry soil (mg kg^{-1}) (see table S1).

Supplementary Text

All reported fluxes were calculated for χ_{in} equal to 0 ppb and, thus, represent fluxes prevailing under clean background conditions (very low atmospheric mixing ratios of trace gases) and may be considered as upper limit estimates. Typical daytime mixing ratios of HONO (50 – 500 ppt) (Rohrer et al., 2005) are much lower than those of NO (1-10 ppb) (Gelfand et al., 2009; Stella et al., 2012; Rummel et al., 2002) in remote regions. Hence, the ratio of net HONO to NO fluxes should be even higher under these conditions.

$F_{N,opt}$(HONO) and $F_{N,opt}$(NO) were found to correlate only slightly with the calculated NO_2^- concentration at optimum SWC (R^2 = 0.52 and 0.51, respectively) and even less with NH_4^+ concentrations at optimum SWC (R^2 = 0.39 and 0.41, respectively).

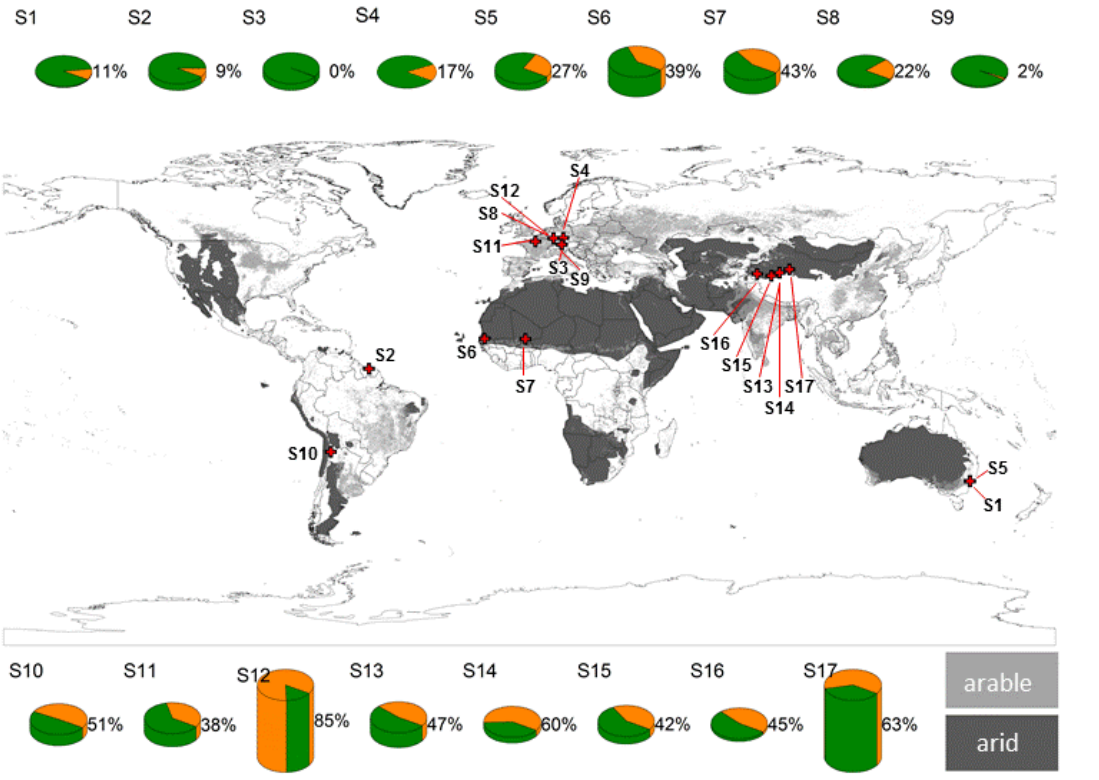

Figure 34. Global map (2000-2013) showing the contribution of $F_{N,opt}$(HONO) (orange) and $F_{N,opt}$(NO) (green) to their sum for the soil samples analyzed in this study. The height of the pie chart reflects the total emission flux (sum of $F_{N,opt}$(HONO) and $F_{N,opt}$(NO)). Light and dark grey shading of the map represent arable land use and arid climate according to Koeppen-Geiger climate zones (Kottek et al., 2006). Black bordered red crosses mark the soil sampling sites (see Materials and Methods).

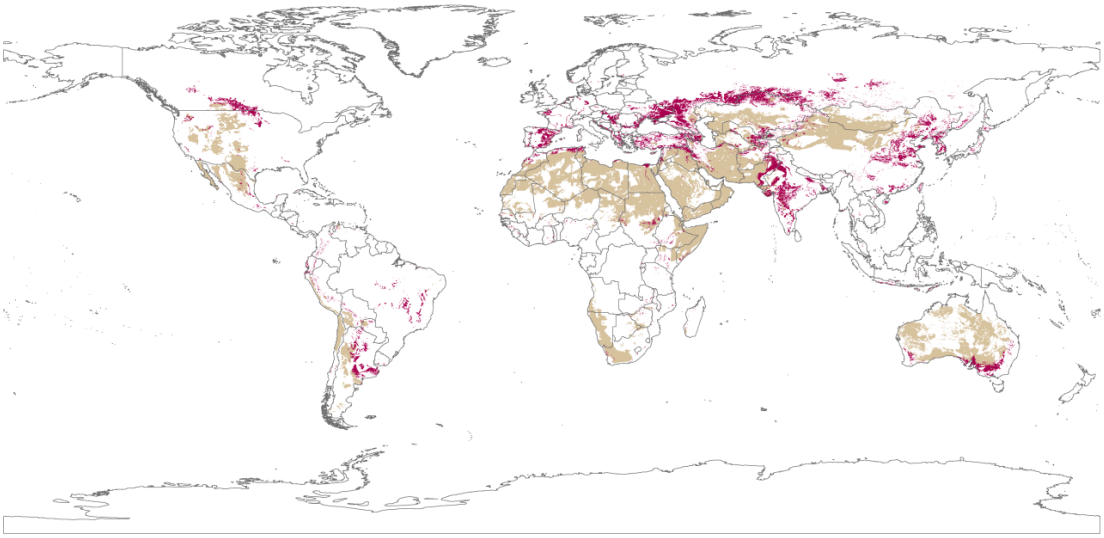

Figure 35. Global map (2000-2013) showing the potential HONO soil emission hot spots. The light brown color-code represents arid land with pH ≥ 7 and the dark red color-code refers to arable land with pH ≥ 7. The pH values were taken from (1998).

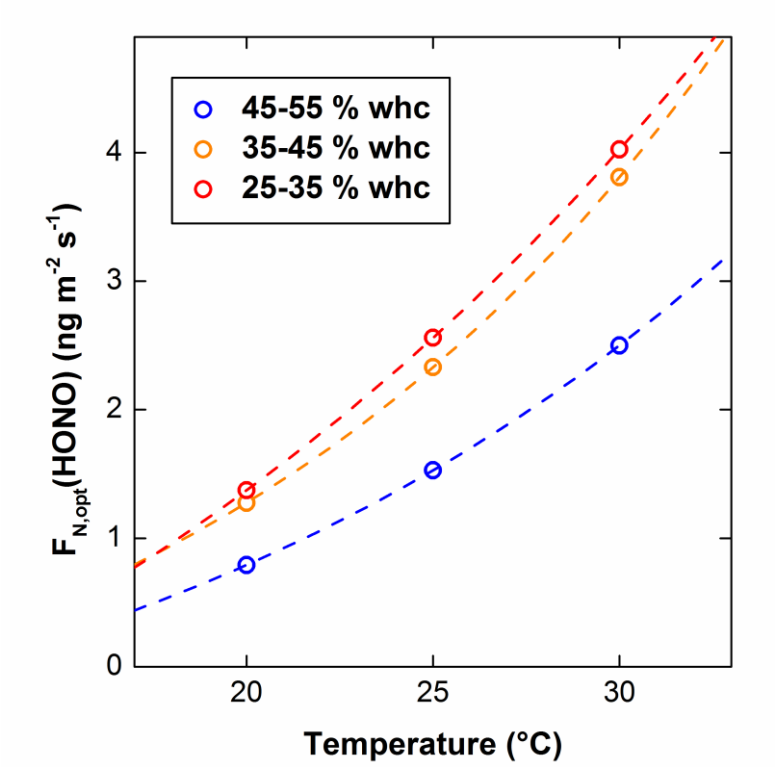

Figure 36. Temperature dependency of $F_{N,opt}$(HONO) measured for soil sample S8 for three different SWC ranges.

Table S1.

Physicochemical soil properties (nutrient content is shown in terms of N; n.a. = not analyzed, LOD of NO_2^- is 0.15 mg kg^{-1}).

soil sample	pH	nitrite	nitrate	ammonium	loss on ignition	C/N	sand	clay	gravimetric soil water content at whc
	1	mg kg^{-1}	mg kg^{-1}	mg kg^{-1}	%	1	%	%	%
S1	3.7	<LOD	12.3	1.3	4.4	39.2	77.4	8.7	68.8
S2	4.0	<LOD	4.9	83.4	18.2	13.8	n.a.	n.a.	143.3
S3	4.6	<LOD	3.5	36.6	37.1	18.9	n.a.	n.a.	188.8
S4	4.8	1.0	5.7	48.4	85.3	20.1	n.a.	n.a.	577.1
S5	5.4	<LOD	17.5	2.9	3.5	12.8	79.2	8.3	62.7
S6	5.6	<LOD	6.4	7.1	0.8	5.4	89.7	7.2	36.0
S7	5.9	0.3	5.6	2.7	0.7	10.0	90.3	8.7	37.1
S8	6.1	<LOD	0.7	19.4	10.0	14.6	38.4	25.6	74.9
S9	6.4	1.6	14.6	4.6	18.3	10.6	17.2	32.9	116.1
S10	6.5	<LOD	0.1	5.3	n.a.	n.a.	n.a.	n.a.	35.0
S11	6.9	<LOD	25.3	6.0	5.3	11.7	5.0	25.3	54.9
S12	7.2	1.0	77.7	18.1	5.2	10.5	21.7	27.8	63.5
S13	7.8	0.2	37.8	4.2	2.7	42.2	29.9	11.7	28.9
S14	8.0	<LOD	41.5	2.6	4.0	41.5	21.0	17.0	33.1
S15	8.2	<LOD	14.2	1.8	1.9	98.0	29.9	5.2	29.7
S16	8.4	<LOD	4.2	0.8	2.1	82.0	55.3	3.4	24.0
S17	8.8	1.1	691.7	83.0	7.4	40.6	21.4	11.2	30.6

Appendix B: Co-author publications

- Su, H., Cheng, Y., Oswald, R., Behrendt, T., Trebs, I., Meixner, F. X., Andreae, M. O., Cheng, P., Zhang, Y., and Pöschl, U.: Soil Nitrite as a Source of Atmospheric HONO and OH Radicals, Science, 333, 1616-1618, 10.1126/science.1207687, 2011.

- Williams, J., Crowley, J., Fischer, H., Harder, H., Martinez, M., Petaja, T., Rinne, J., Back, J., Boy, M., Dal Maso, M., Hakala, J., Kajos, M., Keronen, P., Rantala, P., Aalto, J., Aaltonen, H., Paatero, J., Vesala, T., Hakola, H., Levula, J., Pohja, T., Herrmann, F., Auld, J., Mesarchaki, E., Song, W., Yassaa, N., Nolscher, A., Johnson, A. M., Custer, T., Sinha, V., Thieser, J., Pouvesle, N., Taraborrelli, D., Tang, M. J., Bozem, H., Hosaynali-Beygi, Z., Axinte, R., Oswald, R., Novelli, A., Kubistin, D., Hens, K., Javed, U., Trawny, K., Breitenberger, C., Hidalgo, P. J., Ebben, C. J., Geiger, F. M., Corrigan, A. L., Russell, L. M., Ouwersloot, H. G., de Arellano, J. V. G., Ganzeveld, L., Vogel, A., Beck, M., Bayerle, A., Kampf, C. J., Bertelmann, M., Kollner, F., Hoffmann, T., Valverde, J., Gonzalez, D., Riekkola, M. L., Kulmala, M., and Lelieveld, J.: The summertime Boreal forest field measurement intensive (HUMPPA-COPEC-2010): an overview of meteorological and chemical influences, Atmospheric Chemistry and Physics, 11, 10599-10618, 10.5194/acp-11-10599-2011, 2011.

- Trebs, I., Oswald, R., Behrendt, T., and Meixner, F. X.: From the Soil into the Air, Nachrichten Aus Der Chemie, 60, 29-30, 2012.

- Breuninger, C., Oswald, R., Kesselmeier, J., and Meixner, F. X.: The dynamic chamber method: trace gas exchange fluxes (NO, NO2, O3) between plants and the atmosphere in the laboratory and in the field, Atmospheric Measurement Techniques, 5, 955-989, 10.5194/amt-5-955-2012, 2012.

- Hens, K., Novelli, A., Martinez, M., Auld, J., Axinte, R., Bohn, B., Fischer, H., Keronen, P., Kubistin, D., Nölscher, A. C., Oswald, R., Paasonen, P., Petäjä, T., Regelin, E., Sander, R., Sinha, V., Sipilä, M., Taraborrelli, D., Tatum Ernest, C., Williams, J., Lelieveld, J., and Harder, H.: Observation and modelling of HOx radicals in a boreal forest, Atmos. Chem. Phys. Discuss., 13, 28561-28629, 10.5194/acpd-13-28561-2013, 2013.

- Ermel, M., Oswald, R., Mayer, J. C., Moravek, A., Song, G., Beck, M., Meixner, F. X., and Trebs, I.: Preparation Methods to Optimize the Performance of Sensor Discs for Fast Chemiluminescence Ozone Analyzers, Environmental Science & Technology, 47, 1930-1936, 10.1021/es3040363, 2013.

Appendix C: List of figures

References

See supplementary materials.

Data from IGBP-DIS SoilData: A program for creating global soil-property databases, 2013, 1998.

VDS Technologies, World Data, 2000-2013.

Abida, O., Du, J., and Zhu, L.: Investigation of the photolysis of the surface-adsorbed HNO_3 by combining laser photolysis with Brewster angle cavity ring-down spectroscopy, Chem. Phys. Lett., 534, 77-82, 10.1016/j.cplett.2012.03.034, 2012.

Acker, K., Moller, D., Wieprecht, W., Meixner, F. X., Bohn, B., Gilge, S., Plass-Dülmer, C., and Berresheim, H.: Strong daytime production of OH from HNO_2 at a rural mountain site, Geophysical Research Letters, 33, L02809, doi:02810.01029/02005GL024643, 2006.

Alicke, B., Platt, U., and Stutz, J.: Impact of nitrous acid photolysis on the total hydroxyl radical budget during the Limitation of Oxidant Production/Pianura Padana Produzione di Ozono study in Milan, J. Geophys. Res., 107, LOP9-1-LOP9-LOP9-17, 10.1029/2000jd000075, 2002.

Allison, F. E.: Losses of gaseous nitrogen from soils by chemical mechanisms involving nitrous acid and nitrites, Soil Sci, 96, 404-409, 10.1097/00010694-196312000-00007, 1963.

Anthonisen, A. C., Loehr, R. C., Prakasam, T. B. S., and Srinath, E. G.: Inhibition of Nitrification by Ammonia and Nitrous Acid, Journal (Water Pollution Control Federation), 48, 835-852, 1976.

Asahi, R., and Morikawa, T.: Nitrogen complex species and its chemical nature in TiO2 for visible-light sensitized photocatalysis, Chemical Physics, 339, 57-63, 2007.

Asatryan, R., Bozzelli, J. W., and Simmie, J. M.: Thermochemistry for enthalpies and reaction paths of nitrous acid isomers, Int. J. Chem. Kinet., 39, 378-398, 2007.

Atkinson, R., Baulch, D. L., Cox, R. A., Crowley, J. N., Hampson, R. F., Hynes, R. G., Jenkin, M. E., Rossi, M. J., and Troe, J.: Evaluated kinetic and photochemical data for atmospheric chemistry:

Volume I - gas phase reactions of O_x, HO_x, NO_x and SO_x species, Atmospheric Chemistry and Physics, 4, 1461-1738, 2004.

Aubin, D. G., and Abbatt, J. P. D.: Interaction of NO_2 with hydrocarbon soot: Focus on HONO yield, surface modification, and mechanism, Journal of Physical Chemistry A, 111, 6263-6273, 2007.

Baergen, A. M., and Donaldson, D. J.: Photochemical Renoxification of Nitric Acid on Real Urban Grime, Environmental Science & Technology, 47, 815-820, 10.1021/es3037862, 2013.

Bargsten, A., Falge, E., Pritsch, K., Huwe, B., and Meixner, F. X.: Laboratory measurements of nitric oxide release from forest soil with a thick organic layer under different understory types, Biogeosciences, 7, 1425-1441, 10.5194/bg-7-1425-2010, 2010.

Becker, K. H., Kleffmann, J., Kurtenbach, R., and Wiesen, P.: Solubility of nitrous acid (HONO) in sulfuric acid solutions, J. Phys. Chem., 100, 14984-14990, 10.1021/jp961140r, 1996.

Becker, K. H., Kleffmann, J., Negri, R. M., and Wiesen, P.: Solubility of nitrous acid (HONO) in ammonium sulfate solutions, J. Chem. Soc.-Faraday Trans., 94, 1583-1586, 10.1039/a800458g, 1998.

Bedjanian, Y., and El Zein, A.: Interaction of NO2 with TiO2 Surface Under UV Irradiation: Products Study, Journal of Physical Chemistry A, 116, 1758-1764, 10.1021/jp210078b, 2012.

Bejan, I., Abd El Aal, Y., Barnes, I., Benter, T., Bohn, B., Wiesen, P., and Kleffmann, J.: The photolysis of ortho-nitrophenols: a new gas phase source of HONO, Physical Chemistry Chemical Physics, 8, 2028-2035, 2006.

Blume, H.-P., Deller, B., Furtmann, K., Leschber, R., Paetz, A., and Wilke, B.-M.: Handbuch der Bodenuntersuchung, 1 ed., Wiley-VCH, Weinheim, 2000.

Bohn, B., Corlett, G. K., Gillmann, M., Sanghavi, S., Stange, G., Tensing, E., Vrekoussis, M., Bloss, W. J., Clapp, L. J., Kortner, M., Dorn, H. P., Monks, P. S., Platt, U., Plass-Dulmer, C., Mihalopoulos, N., Heard, D. E., Clemitshaw, K. C., Meixner, F. X., Prevot, A. S. H., and Schmitt, R.: Photolysis frequency measurement techniques: results of a comparison within the ACCENT project, Atmospheric Chemistry and Physics, 8, 5373-5391, 2008.

Borrell, P., Builtjes, P., Grennfelt, P., Hov, O., van Aalst, R., Fowler, D., Megie, G., Moussiopoulos, N., Warneck, P., Volz-Thomas, A., and Wayne, R.: EUROTRAC: Applications to photo-oxidants and the future project, in: Atmospheric Ozone Dynamics: Observations in the Mediterranean Region, edited by: Varotsos, C., Nato Advanced Science Institute Series, Series I, Global Environment Change, Springer-Verlag Berlin, Berlin, 1-7, 1997.

Breuer, L., Kiese, R., and Butterbach-Bahl, K.: Temperature and moisture effects on nitrification rates in tropical rain-forest soils, Soil Science Society of America Journal, 66, 834-844, 2002.

Breuninger, C., Oswald, R., Kesselmeier, J., and Meixner, F. X.: The dynamic chamber method: trace gas exchange fluxes (NO, NO_2, O_3) between plants and the atmosphere in the laboratory and in the field, Atmospheric Measurement Techniques, 5, 955-989, 10.5194/amt-5-955-2012, 2012.

Burkholder, J. B., Mellouki, A., Talukdar, R., and Ravishankara, A. R.: Rate coefficients for the reaction of OH with HONO between 298 K and 373 K, Int. J. Chem. Kinet., 24, 711-725, 10.1002/kin.550240805, 1992.

Campbell, G. s.: A Simple Method for Determining Unsaturated Conductivity From Moisture Retention Data, Soil Sci., 117, 311-314, 1974.

Canfield, D. E., Glazer, A. N., and Falkowski, P. G.: The Evolution and Future of Earth's Nitrogen Cycle, Science, 330, 192-196, 10.1126/science.1186120, 2010.

Chan, W.-T., Heck, S. M., and Pritchard, H. O.: Reaction of nitrogen dioxide with hydrocarbons and its influence on spontaneous ignition. A computational study, Physical Chemistry Chemical Physics, 3, 56-62, 10.1039/B006088G, 2001.

Chan, W. H., Nordstrom, R. J., Calvert, J. G., and Shaw, J. H.: Kinetic study of HONO formation and decay reactions in gaseous mixtures of HONO, NO, NO2, H2O, AND N2, Environmental Science & Technology, 10, 674-682, 10.1021/es60118a007, 1976.

Chen, G., Shen, Y., Zhang, Q., Yao, M., Zheng, Z., and Liu, H.: Experimental study on combustion and emission characteristics of a diesel engine fueled with 2,5-dimethylfuran–diesel, n-butanol–diesel and gasoline–diesel blends, Energy, 54, 333-342, http://dx.doi.org/10.1016/j.energy.2013.02.069, 2013.

Clayden, J.: Organic chemistry, Oxford University Press, Oxford, 1508p : ill. (chiefly col.) ; 1528 cm. pp., 2001.

Clothier, P. Q. E., Aguda, B. D., Moise, A., and Pritchard, H. O.: How do diesel-fuel ignition improvers work?, Chemical Society Reviews, 22, 101-108, 10.1039/CS9932200101, 1993a.

Clothier, P. Q. E., Pritchard, H. O., and Poirier, M. A.: Synergy between additives in stimulating diesel-fuel ignition, Combust. Flame, 95, 427-429, 10.1016/0010-2180(93)90008-q, 1993b.

Conrad, R.: Compensation concentration as critical variable for regulating the flux of trace gases between soil and atmosphere, Biogeochemistry, 27, 155-170, 1994.

Conrad, R.: Soil microorganisms as controllers of atmospheric trace gases (H_2, CO, CH_4, OCS, N_2O, and NO), Microbiological Reviews, 60, 609-+, 1996.

Cook, M. J., Dassanayake, N. L., Johnson, C. D., Katritzky, A. R., and Toone, T. W.: Acidity functions and protonation of weak bases - Temperature-variation of hr-acidity function in aqueous sulfuric-acid, J. Am. Chem. Soc., 97, 760-764, 10.1021/ja00837a012, 1975.

Cox, R. A., Derwent, R. G., and Holt, P. M.: RELATIVE RATE CONSTANTS FOR REACTIONS OF OH RADICALS WITH H-2, CH4, CO, NO AND HONO AT ATMOSPHERIC-PRESSURE AND 296 K, Journal of the Chemical Society-Faraday Transactions I, 72, 2031-2043, 10.1039/f19767202031, 1976.

Crutzen, P. J.: Role of NO and NO_2 in the chemistry of the troposphere and stratosphere, Annu. Rev. Earth Planet. Sci., 7, 443-472, 10.1146/annurev.ea.07.050179.002303, 1979.

Currie, J. A.: Gaseous diffusion in porous media. III. Wet granular materials, Br. J. Appl. Phys., 12, 275-281281, 10.1088/0508-3443/12/6/303, 1961.

da Silva, G., Kennedy, E. M., and Dlugogorski, B. Z.: Ab initio procedure for aqueous-phase pKa calculation: The acidity of nitrous acid, Journal of Physical Chemistry A, 110, 11371-11376, 10.1021/jp0639243, 2006.

Davidson, E. A., Janssens, I. A., and Luo, Y. Q.: On the variability of respiration in terrestrial ecosystems: moving beyond Q(10), Global Change Biology, 12, 154-164, 10.1111/j.1365-2486.2005.01065.x, 2006.

De Jesus Medeiros, D., and Pimentel, A. S.: New insights in the atmospheric HONO formation: New pathways for N_2O_4 isomerization and NO_2 dimerization in the presence of water, Journal of Physical Chemistry A, 115, 6357-6365, 2011.

de Lima, R. G., Sauaia, M. G., Bonaventura, D., Tedesco, A. C., Vianna Lopez, R. F., Bendhack, L. M., and da Silva, R. S.: Controlled nitric oxide photo-release from nitro ruthenium complexes: The vasodilator response produced by UV light irradiation, Inorganica Chimica Acta, 358, 2643-2650, http://dx.doi.org/10.1016/j.ica.2005.03.019, 2005.

De Mare, G. R., and Moussaoui, Y.: Theoretical study of the nitrous acid conformers: Comparison of theoretical and experimental structures, relative energies, barrier to rotation and vibrational frequencies, International Reviews in Physical Chemistry, 18, 91-117, 10.1080/014423599230017, 1999.

El Zein, A., and Bedjanian, Y.: Reactive Uptake of HONO to TiO2 Surface: "Dark" Reaction, Journal of Physical Chemistry A, 116, 3665-3672, 10.1021/jp300859w, 2012.

Elshorbany, Y. F., Steil, B., Brühl, C., and Lelieveld, J.: Impact of HONO on global atmospheric chemistry calculated with an empirical parameterization in the EMAC model, Atmospheric Chemistry and Physics, 12, 9977-10000, 10.5194/acp-12-9977-2012, 2012.

Estabrook, R. W.: A passion for P450s (remembrances of the early history of research on cytochrome P450), Drug Metabolism and Disposition, 31, 1461-1473, 10.1124/dmd.31.12.1461, 2003.

Feig, G. T., Mamtimin, B., and Meixner, F. X.: Soil biogenic emissions of nitric oxide from a semi-arid savanna in South Africa, Biogeosciences, 5, 1723-1738, 2008.

Ferm, M., and Sjödin, A.: A sodium carbonate coated denuder for determination of nitrous acid in the atmosphere, Atmospheric Environment (1967), 19, 979-983, http://dx.doi.org/10.1016/0004-6981(85)90243-4, 1985.

Finlayson-Pitts, B. J., and Pitts, J. N.: Tropospheric air pollution: Ozone, airborne toxics, polycyclic aromatic hydrocarbons, and particles, Science, 276, 1045-1052, 10.1126/science.276.5315.1045, 1997.

Finlayson-Pitts, B. J., Wingen, L. M., Sumner, A. L., Syomin, D., and Ramazan, K. A.: The heterogeneous hydrolysis of NO_2 in laboratory systems and in outdoor and indoor atmospheres: An integrated mechanism, Physical Chemistry Chemical Physics, 5, 223-242, 10.1039/b208564j, 2003.

Firestone, M. K., and Davidson, E. A.: Microbiological basis of NO and N2O production and consumption in soil, in: Exchange of trace gases between terrestrial ecosystems and the atmosphere, edited by: Andreae, M. O., and Schimel, D. S., Wiley, Chichester, 7-21, 1989.

Fowler, D., Coyle, M., Skiba, U., Sutton, M. A., Cape, J. N., Reis, S., Sheppard, L. J., Jenkins, A., Grizzetti, B., Galloway, J. N., Vitousek, P., Leach, A., Bouwman, A. F., Butterbach-Bahl, K., Dentener, F., Stevenson, D., Amann, M., and Voss, M.: The global nitrogen cycle in the twenty-first century, Philosophical Transactions of the Royal Society B: Biological Sciences, 368, 10.1098/rstb.2013.0164, 2013.

Galloway, J. N., Leach, A. M., Bleeker, A., and Erisman, J. W.: A chronology of human understanding of the nitrogen cycle, Philosophical Transactions of the Royal Society B: Biological Sciences, 368, 10.1098/rstb.2013.0120, 2013.

Gelfand, I., Feig, G., Meixner, F. X., and Yakir, D.: Afforestation of semi-arid shrubland reduces biogenic NO emission from soil, Soil Biology & Biochemistry, 41, 1561-1570, 10.1016/j.soilbio.2009.04.018, 2009.

Dicke Luft? Pusteblume! - AirClean® das aktive Betonpflaster: http://braun-steine.de/stadt-und-objektbau/airclean/, 2014.

Gödde, M., and Conrad, R.: Simultaneous measurement of nitric oxide production and consumption in soil using a simple static incubation system, and the effect of soil water content on the contribution of nitrification, Soil Biology & Biochemistry, 30, 433-442, 10.1016/s0038-0717(97)00197-1, 1998.

Gödde, M., and Conrad, R.: Influence of soil properties on the turnover of nitric oxide and nitrous oxide by nitrification and denitrification at constant temperature and moisture, Biology and Fertility of Soils, 32, 120-128, 2000.

Goedde, M., and Conrad, R.: Immediate and adaptational temperature effects on nitric oxide production and nitrous oxide release from nitrification and denitrification in two soils, Biology and Fertility of Soils, 30, 33-40, 1999.

Goodman, A. L., Bernard, E. T., and Grassian, V. H.: Spectroscopic Study of Nitric Acid and Water Adsorption on Oxide Particles: Enhanced Nitric Acid Uptake Kinetics in the Presence of Adsorbed Water, The Journal of Physical Chemistry A, 105, 6443-6457, 10.1021/jp003722l, 2001.

Harrison, R. M., and Kitto, A. M. N.: Evidence for a Surface Source of Atmospheric Nitrous-Acid, Atmospheric Environment, 28, 1089-1094, 1994.

Harrison, R. M., Peak, J. D., and Collins, G. M.: Tropospheric cycle of nitrous acid, Journal of Geophysical Research-Atmospheres, 101, 14429-14439, 1996.

Haynes, W. M., and Lide, D. R.: Handbook of chemistry and physics [electronic resource] : editor-in-chief W. M. Haynes, 92nd ed. ed., CRC Press, Cleveland, Ohio, ill., 2011.

Heland, J., Kleffmann, J., Kurtenbach, R., and Wiesen, P.: A new instrument to measure gaseous nitrous acid (HONO) in the atmosphere, Environmental Science & Technology, 35, 3207-3212, 10.1021/es000303t, 2001.

Hens, K., Novelli, A., Martinez, M., Auld, J., Axinte, R., Bohn, B., Fischer, H., Keronen, P., Kubistin, D., Nölscher, A. C., Oswald, R., Paasonen, P., Petäjä, T., Regelin, E., Sander, R., Sinha, V., Sipilä, M., Taraborrelli, D., Tatum Ernest, C., Williams, J., Lelieveld, J., and Harder, H.: Observation and modelling of HO_x radicals in a boreal forest, Atmos. Chem. Phys. Discuss., 13, 28561-28629, 10.5194/acpd-13-28561-2013, 2013.

Hillel, D., Warrick, A. W., Baker, R. S., Rosenzweig, C., and ebrary, I.: Environmental soil physics, Academic Press, San Diego, Calif. ;

London, xxvii, 771p. : ill. ; 726cm. pp., 1998.

Horowitz, L. W., and Jacob, D. J.: Global impact of fossil fuel combustion on atmospheric NOx, Journal of Geophysical Research: Atmospheres, 104, 23823-23840, 10.1029/1999JD900205, 1999.

Hosaynali Beygi, Z., Fischer, H., Harder, H. D., Martinez, M., Sander, R., Williams, J., Brookes, D. M., Monks, P. S., and Lelieveld, J.: Oxidation photochemistry in the Southern Atlantic boundary layer: unexpected deviations of photochemical steady state, Atmos. Chem. Phys., 11, 8497-8513, 10.5194/acp-11-8497-2011, 2011.

Hov, O.: Photo-oxidants, acidification and tools: Policy application of EUROTRAC results, Proceedings of Eurotrac Symposium '96 - Transport and Transformation of Pollutants in the Troposphere, Vol 1: Clouds, Aerosols, Modelling and Photo-Oxidants, edited by: Borrell, P. M., Borrell, P., Kelly, K., Cvitas, T., and Seiler, W., Computational Mechanics Publications Ltd, Southampton, 1029-1029 pp., 1997.

IPCC: Climate Change 2007: The Physical Science Basis. Contribution of Working Group I to the Fourth Assessment Report of the Intergovernmental Panel on Climate Change, Cambridge, United Kindom and New York, USA, 2007.

Islam, A., Chen, D., White, R. E., and Weatherley, A.: Chemical decomposition and fixation of nitrite in acidic pasture soils and implications for measurement of nitrification, Soil Biology & Biochemistry, 40, 262-265, 10.1016/j.soilbio.2007.07.008, 2008.

Jacob, D. J.: Heterogeneous chemistry and tropospheric ozone, Atmospheric Environment, 34, 2131-2159, 10.1016/s1352-2310(99)00462-8, 2000.

Jiang, Q. Q., and Bakken, L. R.: Comparison of Nitrosospira strains isolated from terrestrial environments, Fems Microbiology Ecology, 30, 171-186, 10.1111/j.1574-6941.1999.tb00646.x, 1999.

Junninen, H., Lauri, A., Keronen, P., Aalto, P., Hiltunen, V., Hari, P., and Kulmala, M.: Smart-SMEAR: on-line data exploration and visualization tool for SMEAR stations., Boreal Environ. Res., 14, 447-457, 2009.

Jurkat, T., Voigt, C., Arnold, F., Schlager, H., Kleffmann, J., Aufmhoff, H., Schauble, D., Schaefer, M., and Schumann, U.: Measurements of HONO, NO, NOy and SO2 in aircraft exhaust plumes at cruise, Geophysical Research Letters, 38, 10.1029/2011gl046884, 2011.

Kaiser, E. W., and Wu, C. H.: Measurement of rate constant of reaction of nitrous-acid with nitric-acid, J. Phys. Chem., 81, 187-190, 10.1021/j100518a001, 1977.

Kebede, M. A., Scharko, N. K., Appelt, L. E., and Raff, J. D.: Formation of Nitrous Acid during Ammonia Photooxidation on TiO2 under Atmospherically Relevant Conditions, The Journal of Physical Chemistry Letters, 4, 2618-2623, 10.1021/jz401250k, 2013.

Kerbrat, M., Huthwelker, T., Gaggeler, H. W., and Ammann, M.: Interaction of Nitrous Acid with Polycrystalline Ice: Adsorption on the Surface and Diffusion into the Bulk, J. Phys. Chem. C, 114, 2208-2219, 10.1021/jp909535c, 2010.

Khalizov, A. F., Cruz-Quinones, M., and Zhang, R. Y.: Heterogeneous Reaction of NO2 on Fresh and Coated Soot Surfaces, Journal of Physical Chemistry A, 114, 7516-7524, 10.1021/jp1021938, 2010.

Kleffmann, J., Heland, J., Kurtenbach, R., Lörzer, J., and Wiesen, P.: A new instrument (LOPAP) for the detection of nitrous acid (HONO), Environmental Science and Pollution Research, 48-54, 2002.

Kleffmann, J., Kurtenbach, R., Lörzer, J., Wiesen, P., Kalthoff, N., Vogel, B., and Vogel, H.: Measured and simulated vertical profiles of nitrous acid - Part I: Field measurements, Atmospheric Environment, 37, 2949-2955, 10.1016/s1352-2310(03)00242-5, 2003.

Kleffmann, J., Gavriloaiei, T., Hofzumahaus, A., Holland, F., Koppmann, R., Rupp, L., Schlosser, E., Siese, M., and Wahner, A.: Daytime formation of nitrous acid: A major source of OH radicals in a forest, Geophysical Research Letters, 32, 2005.

Kleffmann, J.: Daytime sources of nitrous acid (HONO) in the atmospheric boundary layer, ChemPhysChem, 8, 1137-1144, 2007.

Koops, H.-P., Purkhold, U., Pommerening-Röser, A., Timmermann, G., and Wagner, M.: The Lithoautotrophic Ammonia-Oxidizing Bacteria, Prokaryotes: A Handbook on the Biology of Bacteria, Vol 5, Third Edition:Proteobacteria: Alpha and beta subclasses, edited by: Dworkin, M., Falkow, S., Rosenberg, E., Schleifer, K. H., and Stackebrandt, E., 778-811 pp., 2006.

Koops, H. P., and Pommerening-Röser, A.: Distribution and ecophysiology of the nitrifying bacteria emphasizing cultured species, Fems Microbiology Ecology, 37, 1-9, 10.1111/j.1574-6941.2001.tb00847.x, 2001.

Kottek, M., Grieser, J., rgen, Beck, C., Rudolf, B., and Rubel, F.: World Map of the Koppen-Geiger climate classification updated, Meteorologische Zeitschrift, 15, 259-263, 10.1127/0941-2948/2006/0130, 2006.

Kourtchev, I., Fuller, S., Aalto, J., Ruuskanen, T. M., McLeod, M. W., Maenhaut, W., Jones, R., Kulmala, M., and Kalberer, M.: Molecular Composition of Boreal Forest Aerosol from Hyytiala, Finland, Using Ultrahigh Resolution Mass Spectrometry, Environmental Science & Technology, 47, 4069-4079, 10.1021/es3051636, 2013.

Kraus, A., and Hofzumahaus, A.: Field measurements of atmospheric photolysis frequencies for O_3, NO_2, HCHO, CH_3CHO, H_2O_2, and HONO by UV spectroradiometry, J. Atmos. Chem., 31, 161-180, 1998.

Krümmel, A., and Harms, H.: Effect of organic matter on growth and cell yield of ammonia oxidizing bacteria, Archives of Microbiology, 133, 50-54, 1982.

Kubota, M., and Asami, T.: Source of nitrous-acid volatilized from upland soils, Soil Sci. Plant Nutr., 31, 35-42, 1985a.

Kubota, M., and Asami, T.: Volatilization of nitrous-acid from upland soils, Soil Sci. Plant Nutr., 31, 27-34, 1985b.

Lammel, G., and Cape, J. N.: Nitrous acid and nitrite in the atmosphere, Chemical Society Reviews, 25, 361-369, 1996.

Lee, B. H., Wood, E. C., Herndon, S. C., Lefer, B. L., Luke, W. T., Brune, W. H., Nelson, D. D., Zahniser, M. S., and Munger, J. W.: Urban measurements of atmospheric nitrous acid: A caveat on the interpretation of the HONO photostationary state, Journal of Geophysical Research: Atmospheres, 118, 2013JD020341, 10.1002/2013JD020341, 2013.

Lee, Y. N., and Schwartz, S. E.: Evaluation of the rate of uptake of nitrogen-dioxide by atmospheric and surface liquid water, Journal of Geophysical Research-Oceans and Atmospheres, 86, 1971-1983, 10.1029/JC086iC12p11971, 1981.

Levine, J. S., Winstead, E. L., Parsons, D. A. B., Scholes, M. C., Scholes, R. J., Cofer, W. R., Cahoon, D. R., and Sebacher, D. I.: Biogenic soil emissions of nitric oxide (NO) and nitrous oxide (N_2O) from savannas in South Africa: The impact of wetting and burning, Journal of Geophysical Research-Atmospheres, 101, 23689-23697, 10.1029/96jd01661, 1996.

Li, X., Brauers, T., Haseler, R., Bohn, B., Fuchs, H., Hofzumahaus, A., Holland, F., Lou, S., Lu, K. D., Rohrer, F., Hu, M., Zeng, L. M., Zhang, Y. H., Garland, R. M., Su, H., Nowak, A., Wiedensohler, A., Takegawa, N., Shao, M., and Wahner, A.: Exploring the atmospheric chemistry of nitrous acid (HONO) at a rural site in Southern China, Atmospheric Chemistry and Physics, 12, 1497-1513, 10.5194/acp-12-1497-2012, 2012.

Linn, D. M., and Doran, J. W.: Effect of water-filled pore-space on carbon-dioxide and nitrous-oxide production in tilled and nontilled soils, Soil Science Society of America Journal, 48, 1267-1272, 1984.

Ludwig, J., Meixner, F. X., Vogel, B., and Forstner, J.: Soil-air exchange of nitric oxide: An overview of processes, environmental factors, and modeling studies, Biogeochemistry, 52, 225-257, 10.1023/a:1006424330555, 2001.

Maljanen, M., Yli-Pirilä, P., Hytönen, J., Joutsensaari, J., and Martikainen, P. J.: Acidic northern soils as sources of atmospheric nitrous acid (HONO), Soil Biology and Biochemistry, 67, 94-97, http://dx.doi.org/10.1016/j.soilbio.2013.08.013, 2013.

Mamtimin, B., Behrendt, T., Hempelmann, N., Qi, Y., Song, G., Wagner, T., Beirle, S., Bruse, M., Falge, E., Wu, Z., Li, Y., Li, J., Jin, H., Chu, X., Dong, Y., Zhu, Z., Yu, J., and Meixner, F. X.: The project “Desert encroachment in central Asia – Quantification of soil biogenic nitric oxide emissions by ground- and satellite-based methodologies (DEQNO)” – An overview, 2011.

Marshall, T. J.: The diffusion of gases through porous media, Journal of Soil Science, 10, 79-82, 10.1111/j.1365-2389.1959.tb00667.x, 1959.

Massman, W. J.: A review of the molecular diffusivities of H2O, CO2, CH4, CO, O3, SO2, NH3, N2O, NO, and NO2 in air, O2 and N2 near STP, Atmospheric Environment, 32, 1111-1127, http://dx.doi.org/10.1016/S1352-2310(97)00391-9, 1998.

McCaulley, J. A., Anderson, S. M., Jeffries, J. B., and Kaufman, F.: Kinetics of the reaction of CH_3O with NO_2, Chem. Phys. Lett., 115, 180-186, 10.1016/0009-2614(85)80675-8, 1985.

Meixner, F. X., and Yang, W. X.: Biogenic emissions of nitric oxide and nitrous oxide from arid and semi-arid land, Dryland Ecohydrology, edited by: Dodorico, P. P. A., 233-255 pp., 2006.

Millington, R. J., and Quirk, J. P.: Permeability of porous media, Nature, 183, 387-388, 10.1038/183387a0, 1959.

Mofijur, M., Atabani, A. E., Masjuki, H. H., Kalam, M. A., and Masum, B. M.: A study on the effects of promising edible and non-edible biodiesel feedstocks on engine performance and emissions production: A comparative evaluation, Renewable and Sustainable Energy Reviews, 23, 391-404, http://dx.doi.org/10.1016/j.rser.2013.03.009, 2013.

Moldrup, P., Olesen, T., Rolston, D. E., and Yamaguchi, T.: Modeling diffusion and reaction in soils .7. Predicting gas and ion diffusivity in undisturbed and sieved soils, Soil Sci., 162, 632-640, 10.1097/00010694-199709000-00004, 1997.

Moldrup, P., Olesen, T., Gamst, J., Schjonning, P., Yamaguchi, T., and Rolston, D. E.: Predicting the gas diffusion coefficient in repacked soil: Water-induced linear reduction model, Soil Science Society of America Journal, 64, 1588-1594, 2000.

Monge, M. E., D'Anna, B., Mazri, L., Giroir-Fendler, A., Ammann, M., Donaldson, D. J., and George, C.: Light changes the atmospheric reactivity of soot, Proc. Natl. Acad. Sci. U. S. A., 107, 6605-6609, 10.1073/pnas.0908341107, 2010.

Mougin, E., Hiernaux, P., Kergoat, L., Grippa, M., de Rosnay, P., Timouk, F., Le Dantec, V., Demarez, V., Lavenu, F., Arjounin, M., Lebel, T., Soumaguel, N., Ceschia, E., Mougenot, B., Baup, F., Frappart, F., Frison, P. L., Gardelle, J., Gruhier, C., Jarlan, L., Mangiarotti, S., Sanou, B., Tracol, Y., Guichard, F., Trichon, V., Diarra, L., Soumare, A., Koite, M., Dembele, F., Lloyd, C., Hanan, N. P., Damesin, C., Delon, C., Serca, D., Galy-Lacaux, C., Seghieri, J., Becerra, S., Dia, H., Gangneron, F., and Mazzega, P.: The AMMA-CATCH Gourma observatory site in Mali: Relating climatic variations to changes in vegetation, surface hydrology, fluxes and natural resources, Journal of Hydrology, 375, 14-33, 10.1016/j.jhydrol.2009.06.045, 2009.

Naegele, W., and Conrad, R.: Influence of soil pH on the nitrate-reducing microbial population and their potential to reduce nitrate tor nitric oxide and nitrous oxide, FEMS Microbiology Ecology, 74, 49-58, 1990.

Nash, T.: Nitrous-acid in atmosphere and laboratory experiments on its photolysis, Tellus, 26, 175-179, 1974.

The Nobel Prize in Physiology or Medicine 1998: http://www.nobelprize.org/nobel_prizes/medicine/laureates/1998/, access: 11.07.2013.

Nölscher, A. C., Williams, J., Sinha, V., Custer, T., Song, W., Johnson, A. M., Axinte, R., Bozem, H., Fischer, H., Pouvesle, N., Phillips, G., Crowley, J. N., Rantala, P., Rinne, J., Kulmala, M., Gonzales, D., Valverde-Canossa, J., Vogel, A., Hoffmann, T., Ouwersloot, H. G., de Arellano, J. V. G., and Lelieveld, J.: Summertime total OH reactivity measurements from boreal forest during HUMPPA-COPEC 2010, Atmospheric Chemistry and Physics, 12, 8257-8270, 10.5194/acp-12-8257-2012, 2012.

Novelli, A., Hens, K., Tatum Ernest, C., Kubistin, D., Regelin, E., Elste, T., Plass-Dülmer, C., Martinez, M., Lelieveld, J., and Harder, H.: Characterisation of an inlet pre-injector laser induced fluorescence instrument for the measurement of ambient hydroxyl radicals, Atmos. Meas. Tech. Discuss., 7, 819-858, 10.5194/amtd-7-819-2014, 2014.

Olesen, T., Moldrup, P., Henriksen, K., and Petersen, L. W.: Modeling diffusion and reaction in soils .4. New models for predicting ion diffusivity, Soil Sci., 161, 633-645, 10.1097/00010694-199610000-00001, 1996.

Ostwald, W.: Improvements in the Manufacture of Nitric Acid and Nitrogen Oxides., GBD190200698 19020109, 1902.

Oswald, R., Behrendt, T., Ermel, M., Wu, D., Su, H., Cheng, Y., Breuninger, C., Moravek, A., Mougin, E., Delon, C., Loubet, B., Pommerening-Röser, A., Sorgel, M., Pöschl, U., Hoffmann, T., Andreae, M. O., Meixner, F. X., and Trebs, I.: HONO Emissions from Soil Bacteria as a Major Source of Atmospheric Reactive Nitrogen, Science, 341, 1233-1235, 10.1126/science.1242266, 2013.

Ouwersloot, H. G., de Arellano, J. V. G., Nölscher, A. C., Krol, M. C., Ganzeveld, L. N., Breitenberger, C., Mammarella, I., Williams, J., and Lelieveld, J.: Characterization of a boreal convective boundary layer and its impact on atmospheric chemistry during HUMPPA-COPEC-2010, Atmospheric Chemistry and Physics, 12, 9335-9353, 10.5194/acp-12-9335-2012, 2012.

Pape, L., Ammann, C., Nyfeler-Brunner, A., Spirig, C., Hens, K., and Meixner, F. X.: An automated dynamic chamber system for surface exchange measurement of non-reactive and reactive trace gases of grassland ecosystems, Biogeosciences, 6, 405-429, 10.5194/bg-6-405-2009, 2009.

Park, J. Y., and Lee, Y. N.: Solubility and decomposition kinetics of nitrous-acid in aqueous-solution, J. Phys. Chem., 92, 6294-6302, 10.1021/j100333a025, 1988.

Park, S., Bae, W., Chung, J., and Baek, S.-C.: Empirical model of the pH dependence of the maximum specific nitrification rate, Process Biochemistry, 42, 1671-1676, 10.1016/j.procbio.2007.09.010, 2007.

Paul, E. A.: Soil microbiology, ecology, and biochemistry, 3rd ed. ed., Academic Press, Amsterdam ;

Boston, xx, 532 p. pp., 2007.

Penman, H. L.: Gas and vapour movements in the soil I. The diffusion of vapours through porous solids, Journal of Agricultural Science, 30, 437-462, 1940.

Perner, D., and Platt, U.: Detection of nitrous-acid in the atmosphere by differential optical-absorption, Geophysical Research Letters, 6, 917-920, 10.1029/GL006i012p00917, 1979.

Petäjä, T., Mauldin Iii, R. L., Kosciuch, E., McGrath, J., Nieminen, T., Paasonen, P., Boy, M., Adamov, A., Kotiaho, T., and Kulmala, M.: Sulfuric acid and OH concentrations in a boreal forest site, Atmos. Chem. Phys., 9, 7435-7448, 10.5194/acp-9-7435-2009, 2009.

Pilegaard, K.: Processes regulating nitric oxide emissions from soils, Philosophical transactions of the Royal Society of London. Series B, Biological sciences, 368, 20130126-20130126, 10.1098/rstb.2013.0126, 2013.

Pitts, J. N., Grosjean, D., Van Cauwenberghe, K., Schmid, J. P., and Fitz, D. R.: Photooxidation of aliphatic amines under simulated atmospheric conditions: formation of nitrosamines, nitramines, amides, and photochemical oxidant, Environmental Science & Technology, 12, 946-953, 10.1021/es60144a009, 1978.

Pitts, J. N., Biermann, H. W., Winer, A. M., and Tuazon, E. C.: Spectroscopic identification and measurement of gaseous nitrous-acid in dilute auto exhaust, Atmospheric Environment, 18, 847-854, 10.1016/0004-6981(84)90270-1, 1984.

Plake, D., and Trebs, I.: An automated system for selective and continuous measurements of vertical thoron profiles for the determination of transport times near the ground, Atmos. Meas. Tech., 6, 1017-1030, 10.5194/amt-6-1017-2013, 2013.

Pryor, W. A., Lightsey, J. W., and Church, D. F.: Reaction of nitrogen-dioxide with alkenes and poly-unsaturated fatty-acids - addition and hydrogen abstraction mechanisms, J. Am. Chem. Soc., 104, 6685-6692, 10.1021/ja00388a035, 1982.

Quastel, J. H.: soil metabolism, Annual Review of Plant Physiology, 16, 217-&, 10.1146/annurev.pp.16.060165.001245, 1965.

QUMA: Elektronik und Analytik GmbH, LOPAP - 03 Benutzerhandbuch Messgerät zur Bestimmung von salpetriger Säure (HONO), 2006.

Raivonen, M., Bonn, B., Sanz, M. J., Vesala, T., Kulmala, M., and Hari, P.: UV-induced NOy emissions from Scots pine: Could they originate from photolysis of deposited HNO3?, Atmospheric Environment, 40, 6201-6213, 10.1016/j.atmosenv.2006.03.063, 2006.

Ramazan, K. A., Syomin, D., and Finlayson-Pitts, B. J.: The photochemical production of HONO during the heterogeneous hydrolysis of NO_2, Physical Chemistry Chemical Physics, 6, 3836-3843, 2004.

Remde, A., Ludwig, J., Meixner, F. X., and Conrad, R.: A study to explain the emission of nitric-oxide from a marsh soil, J. Atmos. Chem., 17, 249-275, 10.1007/bf00694400, 1993.

Ren, X., Sanders, J. E., Rajendran, A., Weber, R. J., Goldstein, A. H., Pusede, S. E., Browne, E. C., Min, K. E., and Cohen, R. C.: A relaxed eddy accumulation system for measuring vertical fluxes of nitrous acid, Atmospheric Measurement Techniques, 4, 2093-2103, 10.5194/amt-4-2093-2011, 2011.

Rohrer, F., Bohn, B., Brauers, T., Bruning, D., Johnen, F. J., Wahner, A., and Kleffmann, J.: Characterisation of the photolytic HONO-source in the atmosphere simulation chamber SAPHIR, Atmospheric Chemistry and Physics, 5, 2189-2201, 2005.

Rohrer, F., and Berresheim, H.: Strong correlation between levels of tropospheric hydroxyl radicals and solar ultraviolet radiation, Nature, 442, 184-187, 10.1038/nature04924, 2006.

Roncaroli, F., Videla, M., Slep, L. D., and Olabe, J. A.: New features in the redox coordination chemistry of metal nitrosyls {M-NO+; M-NO center dot; M-NO- (HNO)}, Coordination Chemistry Reviews, 251, 1903-1930, 10.1016/j.ccr.2007.04.012, 2007.

Rousk, J., Baath, E., Brookes, P. C., Lauber, C. L., Lozupone, C., Caporaso, J. G., Knight, R., and Fierer, N.: Soil bacterial and fungal communities across a pH gradient in an arable soil, Isme Journal, 4, 1340-1351, 10.1038/ismej.2010.58, 2010.

Rummel, U., Ammann, C., Gut, A., Meixner, F. X., and Andreae, M. O.: Eddy covariance measurements of nitric oxide flux within an Amazonian rain forest, J. Geophys. Res., 107, LBA17-11-19, 10.1029/2601jd000520, 2002.

Russow, R., Stange, C. F., and Neue, H. U.: Role of nitrite and nitric oxide in the processes of nitrification and denitrification in soil: Results from N-15 tracer experiments, Soil Biology & Biochemistry, 41, 785-795, 10.1016/j.soilbio.2009.01.017, 2009.

Saad, O., and Conrad, R.: Temperature-dependence of nitrification, denitrification, and turnover of nitric-oxide in different soils, Biology and Fertility of Soils, 15, 21-27, 10.1007/bf00336283, 1993.

Sander, S. P., Abbatt, J. P. D., Barker, J. R., Burkholder, J. B., Friedl, R. R., Golden, D. M., Huie, R. E., Kolb, C. E., Kurylo, M. J., Moortgat, G. K., Orkin, V. L., and Wine, P. H.: Chemical Kinetics and Photochemical Data for Use in Atmospheric Studies, Evaluation No. 17, in: JPL Publication 10-6, Jet Propulsion Laboratory, Pasadena, 2011.

Schimang, R., Folkers, A., Kleffmann, J., Kleist, E., Miebach, M., and Wildt, J.: Uptake of gaseous nitrous acid (HONO) by several plant species, Atmospheric Environment, 40, 1324-1335, 10.1016/j.atmosenv.2005.10.028, 2006.

Schlögl, R.: Katalytische Ammoniaksynthese – eine “unendliche Geschichte”?, Angewandte Chemie, 115, 2050-2055, 10.1002/ange.200301553, 2003.

Schmidt, I., Look, C., Bock, E., and Jetten, M. S. M.: Ammonium and hydroxylamine uptake and accumulation in Nitrosomonas, Microbiology-(UK), 150, 1405-1412, 10.1099/mic.0.26719-0, 2004.

Seinfeld, J. H., Pandis, S. N., and Knovel: Atmospheric chemistry and physics [electronic resource] : from air pollution to climate change, 2nd ed. ed., J. Wiley, Hoboken, N.J., 1 online resource (xxviii, 1203 p.) : ill. pp., 2006.

Shen, Q. R., Ran, W., and Cao, Z. H.: Mechanisms of nitrite accumulation occurring in soilnitrification, Chemosphere, 50, 747-753, Pii s0045-6535(02)00215-1

10.1016/s0045-6535(02)00215-1, 2003.

Skopp, J., Jawson, M. D., and Doran, J. W.: Steady-state aerobic microbial activity as a function of soil-water content, Soil Science Society of America Journal, 54, 1619-1625, 1990.

Sörgel, M., Regelin, E., Bozem, H., Diesch, J. M., Drewnick, F., Fischer, H., Harder, H., Held, A., Hosaynali-Beygi, Z., Martinez, M., and Zetzsch, C.: Quantification of the unknown HONO daytime source and its relation to NO_2, Atmospheric Chemistry and Physics, 11, 10433-10447, 10.5194/acp-11-10433-2011, 2011a.

Sörgel, M., Trebs, I., Serafimovich, A., Moravek, A., Held, A., and Zetzsch, C.: Simultaneous HONO measurements in and above a forest canopy: influence of turbulent exchange on mixing ratio differences, Atmospheric Chemistry and Physics, 11, 841-855, 10.5194/acp-11-841-2011, 2011b.

Sörgel, M., Wu, D., Trebs, I., and Held, A.: Sources and sinks of HONO in a heterogeneous forest landscape., in preparation, 2014.

Steinkamp, J., and Lawrence, M. G.: Improvement and evaluation of simulated global biogenic soil NO emissions in an AC-GCM, Atmospheric Chemistry and Physics, 11, 6063-6082, 10.5194/acp-11-6063-2011, 2011.

Stella, P., Loubet, B., Laville, P., Lamaud, E., Cazaunau, M., Laufs, S., Bernard, F., Grosselin, B., Mascher, N., Kurtenbach, R., Mellouki, A., Kleffmann, J., and Cellier, P.: Comparison of methods for the determination of NO-O_3-NO_2 fluxes and chemical interactions over a bare soil, Atmospheric Measurement Techniques, 5, 1241-1257, 10.5194/amt-5-1241-2012, 2012.

Stemmler, K., Ammann, M., Donders, C., Kleffmann, J., and George, C.: Photosensitized reduction of nitrogen dioxide on humic acid as a source of nitrous acid, Nature, 440, 195-198, 2006.

Stemmler, K., Ndour, M., Elshorbany, Y., Kleffmann, J., D'Anna, B., George, C., Bohn, B., and Ammann, M.: Light induced conversion of nitrogen dioxide into nitrous acid on submicron humic acid aerosol, Atmospheric Chemistry and Physics, 7, 4237-4248, 2007.

Stromberger, M. E., Klose, S., Ajwa, H., Trout, T., and Fennimore, S.: Microbial populations and enzyme activities in soils fumigated with methyl bromide alternatives, Soil Science Society of America Journal, 69, 1987-1999, 10.2136/sssaj2005.0076, 2005.

Su, H., Cheng, Y. F., Cheng, P., Zhang, Y. H., Dong, S., Zeng, L. M., Wang, X., Slanina, J., Shao, M., and Wiedensohler, A.: Observation of nighttime nitrous acid (HONO) formation at a non-urban site during PRIDE-PRD2004 in China, Atmospheric Environment, 42, 6219-6232, 10.1016/j.atmosenv.2008.04.006, 2008a.

Su, H., Cheng, Y. F., Min, S., Dong Feng, G., Zhong Ying, Y., Li Min, Z., Slanina, J., Yuan Hang, Z., and Wiedensohler, A.: Nitrous acid (HONO) and its daytime sources at a rural site during the 2004 PRIDE-PRD experiment in China, Journal of Geophysical Research - Part D - Atmospheres, 114, 10.1029/2007jd009060, 2008b.

Su, H., Cheng, Y. F., Shao, M., Gao, D. F., Yu, Z. Y., Zeng, L. M., Slanina, J., Zhang, Y. H., and Wiedensohler, A.: Nitrous acid (HONO) and its daytime sources at a rural site during the 2004 PRIDE-PRD experiment in China, Journal of Geophysical Research-Atmospheres, 113, D14312

10.1029/2007jd009060, 2008c.

Su, H., Cheng, Y., Oswald, R., Behrendt, T., Trebs, I., Meixner, F. X., Andreae, M. O., Cheng, P., Zhang, Y., and Pöschl, U.: Soil Nitrite as a Source of Atmospheric HONO and OH Radicals, Science, 333, 1616-1618, 10.1126/science.1207687, 2011.

Ten Brink, H. M., and Spoelstra, H.: The dark decay of HONO in environmental (smog) chambers, Atmospheric Environment, 32, 247-251, 1998.

Trebs, I., Bohn, B., Ammann, C., Rummel, U., Blumthaler, M., Königstedt, R., Meixner, F. X., Fan, S., and Andreae, M. O.: Relationship between the NO_2 photolysis frequency and the solar global irradiance, Atmospheric Measurement Techniques, 2, 725-739, 2009.

Twigg, M. M., House, E., Thomas, R., Whitehead, J., Phillips, G. J., Famulari, D., Fowler, D., Gallagher, M. W., Cape, J. N., Sutton, M. A., and Nemitz, E.: Surface/atmosphere exchange and chemical interactions of reactive nitrogen compounds above a manured grassland, Agricultural and Forest Meteorology, 151, 1488-1503, 10.1016/j.agrformet.2011.06.005, 2011.

Tyndall, G. S., Orlando, J. J., and Calvert, J. G.: Upper limit for the rate coefficient for the reaction HO_2+NO_2^- HONO+O^{-2}, Environmental Science & Technology, 29, 202-206, 10.1021/es00001a026, 1995.

van Breemen, N., Burrough, P. A., Velthorst, E. J., van Dobben, H. F., de Wit, T., Ridder, T. B., and Reijnders, H. F. R.: Soil acidification from atmospheric ammonium sulphate in forest canopy throughfall, Nature, 299, 548-550, 1982.

Van Cleemput, O., and Samater, A. H.: Nitrite in soils: Accumulation and role in the formation of gaseous N compounds, Fertilizer Research, 45, 81-89, 1995.

van Dijk, S. M., Gut, A., Kirkman, G. A., Meixner, F. X., Andreae, M. O., and Gomes, B. M.: Biogenic NO emissions from forest and pasture soils: Relating laboratory studies to field measurements, Journal of Geophysical Research-Atmospheres, 107, 8058

10.1029/2001jd000358, 2002.

Vancleemput, O., and Baert, L.: Nitrite - a key compound in n-loss processes under acid conditions, Plant Soil, 76, 233-241, 1984.

VandenBoer, T. C., Brown, S. S., Murphy, J. G., Keene, W. C., Young, C. J., Pszenny, A. A. P., Kim, S., Warneke, C., de Gouw, J. A., Maben, J. R., Wagner, N. L., Riedel, T. P., Thornton, J. A., Wolfe, D. E., Dubé, W. P., Öztürk, F., Brock, C. A., Grossberg, N., Lefer, B., Lerner, B., Middlebrook, A. M., and Roberts, J. M.: Understanding the role of the ground surface in HONO vertical structure: High resolution vertical profiles during NACHTT-11, Journal of Geophysical Research: Atmospheres, 118, 10,155-110,171, 10.1002/jgrd.50721, 2013.

Wall, K. J., Schiller, C. L., and Harris, G. W.: Measurements of the HONO photodissociation constant, J. Atmos. Chem., 55, 31-54, 10.1007/s10874-006-9021-2, 2006.

Wiesen, P., Kleffmann, J., Kurtenbach, R., and Becker, K. H.: Mechanistic study of the heterogeneous conversion of NO2 into HONO and N2O on acid surfaces, Faraday Discussions, 100, 121-127, 1995.

Williams, J., Crowley, J., Fischer, H., Harder, H., Martinez, M., Petaja, T., Rinne, J., Back, J., Boy, M., Dal Maso, M., Hakala, J., Kajos, M., Keronen, P., Rantala, P., Aalto, J., Aaltonen, H., Paatero, J., Vesala, T., Hakola, H., Levula, J., Pohja, T., Herrmann, F., Auld, J., Mesarchaki, E., Song, W., Yassaa, N., Nolscher, A., Johnson, A. M., Custer, T., Sinha, V., Thieser, J., Pouvesle, N., Taraborrelli, D., Tang, M. J., Bozem, H., Hosaynali-Beygi, Z., Axinte, R., Oswald, R., Novelli, A., Kubistin, D., Hens, K., Javed, U., Trawny, K., Breitenberger, C., Hidalgo, P. J., Ebben, C. J., Geiger, F. M., Corrigan, A. L., Russell, L. M., Ouwersloot, H. G., de Arellano, J. V. G., Ganzeveld, L., Vogel, A., Beck, M., Bayerle, A., Kampf, C. J., Bertelmann, M., Kollner, F., Hoffmann, T., Valverde, J., Gonzalez, D., Riekkola, M. L., Kulmala, M., and Lelieveld, J.: The summertime Boreal forest field measurement intensive (HUMPPA-COPEC-2010): an overview of

meteorological and chemical influences, Atmospheric Chemistry and Physics, 11, 10599-10618, 10.5194/acp-11-10599-2011, 2011.

Wong, K. W., Tsai, C., Lefer, B., Haman, C., Grossberg, N., Brune, W. H., Ren, X., Luke, W., and Stutz, J.: Daytime HONO vertical gradients during SHARP 2009 in Houston, TX, Atmospheric Chemistry and Physics, 12, 635-652, 10.5194/acp-12-635-2012, 2012.

Wong, K. W., Tsai, C., Lefer, B., Grossberg, N., and Stutz, J.: Modeling of daytime HONO vertical gradients during SHARP 2009, Atmos. Chem. Phys., 13, 3587-3601, 10.5194/acp-13-3587-2013, 2013.

Yabushita, A., Enami, S., Sakamoto, Y., Kawasaki, M., Hoffmann, M. R., and Colussi, A. J.: Anion-Catalyzed Dissolution of NO_2 on Aqueous Microdroplets, The Journal of Physical Chemistry A, 113, 4844-4848, 10.1021/jp900685f, 2009.

Yan, D., Wang, Q., Mao, L., Ma, T., Li, Y., Guo, M., and Cao, A.: Nitrification dynamics in a soil after addition of different fumigants, Soil Sci. Plant Nutr., 59, 142-148, 10.1080/00380768.2012.754727, 2013.

Yienger, J. J., and Levy, H.: Empirical-model of global soil-biogenic NO_x emissions, Journal of Geophysical Research-Atmospheres, 100, 11447-11464, 10.1029/95jd00370, 1995.

York, D., Evensen, N. M., Martínez, M. L., and De Basabe Delgado, J.: Unified equations for the slope, intercept, and standard errors of the best straight line, American Journal of Physics, 72, 367-375, doi:http://dx.doi.org/10.1119/1.1632486, 2004.

Zhang, N., Zhou, X., Bertman, S., Tang, D., Alaghmand, M., Shepson, P. B., and Carroll, M. A.: Measurements of ambient HONO concentrations and vertical HONO flux above a northern Michigan forest canopy, Atmospheric Chemistry and Physics, 12, 8285-8296, 10.5194/acp-12-8285-2012, 2012.

Zhou, X. L., Gao, H. L., He, Y., Huang, G., Bertman, S. B., Civerolo, K., and Schwab, J.: Nitric acid photolysis on surfaces in low-NO_x environments: Significant atmospheric implications, Geophysical Research Letters, 30, 2217

10.1029/2003gl018620, 2003.

Zhou, X. L., Zhang, N., TerAvest, M., Tang, D., Hou, J., Bertman, S., Alaghmand, M., Shepson, P. B., Carroll, M. A., Griffith, S., Dusanter, S., and Stevens, P. S.: Nitric acid photolysis on forest

canopy surface as a source for tropospheric nitrous acid, Nat. Geosci., 4, 440-443, 10.1038/ngeo1164, 2011.

Zhu, C., Xiang, B., Zhu, L., and Cole, R.: Determination of absorption cross sections of surface-adsorbed HNO_3 in the 290–330 nm region by Brewster angle cavity ring-down spectroscopy, Chem. Phys. Lett., 458, 373-377, http://dx.doi.org/10.1016/j.cplett.2008.04.125, 2008.

Zhu, C. Z., Xiang, B., Chu, L. T., and Zhu, L.: 308 nm Photolysis of Nitric Acid in the Gas Phase, on Aluminum Surfaces, and on Ice Films, Journal of Physical Chemistry A, 114, 2561-2568, 10.1021/jp909867a, 2010.

I hereby declare that I wrote the dissertation submitted without any unauthorized external assistance and used only sources acknowledged in the work. All textual passages which are appropriated verbatim or paraphrased from published and unpublished texts as well as all information obtained from oral sources are duly indicated and listed in accordance with bibliographical rules. In carrying out this research, I complied with the rules of standard scientific practice as formulated in the statutes of Johannes Gutenberg-University Mainz to insure standard scientific practice.

Mainz, 12 February 2014_____